

UNIVERSITA' DEGLI STUDI DI PADOVA

DIPARTIMENTO DI SCIENZE DEL FARMACO

**CORSO DI LAUREA MAGISTRALE IN
CHIMICA E TECNOLOGIA
FARMACEUTICHE**

TESI DI LAUREA

Simultaneous quantification of abiraterone,
enzalutamide, darolutamide, apalutamide, and
their active metabolites: development and
analytical validation of a new LC-MS/MS method
for the PRECISION study

RELATRICE: Chiar.ma Prof.ssa Bolego Chiara

CORRELATRICI: Dr.ssa Cecchin Erika

Dr.ssa Posocco Bianca

LAUREANDA: De Cesaro Nicoletta

ANNO ACCADEMICO: 2024/2025

Questo lavoro di tesi è stato svolto presso
la Struttura Operativa Semplice Dipartimentale
di Farmacologia Sperimentale e Clinica
del Centro di Riferimento Oncologico di Aviano
(Istituto di Ricovero e Cura a Carattere Scientifico),
sotto la direzione della Dott.ssa Erika Cecchin.

CONTENTS

ABSTRACT.....	1
1. INTRODUCTION.....	3
1.1 Prostate cancer.....	4
1.1.1 Pharmacological treatment.....	7
1.1.1.1 Abiraterone.....	9
1.1.1.2 Apalutamide.....	11
1.1.1.3 Darolutamide.....	13
1.1.1.4 Enzalutamide.....	14
1.2 Therapeutic Drug Monitoring.....	16
1.2.1 TDM in the context of anticancer therapy.....	17
1.3 LC-MS/MS as a tool for TDM.....	20
1.3.1 Principles of liquid chromatography.....	20
1.1.1.5 HPLC.....	25
1.3.2 Principles of tandem mass spectrometry.....	26
1.3.3 Validation of a LC-MS/MS method.....	31
1.4 Precision study.....	33
2. AIMS.....	35
3. MATERIALS AND METHODS.....	38
3.1 LC-MS/MS method development of abiraterone, enzalutamide, darolutamide, apalutamide and their metabolites in human plasma.....	39
3.1.1 Instrumentation.....	39
3.1.2 Standard and chemicals.....	40
3.1.3 Mass spectrometric conditions optimisation.....	41
3.1.3.1 Compound-dependent parameters optimisation.....	41
3.1.3.1 Source-dependent parameters optimisation.....	44
3.1.4 Chromatographic conditions optimisation.....	46
3.1.5 Calibration curve and quality controls preparation.....	48
3.1.6 Internal Standard.....	51
3.1.7 Sample preparation.....	53
3.1.7.1 Sample extraction optimisation.....	53
3.2 LC-MS/MS validation study.....	55

3.2.1	Selectivity.....	55
3.2.2	Matrix effect.....	55
3.2.3	Recovery	56
3.2.4	Calibration curve and range	57
3.2.5	Accuracy and precision	57
3.2.6	Carry-over	58
3.2.7	Dilution integrity.....	59
3.2.8	Stability and reinjection reproducibility.....	59
3.3	Patient enrolment	61
3.3.1	Patient characteristics.....	61
3.3.2	Treatment and sampling.....	61
3.3.3	Patients' samples processing procedures	62
4.	RESULTS AND DISCUSSION	64
4.1	LC-MS/MS method development of abiraterone, enzalutamide, darolutamide, apalutamide and their metabolites in human plasma	65
4.1.1	Mass spectrometric conditions optimisation.....	65
4.1.1.1	Compound-dependent parameters optimisation	65
4.1.1.2	Source-dependent parameters optimisation.....	70
4.1.2	Chromatographic conditions optimisation	73
4.1.3	Sample preparation.....	78
4.1.3.1	Sample extraction optimisation	78
4.1.3.2	Calibration curve and quality controls preparation	79
4.2	LC-MS/MS validation study.....	80
4.2.1	Selectivity.....	80
4.2.2	Matrix effect.....	80
4.2.3	Recovery	82
4.2.4	Calibration curve and range	83
4.2.5	Accuracy and precision	85
4.2.6	Carry-over	89
4.2.7	Dilution integrity.....	89
4.2.8	Stability and reinjection reproducibility.....	90
4.3	Application of the method in human plasma samples	93
4.3.1	Abiraterone.....	94

4.3.2	Apalutamide	97
4.3.3	Darolutamide	100
4.3.4	Enzalutamide	102
5.	CONCLUSIONS	106
	REFERENCES	109

ABSTRACT

Prostate cancer is among the most prevalent malignancies in men and becomes life-threatening in its advanced stages. Therapeutic advances for metastatic castration-resistant prostate cancer (mCRPC) include next-generation androgen receptor signaling inhibitors (ARSIs) such as abiraterone (ABI), enzalutamide (ENZA), apalutamide (APA), and darolutamide (DARO). ABI is a CYP17A1 inhibitor, while ENZA, APA, and DARO are potent anti-androgens that directly antagonize the androgen receptor. All are administered at fixed high doses and are metabolized to active derivatives. These agents significantly improve patient outcomes, but their pharmacokinetic profiles exhibit high inter-individual variability. This highlights the rationale for therapeutic drug monitoring (TDM) of ARSIs to optimize efficacy and minimize toxicity. Despite emerging exposure–response data, especially for ABI, TDM remains largely investigational, partly due to the lack of robust analytical methods covering all four agents and their metabolites.

This thesis aimed to develop and validate a novel LC–MS/MS method capable of simultaneously quantifying ABI, APA, DARO, ENZA, and their respective active metabolites in human plasma. The method was tailored to support TDM applications in prostate cancer patients enrolled in the PRECISION study (protocol N: CRO-2025-12).

A triple quadrupole LC–MS/MS system Nexera LC-40 X3 (Shimadzu Corporation, Tokyo, Japan) coupled with a CITRINE 6500 QTrap, (SCIEX, Massachusetts, USA) was used. Electrospray ionization in positive mode enabled sensitive detection. Compound-specific MS parameters were optimized for each analyte and its internal standard. Chromatographic separation was achieved using a Kinetex® C18 column with gradient elution (acetonitrile and aqueous formic acid), resulting in a total runtime of 6.5 minutes. Sample preparation was limited to a simple protein precipitation step using 100 μ L of plasma and acetonitrile, yielding high recovery and minimal matrix effects. The method allowed coverage of clinically relevant concentrations for all eight analytes with rapid and reliable quantification.

The method was fully validated following EMA and FDA guidelines. It met all criteria for linearity, accuracy, precision, sensitivity, recovery, and analyte stability, confirming its suitability for clinical application.

The method was applied to plasma samples from prostate cancer patients receiving ARSI therapy in the ongoing PRECISION study. The assay enabled precise measurement of trough concentrations for all ARSIs and their active metabolites. ABI concentrations ranged from ~8 to 60 ng/mL with a mean of 24.7 ng/mL, and its metabolite D4A showed even

greater inter-individual variability. APA levels averaged ~ 2.9 $\mu\text{g/mL}$, while DARO and ENZA troughs averaged ~ 8.7 $\mu\text{g/mL}$ and ~ 10.8 $\mu\text{g/mL}$, respectively. Inter-patient variability was observed for all agents despite fixed dosing, reinforcing the need for pharmacokinetic-guided strategies. The method proved robust in real-world conditions. These results establish the assay as a practical tool for TDM in prostate cancer.

To conclude, a new LC–MS/MS method was developed and validated for the simultaneous quantification of four ARSIs and their metabolites in plasma. It enables efficient, sensitive, and accurate analysis with minimal sample preparation and short runtime. Its successful implementation in the PRECISION study supports its application in personalized prostate cancer therapy and lays the groundwork for broader adoption of TDM to improve clinical outcomes.

1. INTRODUCTION

1.1 Prostate cancer

Prostate cancer is the most common malignancy among men and represents a major cause of cancer-related mortality. It is estimated that in 2022, approximately 1.47 million new cases were diagnosed worldwide, resulting in 397,000 deaths. This disease is one of the most prevalent cancers and remains the leading cause of cancer-related death in the male population.¹ Globally, around 10 million men are currently living with prostate cancer, and roughly 700,000 of them present with metastatic disease.² The incidence of prostate cancer varies significantly across countries, largely due to differences in prostate-specific antigen (PSA) screening programs. In both screened and unscreened populations, prostate cancer accounts for approximately 1–2% of all male deaths.³ According to the International Agency for Research on Cancer (IARC), an estimated 40,500 new prostate cancer cases were diagnosed in Italy in 2022, representing 19.8% of all male cancers, an increase of 1.5% compared to 2020⁴. Furthermore, about 7,200 prostate cancer-related deaths occurred in 2021, while the five-year survival rate after diagnosis reached 91%.⁵

The prostate is a male accessory reproductive gland located just below the bladder, whose main function is to produce seminal fluid components that support sperm viability and fertility. Anatomically, the adult prostate is divided into three zones: the central, transitional, and peripheral regions.² The majority of prostate cancers, over 95% of which are classified as adenocarcinomas, originate in the peripheral zone, the outermost region of the gland.⁶ Both basal and luminal epithelial cells, which together constitute more than 70% of prostate tissue⁷, have been identified as potential cells of origin for prostate cancer, since genetic alterations in either population can drive the development of high-grade lesions characteristic of adenocarcinomas.⁸

Risk factors for prostate cancer include age, family history, ethnicity, and various environmental influences.^{9,10} In men younger than 50 years, the incidence is less than 1 case per 100,000 individuals; however, this rate increases to approximately 100 cases per 100,000 among those aged 51–60 years, and escalates further to more than 500 cases per 100,000 in men older than 60 years.¹ Men with first-degree relatives affected by prostate cancer have about a 50% higher chance of developing the disease compared to those without such a history, with earlier onset often observed in families spanning multiple generations.⁹ Genetic and epidemiological studies, including twin and family analyses, have confirmed a hereditary component, identifying mutations in DNA repair genes, such as *ATM*, *BRCA1*, and *BRCA2*, in about 5.5% of affected men, which markedly increases susceptibility.¹¹ Moreover, men of African descent show genetic variants associated with a

higher risk compared to White and Asian men.^{9,12} The heterogeneity of the disease is also linked to variations in androgen biosynthesis and metabolism, which can influence disease progression and treatment response. Chronic inflammation and urinary tract infections caused by microbial agents may further contribute to carcinogenesis through oxidative stress and the production of reactive oxygen species, which induce DNA damage and clonal selection of mutated cells.²

Given these factors, therapeutic strategies are designed according to both disease stage and androgen responsiveness. Screening plays a crucial role in the early detection of prostate cancer, as the disease often progresses silently and remains asymptomatic in its initial stages. When symptoms do appear, they are usually mild and nonspecific, such as increased urinary frequency or a persistent sensation of incomplete bladder emptying.^{13,14} These subtle signs can easily go unnoticed, underscoring the importance of regular screening for timely diagnosis and effective management. A conclusive diagnosis of prostate cancer is established through histopathological examination, which provides essential information such as the Gleason score, histological subtype, and tumor localization. These pathological parameters serve as crucial prognostic indicators, guiding therapeutic decisions and assisting clinicians in patient management and counseling.¹⁵ The Gleason scoring system is a histopathological grading method used to assess the aggressiveness of prostate cancer. Each biopsy core is assigned a Gleason grade from 1 to 5, where grade 1 resembles normal prostate tissue and grade 5 represents poorly differentiated cells lacking glandular structure.^{16,17} The two most predominant patterns are added to obtain the Gleason score (ranging from 2 to 10), which reflects tumor differentiation.¹⁵ Based on this, tumors are classified into five Grade Groups (1–5), with higher groups indicating more aggressive and less differentiated cancers.¹⁸ When the patient is diagnosed with localized prostate cancer, which accounts for approximately 70% of all cases,¹⁹ the condition is typically treated through prostatectomy, radiotherapy, or cryotherapy, followed by active surveillance. Following these interventions, patients are usually monitored under active surveillance. This management strategy is reserved for men with low or favorable intermediate risk prostate cancer and aims to monitor disease evolution through PSA testing, imaging, and biopsies, initiating curative treatment only in cases of progression. This approach helps balance effective cancer control with the preservation of urinary, sexual, and bowel function, thereby avoiding unnecessary overtreatment.^{2,20}

Following treatment for localised prostate cancer, androgen deprivation therapy (whether achieved through surgical or pharmacological means) often provides an initial favourable response. However, a proportion of patients eventually progress to castration-resistant

prostate cancer (CRPC). This advanced stage is defined by persistent disease progression despite maintaining low circulating testosterone levels (<50 ng/dL).²¹ The rise in PSA level, after initial treatment, is considered a biomarker of disease progression to non-metastatic castration-resistant prostate cancer (M0 CRPC), and if it is untreated or inadequately managed, can also advance to metastatic castration-resistant prostate cancer (mCRPC).²² Individuals diagnosed with metastatic prostate cancer are first managed through surgical or pharmacological castration, collectively referred to as androgen deprivation therapy (ADT). During this phase, the disease is classified as metastatic castration-sensitive prostate cancer (mCSPC), also known as metastatic hormone-sensitive or naive prostate cancer (mHSPC, mHNPC). When the tumor eventually becomes unresponsive to ADT, the condition progresses mCRPC.²³ This represents the most aggressive stage of prostate cancer, marked by the presence of multiple metastatic sites, including bones, lymph nodes, and visceral organs. Approximately 13% of prostate cancer patients develop locoregional metastases, while around 8% present with distant metastatic disease.¹⁹

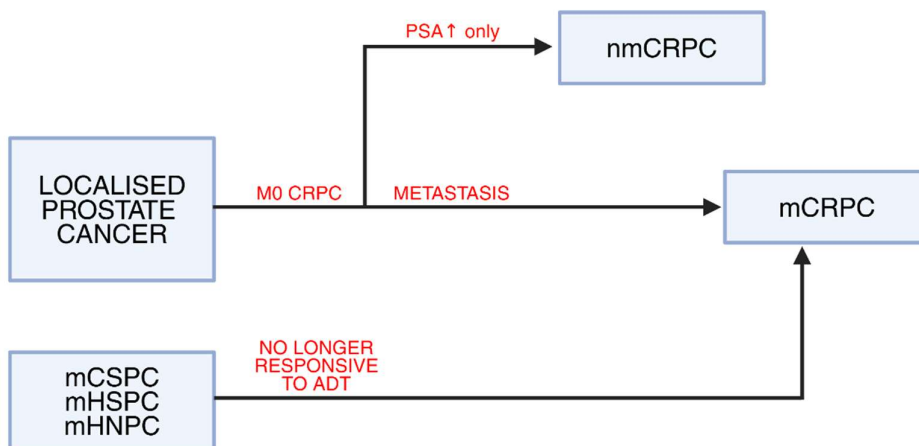


Figure 1, schematic representation of prostate cancer progression and disease stages.

1.1.1 Pharmacological treatment

The treatment of prostate cancer depends primarily on the stage and progression of the disease, as well as on the patient's overall health and life expectancy. Therapeutic strategies are clearly defined and guided by the European Society for Medical Oncology (ESMO) clinical practice guidelines²⁴, which provide evidence-based recommendations for the management of localized, locally advanced, and metastatic prostate cancer.

Localised disease	Low risk	Active surveillance Brachytherapy RP Radical RT
	Intermediate risk	RP Radical RT ± neoadjuvant ADT Brachytherapy Active surveillance
	High risk	Long-term ADT + radical RT ± neoadjuvant docetaxel RP + pelvic lymphadenectomy
Locally advanced disease		Neoadjuvant ADT + radical RT + adjuvant ADT ± neoadjuvant docetaxel RP + pelvic lymphadenectomy
M0 CRPC	High risk	ADT + apalutamide ADT + darolutamide ADT + enzalutamide
Metastatic disease	Hormone-naive	ADT + abiraterone ADT + docetaxel ADT + enzalutamide ADT + apalutamide RT for low volume ADT alone for frail patients who cannot tolerate the above treatments Bone health agent
	Castration-resistant (first line)	Abiraterone Docetaxel Enzalutamide ²²³ Ra for patients unfit for above treatments (and bone-only metastases)
	Second line or post-docetaxel	Abiraterone Cabazitaxel Enzalutamide ²²³ Ra

Table 1, summary of treatment recommendations for localized prostate cancer according to ESMO guidelines.²⁴

In localized prostate cancer, treatment strategies are defined according to the patient's risk category, low, intermediate, or high, based on specific clinical and pathological characteristics. For low-risk disease, the preferred management is usually active surveillance, which involves close monitoring of the patient's condition without immediate invasive therapy.²⁴ However, in selected cases, radical prostatectomy (RP), brachytherapy, or radical radiotherapy (RT) may also be appropriate options. RP, a surgical intervention involving the removal of the prostate gland and adjacent tissues, is particularly indicated in patients experiencing local recurrence without evidence of metastasis after previous external beam RT or brachytherapy, and it can also be performed in combination with RT in certain cases of low-risk prostate cancer.⁹

Already when discussing high-risk localized PC, and then in the subsequent stages, PC management is fundamentally based on the concept, established in the 1940s, that the disease is highly androgen-dependent²⁵. Over time, ADT has evolved from simply reducing gonadal testosterone levels to including approaches that inhibit the production of adrenal and other extragonadal androgens, as well as those that directly block or degrade the Androgen Receptor (AR).²⁶ Currently, the standard of care for advanced prostate cancer combines ADT with novel hormonal agents, particularly androgen biosynthesis inhibitors. This combined approach is strongly recommended as first-line systemic therapy for mHNPC.²⁴ Clinical evidence supports this combination: the LATITUDE trial demonstrated that adding abiraterone plus prednisone to ADT significantly improved Overall Survival (OS) in high-risk mHNPC patients,²⁷ while similar benefits were observed in the TITAN trial with apalutamide plus ADT²⁸, and in the ENZAMET trial with enzalutamide plus ADT.²⁹ These agents are also critical in treating M0 CRPC with a high risk of progression. In this setting, apalutamide (SPARTAN trial)³⁰, enzalutamide (PROSPER trial)³¹, and darolutamide (ARAMIS trial)^{31,32}, have all demonstrated significant increases in median metastasis-free survival (MFS) compared to placebo. Specifically, darolutamide increased median MFS to 40.4 months from 18.4 months with placebo in high-risk M0 CRPC patients.³² For patients with mCRPC, the recommended first-line systemic therapies include either the androgen biosynthesis inhibitor abiraterone, combined with prednisone, or the second-generation AR antagonist enzalutamide. The COU-AA-302 trial demonstrated that abiraterone plus prednisone significantly prolonged OS compared to placebo plus prednisone,³³ while the PREVAIL trial showed that enzalutamide was superior to placebo in improving OS among metastatic patients before chemotherapy.³⁴ Docetaxel chemotherapy is also a recognized systemic option for mCRPC. For patients progressing in the post-docetaxel setting, both abiraterone (COU-301 study) and enzalutamide (AFFIRM

trial) are recommended options and have been shown to improve OS, alongside cabazitaxel chemotherapy.³⁵⁻³⁷ In this thesis, we focused on the study of abiraterone, apalutamide, darolutamide, and enzalutamide, as these oral drugs are particularly suitable for investigation from a Therapeutic Drug Monitoring (TDM) perspective (see section 1.2.1).

1.1.1.1 Abiraterone

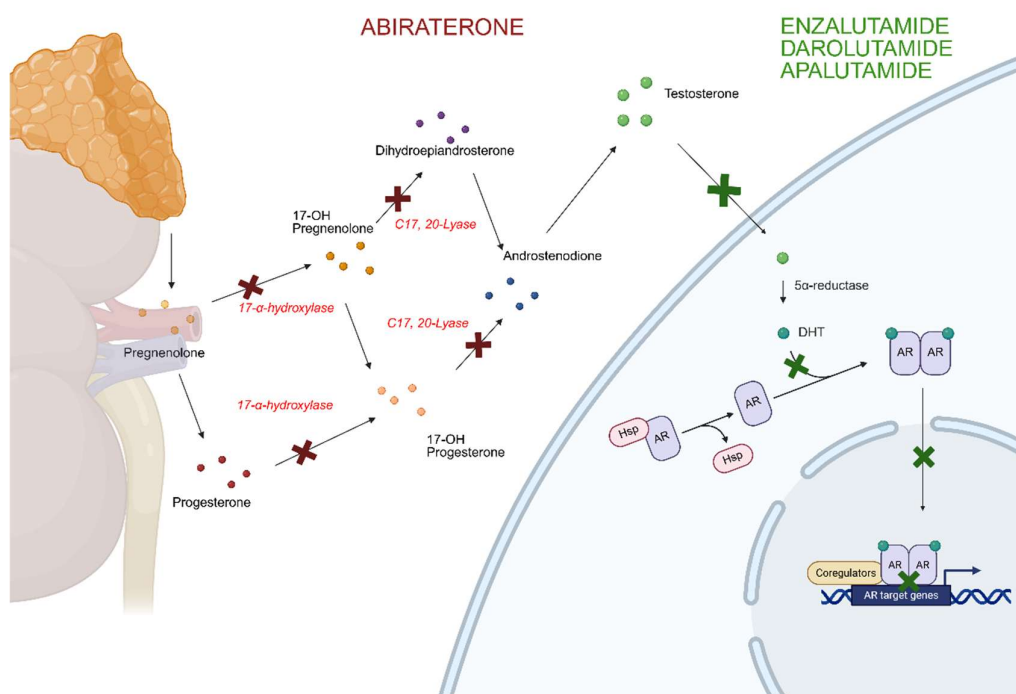


Figure 2, Schematic representation of the mechanisms of action of abiraterone, apalutamide, enzalutamide, and darolutamide.

Abiraterone (ABI) is a steroidal, orally administered, selective, and irreversible inhibitor of the enzyme CYP17A1 (17 α -hydroxylase/C17,20-lyase), which plays a key role in the biosynthesis of androgens derived from the testes, adrenal glands, and tumor tissues (Figure 2). By blocking CYP17A1 activity, ABI reduces the production of dihydrotestosterone (DHT), an androgen capable of binding to and activating the AR, which is crucial in the progression of prostate cancer.^{38,39} ABI is given orally once daily and is administered on an empty stomach, together with prednisone or prednisolone.⁴⁰ Treatment should be maintained until disease progression or the development of unacceptable toxicity. The medication must be taken at least two hours after a meal, and no food should be consumed

for at least one hour afterward, as food intake markedly increases its systemic exposure.³⁹ ABI is administered as a prodrug, abiraterone acetate (AA), which undergoes rapid hepatic hydrolysis to its active metabolite, ABI. Following AA oral administration, the time to reach maximum plasma concentration is approximately 2 hours. ABI is metabolized by several enzymes, primarily CYP3A4 and the sulfotransferase SULT2A1, leading to the formation of its two main inactive metabolites: abiraterone sulfate and N-oxide abiraterone sulfate. Because ABI is a steroidal compound and structurally resembles endogenous steroid precursors processed by 3 β -hydroxysteroid dehydrogenase (3 β -HSD) in the DHT biosynthetic pathway, the 3 β -HSD enzyme can convert ABI into Δ (4)-abiraterone (D4A), its active metabolite.⁴¹ The mean plasma half-life ($t_{1/2}$) of ABI in patients with mCRPC is 12h, a duration largely determined by its metabolism through glucuronidation, which inactivates the drug and facilitates its excretion. 88% of the drug is excreted in the feces, and 5% of ABI is recovered in the urine.^{39,42} In a study investigating ABI pharmacokinetics, the trough concentration (C_{\min}) of ABI, that is the plasma concentration reached just before patient takes the next daily dose of drug, and represent the least point in the dosing interval (This will be better explained in the section 1.2), was found to be 9.9 ng/mL, (range: 1.5–25.4 ng/mL, CV 61%), whereas levels of its active metabolite D4A were considerably lower, with a median of 0.8 ng/mL (range: 0.2–2.5 ng/mL, CV 61%). Repeated measurements in 17 subjects confirmed marked variability, with ABI C_{\min} reaching up to 28.6 ng/mL and intra-patient fluctuations as high as 33.6%. More than 65% of patients exhibited intra-patient variability exceeding 25% for ABI, and nearly half for D4A, indicating a pronounced lack of pharmacokinetic stability even under controlled dosing conditions.⁴³ The relationship between ABI exposure and clinical outcomes, encompassing both efficacy and toxicity, has been investigated. It has been reported that ABI C_{\min} is significantly associated with clinical efficacy, as measured by PSA response at three months. A C_{\min} threshold of 8.4 ng/mL was identified. Patients with C_{\min} above this threshold showed significantly longer PFS compared to those with $C_{\min} \leq 8.4$ ng/mL. No association was observed between ABI exposure and severe acute toxicity.^{44,45} It has also been investigated that the metabolic ratio between ABI and its active metabolite D4A may influence treatment outcomes. A higher D4A/ABI ratio was associated with shorter progression-free survival (PFS) and OS, suggesting that interindividual differences in metabolism can impact efficacy.^{45,46} Conversely, no clear link was observed between this metabolic ratio and clinically significant adverse events in most cohorts, although some studies reported higher ratios to be associated with increased toxicity.⁴⁷ ABI absorption is strongly influenced by food intake, with high-fat meals markedly increasing its plasma

exposure compared to the fasted state, while low-fat meals have a moderate effect.³⁹ Co-administration with food can shorten the time to reach therapeutic levels and improve overall drug bioavailability, potentially allowing lower doses to achieve efficacy comparable to standard fasting doses. This approach represents a promising therapeutic strategy, enhancing patient convenience and optimizing exposure while maintaining effectiveness.⁴⁸ ABI undergoes extensive metabolism and interacts with multiple CYP450 enzymes, strongly inhibiting CYP1A2 and CYP2D6, moderately inhibiting CYP2C9, CYP2C19, and CYP3A4/5, and weakly inhibiting CYP2C8, making it prone to pharmacokinetic drug–drug interactions (DDIs)^{42,49,50}. Caution is advised when co-administered with CYP2D6 substrates with a narrow therapeutic index, such as metoprolol, venlafaxine, or codeine. CYP3A4 inducers like rifampicin can markedly reduce ABI exposure. Co-administration of corticosteroids, routinely given to prevent adrenal insufficiency, may affect CYP activity and requires monitoring for dose-dependent adverse effects. Additionally, drugs affecting steroidogenesis, such as statins or indomethacin, may modulate ABI efficacy by altering intratumoral androgen levels.^{50,51}

1.1.1.2 Apalutamide

As a second-generation nonsteroidal antiandrogen, apalutamide (APA) acts by selectively and competitively inhibiting the ligand-binding domain of the AR (Figure 2)⁵². This mechanism prevents AR activation and subsequent steps such as nuclear translocation, DNA binding, and the transcription of androgen-regulated genes, processes that are essential for the growth and survival of prostate cancer cells^{52–54}. APA is administered orally at a recommended daily dose of 240 mg, which may be taken with or without food⁵⁵. According to EMA and FDA guidelines, no dose adjustment is required in patients with mild to moderate hepatic or renal impairment; however, treatment interruption or dose modification may be necessary in cases of severe adverse events^{55,56}.

The most common adverse effects (AEs) associated with APA include fatigue, rash, falls, weight loss, arthralgia, and hypertension⁵⁶. The drug is primarily metabolized in the liver via CYP2C8 and CYP3A4 enzymes, forming the active metabolite N-desmethyl APA, which retains approximately one-third of the activity of the parent compound^{57,58}. The mean terminal half-life ($t_{1/2}$) of APA is approximately 3–4 days, and steady-state plasma concentrations are typically achieved after about four weeks of daily dosing^{55,57}. Elimination occurs mainly through metabolic pathways, with approximately 65% of the administered dose excreted in urine and 24% in feces, primarily as metabolites⁵².

Additionally, APA acts as a weak inducer of CYP2C9 and a strong inducer of CYP2C19 and CYP3A4, as well as a weak inducer of the P-gp efflux transporter^{55,59}.

Pharmacokinetic (PK) data demonstrated that once-daily administration of APA at the approved 240 mg dose resulted in stable plasma concentrations at steady state after 28 days, with minimal peak-to-trough fluctuation (C_{\max} 6 $\mu\text{g/mL}$; C_{\min} 3.7 $\mu\text{g/mL}$).⁶⁰ Comparable stability was observed for its active metabolite, N-desmethyl-apalutamide (N-desmethyl APA), which exhibited limited variability throughout the dosing interval. Exposure parameters indicated low to moderate interindividual variability ($\leq 27\%$), supporting the use of AUC as a reliable metric for exposure–response analyses⁶¹.

The active metabolite contributes significantly to the overall pharmacological effect due to its comparable activity to the parent compound⁶².

Higher systemic exposure to APA was correlated with an increased incidence of dermatologic adverse events, particularly rash and pruritus. Specifically, higher exposure was significantly associated with rash (OR = 3.98) and pruritus (OR = 2.51), both in univariate regression and exposure–safety modelling. Rash represented the most prominent exposure-related event; however, most patients (92.7%) were able to continue therapy at the full 240 mg dose. In those who developed rash or pruritus, temporary dose reductions generally resulted in symptom resolution, allowing successful re-escalation⁶².

Food intake was found to delay t_{\max} without influencing overall drug exposure or efficacy, and the low intra-day variability of plasma concentrations further supports once-daily dosing⁵⁶.

APA exhibits a complex DDI profile primarily due to its strong induction of CYP3A4 and CYP2C19, and weaker induction of CYP2C9, P-gp, BCRP, and OATP1B1⁶³. This induction leads to increased metabolism and reduced plasma concentrations of co-administered substrates, potentially diminishing their efficacy. Clinically significant interactions have been observed with drugs metabolized by CYP3A4, CYP2C19, and CYP2C9, including anticoagulants, immunosuppressants, and central nervous system agents⁶³. Strong inhibitors of CYP2C8 or CYP3A4, such as gemfibrozil and ketoconazole, can increase APA exposure by up to 50%, warranting close monitoring for tolerability. The induction of enzymes and transporters like P-gp and UGT further enhances its DDI potential, notably with drugs such as apixaban, rivaroxaban, or ticagrelor, potentially raising thromboembolic risk due to decreased systemic exposure⁵⁹. Therefore, individualized management and careful review of concomitant medications are essential when prescribing APA⁶³.

1.1.1.3 Darolutamide

Darolutamide (DARO) is an oral, nonsteroidal AR antagonist composed of two pharmacologically active diastereomers, (S,R)-darolutamide and (S,S)-darolutamide, which interconvert through their primary active metabolite, keto-darolutamide (keto-DARO), with a predominance of the (S,S) form due to its slower elimination rate^{64,65}. It binds to the AR with high affinity, inhibiting receptor activation and thereby blocking prostate cancer cell proliferation^{64,66}(Figure 2). While no formal TDM thresholds have been defined, PK data continue to enhance understanding of APA's exposure–response relationship.^{52,67} Structurally, DARO exhibits unique characteristics compared to other AR antagonists, including low lipophilicity and limited ability to cross the blood–brain barrier, features that contribute to a significantly reduced incidence of central nervous system related adverse events^{64,66,68}. The standard regimen consists of 600 mg administered orally twice daily with food, for a total of 1,200 mg per day, and in non-castrated men it should be combined with a luteinizing hormone-releasing hormone (LHRH) analogue to maintain testosterone suppression⁶⁹. From a pharmacological perspective, DARO demonstrates high target selectivity and a favorable safety profile, which make it suitable for long-term administration in patients with advanced prostate cancer. Its oral bioavailability is strongly influenced by food intake since the absolute bioavailability increases from approximately 30% under fasting conditions to over 70% when administered with food. For this reason, DARO is recommended to be taken with meals to maximize absorption and reduce PK variability. After oral administration, the compound reaches peak plasma concentration (C_{max}) approximately four hours post-dose and displays time-independent PK with steady state achieved within 2–3 days⁶⁵. DARO undergoes extensive hepatic metabolism mainly through the cytochrome P450 isoenzyme CYP3A4, which oxidizes it into its equipotent metabolite keto-darolutamide. This interconversion also involves aldo–keto reductase 1C enzymes, while glucuronidation via UGT1A9, UGT1A1, UGT1A3, and UGT2B10 represents a secondary metabolic pathway^{69,70}. The elimination half-life ($t_{1/2}$) differs between the two diastereomers, being approximately 9 hours for (S,R)-darolutamide and 22 hours for (S,S)-darolutamide, resulting in an overall mean $t_{1/2}$ of around 20 hours⁷¹. At steady state, the mean plasma concentrations of DARO were 3.78 $\mu\text{g/mL}$ (C_{min}) and 4.79 $\mu\text{g/mL}$ (C_{max}) and for its active metabolite, keto-DARO, mean C_{min} and C_{max} values were 6.11 $\mu\text{g/L}$ and 8.48 $\mu\text{g/mL}$, respectively.⁷² The main route of excretion is fecal (around 63%), with about one-third eliminated through urine⁶⁵. Regarding DDIs, darolutamide has a lower potential compared with other second-generation AR antagonists. Although

metabolized by CYP3A4 and serving as a substrate for P-glycoprotein (P-gp) and BCRP, it exerts only weak inhibition or induction of cytochrome P450 isoenzymes^{63,73,74}.

1.1.1.4 Enzalutamide

Enzalutamide (ENZA) is a second-generation, nonsteroidal AR. It acts by competitively binding to the AR and blocking multiple key steps in the androgen signalling cascade, including receptor translocation into the nucleus, DNA binding, and co-activator recruitment^{35,75,76}(Figure 2). This multi-level inhibition translates into a potent suppression of androgen-dependent gene transcription, which is central to prostate cancer progression. From a PK perspective, ENZA is rapidly and extensively absorbed following oral administration, with an estimated absolute bioavailability of at least 84%⁷⁷. The drug reaches its C_{max} within 1–2 hours and achieves steady-state levels by approximately day 28 due to its long elimination half-life^{50,78}. It exhibits linear and time-independent PK, characterized by low interindividual variability ($\leq 30\%$), supporting its suitability for once-daily dosing. The mean C_{min} at week 13 was $11.4 \pm 2.95 \mu\text{g/mL}$ for ENZA ($n = 679$), $13.0 \pm 3.78 \mu\text{g/mL}$ for N-desmethyl ENZA ($n = 680$)⁷⁹. ENZA undergoes hepatic metabolism mainly via CYP2C8, with a minor contribution from CYP3A4/5^{80,81}. It is converted into two major metabolites: the active N-desmethyl ENZA, which retains similar pharmacological potency, and an inactive carboxylic acid derivative. The $t_{1/2}$ of ENZA is about 5.8 days, while that of N-desmethyl ENZA is between 6 and 8 days, leading to notable accumulation at steady state^{82,83}. Food has a minimal effect on ENZA absorption, with only a slight decrease ($\sim 30\%$) in C_{max} and a minor delay (approximately one hour) when taken with meals⁸⁴. Given that overall exposure is unaffected, the drug can be administered with or without food, enhancing convenience and adherence^{78,81}. Regarding DDIs, ENZA acts both as a substrate and as a potent inducer of several CYP450 enzymes. Since it is extensively metabolized by CYP2C8 and CYP3A4, co-administration with strong CYP2C8 inhibitors such as gemfibrozil increases ENZA exposure by approximately 2.2-fold, while CYP3A4 inhibitors like itraconazole cause a smaller (1.3-fold) increase⁵⁰. For this reason, a dose reduction to 80 mg daily is recommended when strong CYP2C8 inhibitors are used concomitantly^{50,77}. Conversely, ENZA strongly induces CYP3A4, CYP2C9, and CYP2C19, and inhibits the P-gp efflux transporter in vitro, potentially decreasing the plasma concentrations of drugs metabolized by these pathways. ENZA can significantly decrease the exposure of compounds that are both CYP3A substrates and P-gp substrates, such as apixaban, edoxaban, and rivaroxaban, with reductions in AUC estimated

between 30% and 45%^{85,86}. For this reason, the European Society of Cardiology (ESC) recommends avoiding these combinations when possible⁸⁷. These data emphasize the importance of careful drug management and potential TDM application, especially in polytreated patients at high risk of adverse or subtherapeutic interactions⁸⁸. Taken together, ENZA exhibits predictable PK, extensive metabolism through CYP450 enzymes, and a well-established safety profile. Nonetheless, its role as a strong enzyme inducer makes it particularly relevant for TDM-based evaluation, especially in patients receiving multiple concomitant medications or experiencing dose-dependent toxicity. Maintaining optimal plasma concentrations is essential to balance efficacy and tolerability, supporting the integration of TDM approaches to optimize personalized treatment in prostate cancer management^{50,77,88}.

1.2 Therapeutic Drug Monitoring

TDM represents a specialized area within clinical chemistry and pharmacology focused on individualizing pharmacological treatments.⁸⁹ Its goal is to optimize drug dosing by measuring and interpreting drug concentrations in biological matrices such as plasma, serum, whole blood, or urine⁹⁰. In practical terms, these measurements are used to assess whether the drug levels fall within the therapeutic window, as illustrated in Figure 3.

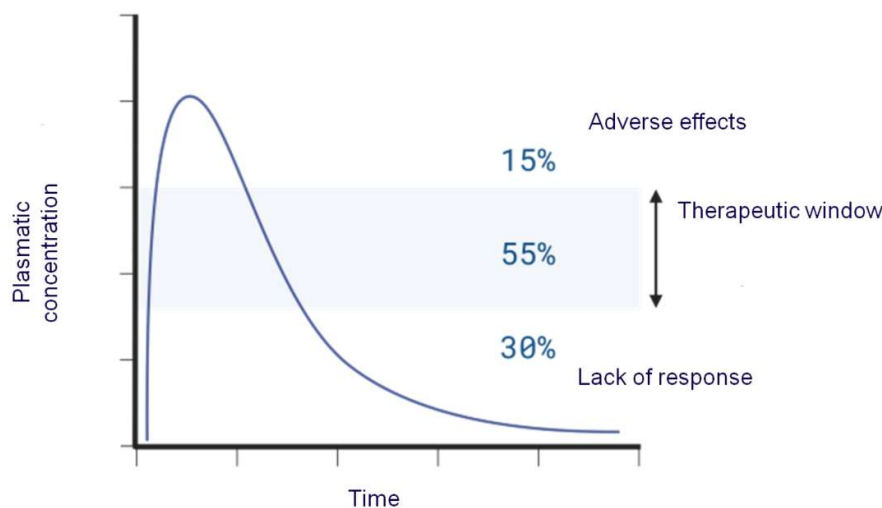


Figure 3, Schematic representation of a therapeutic window.

Since the beginning of the 60s, TDM has been used in the clinical treatment of patients to simultaneously maximize the therapeutic effect and minimize the occurrence of toxicity⁹¹. Nowadays, this approach is widely applied in the pharmacological treatment with antibiotics⁹², cardiovascular drugs⁹³, antiepileptics⁹⁴, antidepressants⁹⁵, immunosuppressants⁹⁶, and some chemotherapeutic agents⁹⁷. To ensure the proper execution of TDM, several key elements must be carefully controlled: correct drug administration, accurate collection and handling of the biological sample, precise quantification of the drug and/or its metabolites, and a sound interpretation of the obtained results⁹⁸. Consequently, TDM relies on a multidisciplinary collaboration involving physicians, pharmacists, nurses, pharmaceutical chemists or technicians, and PK specialists. Each professional plays a defined role and must be aware of the potential challenges and limitations of the process, as an error or oversight in any single step can put it at risk the

accuracy and reliability of the entire procedure⁹⁹. The physician is the initial professional involved in TDM, as they determine the appropriate pharmacological therapy based on the patient's diagnosis. The pharmacist is responsible for providing the medication to the patient or, in cases of intravenous administration, preparing the drug according to the prescribed dosage. The nurse oversees the collection of biological samples, ensuring both the quality of the sample and the timing of collection. Proper timing is crucial in TDM because it directly affects the accuracy of PK assessments; if the sampling time deviates from the planned schedule and is not documented, the resulting PK data may be unreliable, potentially compromising the physician's ability to adjust the dosage optimally for the patient⁹⁹. The next key professional in the TDM workflow is the clinical chemist or pharmaceutical technologist, who is responsible for processing the biological sample and measuring the concentration of the drug and any relevant metabolites. Based on these concentration values, the PK scientist can either calculate PK parameters or compare the results with data from the literature.

1.2.1 TDM in the context of anticancer therapy

The dosage of anticancer agents is traditionally calculated according to patient-specific parameters, such as body surface area (mg/m^2) or body weight (mg/kg). However, this approach often lacks precision, as patients with comparable anthropometric characteristics may experience very different therapeutic responses or toxic effects when administered the same dose of a given drug. Such pronounced inter-individual variability in drug efficacy and safety, combined with other peculiar pharmacological features of anticancer compounds, makes this class of drugs particularly suitable for TDM applications⁹⁷.

To be appropriate for TDM, a drug should meet several fundamental criteria¹⁰⁰:

- it should have a narrow therapeutic window, meaning a small difference between the minimum effective concentration (MEC) and the minimum toxic concentration (MTC);
- it should exhibit limited intra-individual but marked inter-individual PK variability;
- a well-defined relationship must exist between systemic exposure and pharmacological or clinical effects;
- an accurate, validated, and reproducible analytical method must be available for quantification in biological matrices;
- and finally, no alternative, easily measurable biomarkers should exist to evaluate its efficacy¹⁰¹.

In recent decades, the therapeutic landscape in oncology has shifted from the use of conventional cytotoxic agents and nonspecific chemotherapy toward oral molecularly targeted therapies¹⁰².

The term targeted therapy refers to a new class of anticancer drugs designed to selectively interfere with specific cellular targets, often kinases or key signalling molecules, involved in cancer growth and progression¹⁰³. These agents have profoundly changed the clinical management of many cancers, as they are typically administered orally and chronically, allowing certain previously fatal malignancies to become manageable chronic conditions. For many of these targeted drugs, a relationship between systemic exposure and both efficacy and toxicity has been demonstrated¹⁰⁴. Despite being commonly given at fixed doses, inter-patient variability in PKs often leads to a wide range of circulating concentrations, resulting in either excessive toxicity (overexposure) or therapeutic failure and drug resistance (underexposure)¹⁰⁵. Indeed, oral administration frequently produces a broad distribution of plasma concentrations, with inter-individual variability as high as 23-fold.

This variability arises from multiple factors. The oral route, while convenient, introduces complexities related to gastrointestinal absorption and first-pass hepatic metabolism¹⁰⁶. Additional contributors include pharmacogenetic differences, dietary factors, environmental influences, and patient adherence^{106,107}. These factors collectively shape the PK profile of a drug over time and thus determine its pharmacological activity at the site of action¹⁰⁸.

In the case of metronomic therapy, which has been explored as an alternative to conventional chemotherapy¹⁰⁵, TDM can be particularly useful for verifying whether drug levels remain within the therapeutic range. Monitoring the C_{\min} or C_{trough} , the minimum plasma concentration at the steady state, provides valuable information on the lowest drug level during a dosing interval. Steady-state equilibrium is typically reached after 4–5 half-lives from the start of treatment¹⁰⁹.

Despite its strong rationale, TDM is not yet routinely implemented for anticancer agents, even though dosage adjustments could significantly improve safety and efficacy. One notable exception is methotrexate, an antineoplastic and immunosuppressive agent whose serum concentration is routinely monitored in clinical laboratories. In high-dose regimens, methotrexate levels are measured to determine whether folinic acid rescue therapy should be initiated to prevent toxicity caused by delayed drug clearance¹¹⁰.

However, the broader clinical application of TDM in oncology remains limited by several challenges:

- for many anticancer agents, the pharmacokinetic–pharmacodynamic relationship is not fully elucidated, making it difficult to establish a reliable correlation between plasma concentration and therapeutic response. In the absence of a clear dose–response relationship, the therapeutic window cannot be defined, limiting the utility of TDM¹¹¹;
- the intrinsic heterogeneity of cancer also limits standardization, as tumours of similar histology may exhibit different sensitivity and resistance profiles¹¹⁵;
- TDM is inherently a multidisciplinary process, requiring coordination among clinicians, pharmacists, and laboratory scientists, errors at any stage can compromise the entire workflow.
- finally, analytical methods must be robust, rapid, precise, and sensitive, while remaining economically feasible and minimally affected by matrix effects.

Despite these challenges, the potential benefits of TDM in oncology are considerable. Most anticancer drugs have a low therapeutic index and display marked PK variability, both of which strengthen the rationale for individualized monitoring¹¹⁶. Personalized dose optimization through TDM can help achieve maximal therapeutic efficacy while minimizing toxicity. Furthermore, this approach improves patient compliance, by reducing the occurrence of AEs, enables dose adjustments in individuals with hepatic or renal impairment, and facilitates the identification of clinically relevant DDIs^{98,116}.

Overall, the integration of TDM into the management of anticancer therapies represents a powerful strategy to enhance treatment precision, reduce variability, and optimize clinical outcomes, ultimately contributing to a more personalized and effective approach to cancer care.

1.3 LC-MS/MS as a tool for TDM

Over the last decades, analytical techniques in cancer pharmacology have undergone significant advancements, which are essential for accurately determining drug concentrations in biological samples for TDM. Initially, LC-UV/VIS assays were widely used, followed by the introduction of fluorescence detectors, but a major turning point in bioanalysis was represented by the development of bench-top mass spectrometry instruments.¹¹⁷ Key milestones in the history of mass spectrometry include the perfection of electrospray ionisation (ESI) in the 1980s by John Fenn¹¹⁸, which allowed soft ionisation of large biomolecules, and the transition from gas chromatography (GC) to liquid chromatography (LC) as a front-end technique, enabling simpler workflows and faster analysis times.

Currently, the reference method for determining drug concentrations in biological matrices is LC coupled with tandem mass spectrometry (MS/MS)¹¹⁹. LC efficiently separates the components of complex matrices, such as whole blood, serum, or plasma, with high reproducibility and precision, while MS/MS, especially in tandem configuration, provides information on both the identity and the exact quantity of the analytes present. This combination allows simultaneous quantification of multiple compounds from small sample volumes, ensuring reliable and robust results, and has become a widely adopted technique in many laboratories.

1.3.1 Principles of liquid chromatography

Chromatography is a technique used to separate the components of a mixture according to their distinct physicochemical characteristics, such as polarity, charge, or molecular mass. The process relies on the different interactions of analytes with two phases: a stationary phase (SP), which remains fixed, and a mobile phase (MP), which passes through it. Each compound distributes itself between these two phases depending on its relative affinity for them. This distribution is expressed by the partition coefficient (K), defined as the ratio between the analyte concentration in the stationary phase (C_s) and that in the mobile phase (C_m). The value of K is characteristic of each compound and determines its retention behavior during separation.

$$K = \frac{C_s}{C_m}$$

A higher K indicates that a compound has a stronger affinity for the SP. For a given SP, the K value depends both on the chemical nature of the analyte and on the composition of the MP. By adjusting experimental parameters, such as the MP composition or flow rate, it is possible to influence the migration behaviour of the analytes within the column, thus achieving their separation. Based on the interaction mechanisms between the analytes and the two phases, and on the specific characteristics of the SP and MP used, different chromatographic techniques can be distinguished:

- adsorption chromatography: the separation of the compounds is based on the adsorption coefficient relative to the SP;
- partition chromatography: the separation of the compounds is based on the partition coefficient relative to a biphasic (aqueous/organic) system. If the SP is more polar than the MP it will be called normal phase (NP), while in the opposite situation, it is called reverse phase (RP);
- ion exchange chromatography: the separation of the compounds is based on their charge and the ionic bond with the SP, which is an ion exchange resin;
- size exclusion chromatography: the separation of the compounds is based on molecular size. It is also called gel permeation/filtration chromatography.
- affinity chromatography: separation of the compounds is based on biochemical, reversible, and very specific reactions.

In RP chromatography, the technique applied in this thesis, the SP consists of a support material, usually silica, polymer, or a silica-polymer hybrid, chemically modified with apolar functional groups known as bonded phases. These hydrophobic chains, such as C8, C18, or phenyl groups, impart apolarity to the SP. This approach is particularly suitable for the separation of lipophilic analytes, including most drugs, as the retention mechanism is mainly governed by hydrophobic interactions. Therefore, the selectivity of the separation depends on the differences in hydrophobicity among the various compounds. During the chromatographic process, the lipophilic molecules carried by the MP are retained on the SP that fills the chromatographic column, which presents similar characteristics with the analytes. As the MP, constituted by an aqueous-organic mixture, continues to flow through the column, there will be the detachment of the various compounds retained by the SP according to their affinity for the MP. There are many solvents that can be used as MP, mainly classifiable according to their eluting power which is strictly related on their own polarity; moreover, two or more solvents can also be mixed to modulate the elution power of the resulting MP.

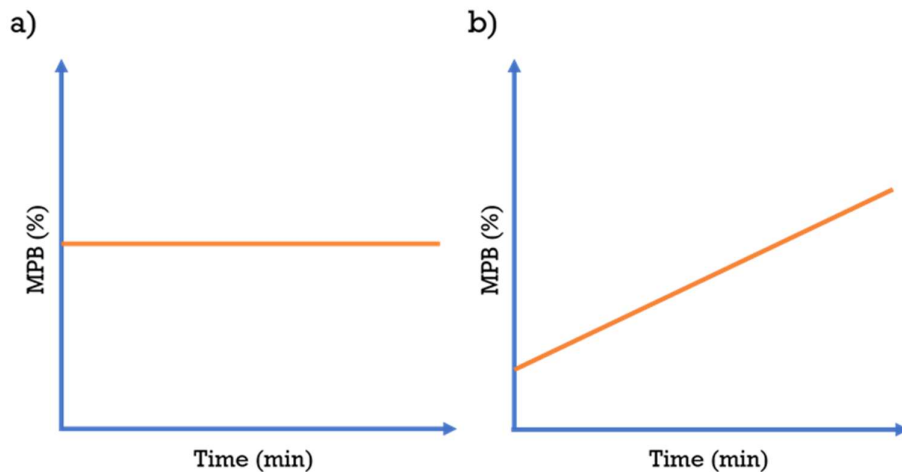


Figure 4, graphic representation of the two elution types: isocratic (a) and gradient (b).

In LC, two main elution modes can be applied (Figure 4): isocratic and gradient elution. In isocratic elution (Figure a), the MP composition remains constant throughout the entire chromatographic run, and the separation of analytes occurs under fixed solvent conditions. In contrast, gradient elution (Figure b) involves a varying ratio of two or more MPs, typically referred to as A (the aqueous or “weak” solvent in RP chromatography) and B (the organic or “strong” solvent in RP chromatography).

Gradient elution usually provides faster and more efficient separations compared to the isocratic mode, since the changing solvent strength allows analytes to desorb from the SP more rapidly. At the end of the analysis, a chromatogram is obtained, showing the detector response (Y-axis) as a function of the chromatographic runtime (X-axis), as illustrated in Figure 5.

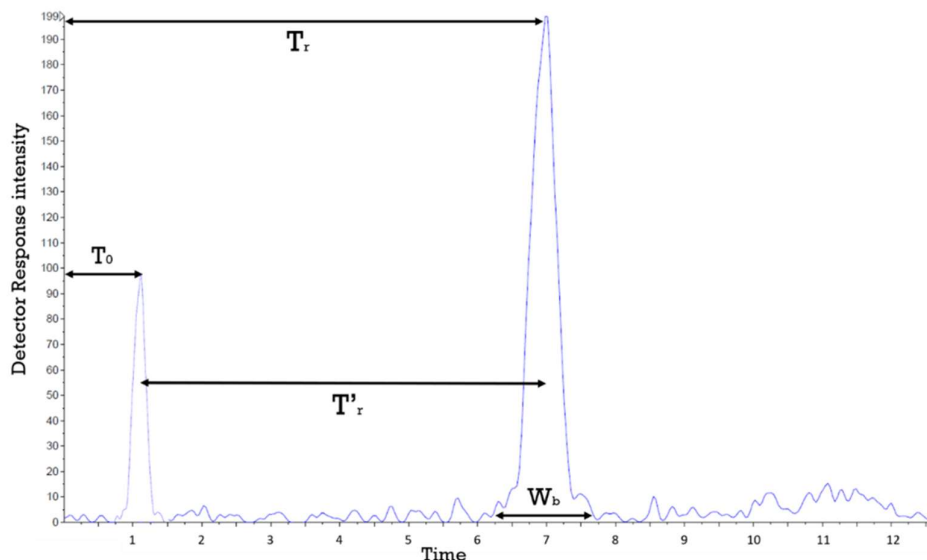


Figure 5, Example of a generic chromatogram. The first lower peak shows the elution of the mobile phase or unretained compound while the second peak describes the elution of the compound of interest. The retention time (T_r), the dead time (T_0) and the adjusted retention time (T'_r) are represented.

Each analyte appears as a peak, corresponding to a transient increase in detector signal during its elution.

For quantitative analysis, the peak area is used as parameter instead of peak height because it is better directly proportioned to the amount of the detected analytes. The retention time (T_r) is the time that the compound of interest takes to be eluted by the MP, while the dead time (T_0) is the elution time of non-retained compound. T_0 also represents the migration rate of the MP molecules, so the adjusted retention time (T'_r) of an analyte, which is a qualitative parameter, is the difference between its T_r and T_0 . A good chromatographic separation is characterized by narrow, symmetrical, and well separated peaks for each substance. The fundamental variables of chromatography are:

- capacity factor (K'): it represents the retention of an analyte into the chromatographic column, and it is equal to the ratio between T'_r and T_0 . As shown in the equation, the higher the K' value, the longer the time spent in the SP and the later the compound elutes from the column.

$$K' = \frac{T'_r}{T_0}$$

- selectivity (α): indicates the ability of the chromatographic system to distinguish between two species A and B. It is expressed by the ratio between the capacity factor of A (K'_A), and the capacity factor of B (K'_B). A and B result distinguished

only with α value higher than 1. A high selectivity can only be achieved by using the optimal SP-MP combination for the analyte of interest;

$$\alpha = \frac{K'_A}{K'_B}$$

- Efficiency (N): this parameter describes how well an analyte band remains compact as it moves through the column. It is expressed in terms of the number of theoretical plates (N), which represent hypothetical sections into which the column volume can be divided. Each theoretical plate corresponds to one equilibrium step of the analyte distribution between the MP and the SP.

A higher N value indicates more equilibrium stages and, consequently, improved separation performance. Efficiency can be enhanced by increasing the column length, though this also extends the total analysis time. Alternatively, columns packed with smaller particles can be used to reduce the plate height (H), thereby increasing N for a given column length (L).

The relationship among these parameters is expressed as:

$$H = \frac{L}{N}$$

N is instead expressed by the following equation where W_b is the width at the peak base:

$$N = 16 \left(\frac{T'_r}{W_b} \right)^2$$

Resolution (R): it is the capacity of the system to separate two chromatographic peaks and it relates the abovementioned three variables as shown in the following formula:

$$R = \frac{\sqrt{N}}{4} \left(\frac{\alpha - 1}{\alpha} \right) \left(\frac{K'}{1 + K'} \right)$$

Indeed, resolution (R) expresses the effectiveness of the separation between two chromatographic peaks. It is determined by comparing the retention times of two compounds that elute successively. A satisfactory resolution is achieved when the peaks are completely distinct, showing no overlap. For two analytes, A and B, the resolution can also be expressed as the ratio between the distance separating their peak apices and the average baseline widths of the two peaks:

$$R = 2 \frac{T_{rB} - T_{rA}}{W_{bA} + W_{bB}}$$

1.1.1.5 HPLC

High-performance liquid chromatography (HPLC) is a form of LC in which the MP is forced through a densely packed SP under high pressure. This technique provides several advantages over other chromatographic methods, including rapid analyte separation, minimal sample volume requirements, high precision and reproducibility, and full automation capabilities.

The SP, regardless of its chemical composition, which varies depending on the separation mechanism, is made up of solid microparticles, typically ranging from 3 to 10 μm in diameter. Their small size increases the surface area available for MP–SP interactions and ensures uniform column packing. The MPs used are of high purity and low viscosity, and they must be immiscible with the SP as well as compatible with the detector. The selection of the eluent depends on both the type of SP used and the physicochemical characteristics of the analytes. Components of a high-performance liquid chromatograph usually include (Figure 6):

- containers for solvents: they are made of inert material, generally glass, and they have enough capacity to ensure the execution of a certain amount of analysis. The MPs are picked up by Teflon dip tubes ending with a porous steel filter, that blocks any coarse particle.
- degasser: removes potential air bubbles present in the MP to prevent them from reaching the column, damaging it or interfering with both the separation process and the detector.
- high-pressure pumps: they push MPs along the chromatographic system. The pumps must be able to exert high pressures and to dump the pulsations in order to guarantee a constant and reproducible flow. For an isocratic elution only one pump is needed, while two pumps (at least) must be used for a gradient one
- mixer: if a gradient elution is used, it is essential to mix the two MPs.
- autosampler: it consists on the sample loading and injection system. Sample loading can occur by interrupting the eluent flow or exploiting an injection valve, which makes it possible to introduce the sample without suspending it; the injection valves are integrated with a tube, called loop, which guarantees high reproducibility of the injected volume.
- pre-column (guard-column): it acts as a mechanical filter to prevent sample impurities from entering the column, risking ruining it.

- column: it is usually made of stainless steel and is suitable for withstanding high pressures; at the ends, it is closed by porous steel septums that retain the SP. The internal diameters and lengths vary according to the type of analysis. If temperature control is needed, it can be obtained by placing the column in a thermostatic ventilation chamber (called oven) or by using columns provided externally with a mantle, inside which a thermostat fluid circulates.
- detector: device used to determine the presence of eluted compounds. It must be sensitive, characterised by rapid response times and must provide stable, reproducible and linear signals according to the analyte concentration. Commonly used detectors are: spectrophotometer (IR, UV/VIS, fluorescence-based), refractometer, electrochemical-based detectors, photodiode array (PDA) or mass spectrometer.

While most of the time HPLC is coupled with UV/VIS detectors, the coupling with mass spectrometry (typically quadrupoles) allows reaching the best selectivity and sensitivity for quantitative analysis of compounds in complex matrices.

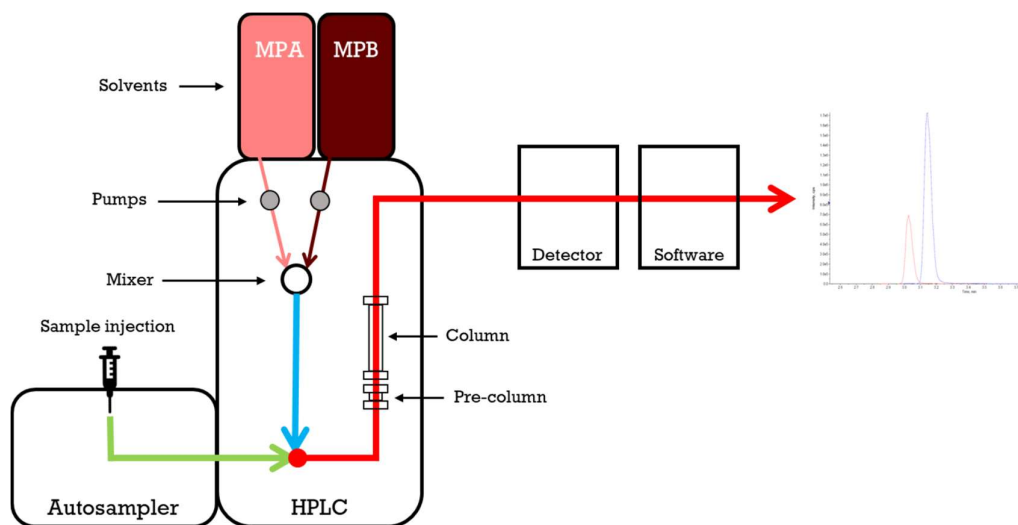


Figure 6, Schematic representation of a HPLC system.

1.3.2 Principles of tandem mass spectrometry

MS is a technique that allows the detection of substances based on the ratio between the molecular mass and the charge (m/z), with an accuracy that may reach 0.01%. Each spectrometer consists of some essential components which are summarized in Figure 7.

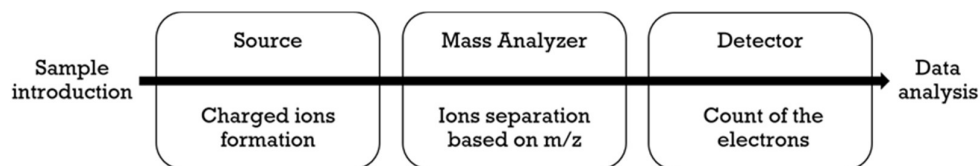


Figure 7, Schematic representation of a mass spectrometer components.

However, some of the conditions and characteristics hereafter described are specific of SCIEX spectrometers, because is the instrument adopted for the method development object of this thesis project. After the sample introduction, the first step in MS is the ionization of the neutral compound of interest mainly through electron ejection, electron capture, protonation, deprotonation, adduct formation. This process takes place into the source, and it is fundamental because the spectrometer can detect only the charged molecules. A wide range of ionisation methods can be employed in MS analysis. Techniques that use high-energy processes, leading to extensive molecular fragmentation, are referred to as “hard” ionisation sources, such as electron ionisation (EI). In contrast, “soft” ionisation sources generate ions of the intact molecular species with minimal fragmentation; these include chemical ionisation (CI), atmospheric-pressure chemical ionisation (APCI), and electrospray ionisation (ESI). Another important soft ionisation technique is matrix-assisted laser desorption ionisation (MALDI), which is particularly suitable for producing intact gas-phase ions from large, non-volatile, and thermally sensitive molecules like proteins, oligonucleotides, and synthetic polymers. Among these, ESI and MALDI are the most widely used in biomolecular analysis. Specifically, ESI is the preferred ionisation technique for samples obtained from RP-LC separations. Since the analytical method developed in this thesis relies on ESI coupled with LC-MS/MS, a detailed explanation of its operating principles is reported below.

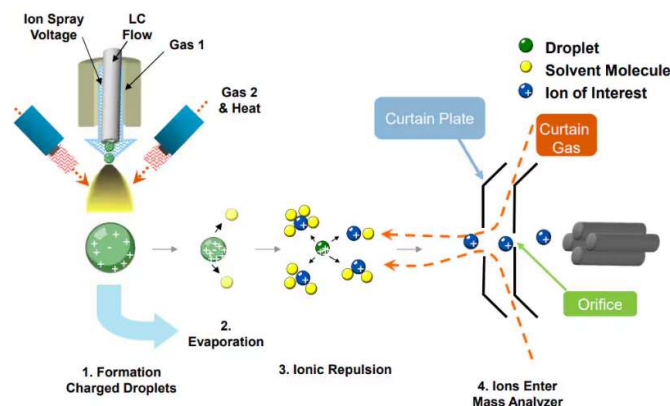


Figure 8, Schematic representation of an ESI source¹²⁰

For analysis in an ESI source (Figure 8), the analyte is first dissolved in a volatile MP containing a small proportion (typically 0.1–0.5% v/v) of an acid or weak base, which facilitates the ionization of the compound. The resulting solution is introduced into a stainless-steel capillary, known as the probe, through which a high voltage (2–5 kV) is applied between the capillary and a counter-electrode. Under these conditions, a nebulized cone-shaped spray, commonly referred to as the Taylor cone, forms at the tip of the capillary. This phenomenon occurs because the charged species within the solution are influenced by the electrostatic field generated between the probe and the counter-electrode.¹²¹ At the tip of the cone, charged droplets are generated and begin to move toward the counter-electrode. Their formation is influenced by several factors, including the physicochemical properties of the solvent, the concentration of analyte ions, the presence of inorganic salts, and the applied electric potential.

Once produced, the droplets gradually shrink in size as the solvent evaporates, though their overall electrical charge remains constant. The energy driving solvent evaporation originates both from the thermal environment, supported by a heated capillary, and from collisions with drying gases, specifically, the nebulizer gas (GS1), which moves along the capillary axis, and the heater gas (GS2), which flows from the sides.

As the droplets continue to lose solvent, their surface charge density increases until they reach the Rayleigh stability limit, a condition in which the electrostatic repulsion among the charges on the droplet surface equals the surface tension that holds it together¹²², resulting in droplet instability. Once this stability threshold is exceeded, the charged droplets become unstable and undergo a process known as Coulombic explosion¹²³, in which electrostatic repulsion causes the droplet to fragment into numerous smaller droplets. This cascade of fissions ultimately leads to the complete desolvation of ions, producing free gas-phase ions ready for analysis.

After ion generation in the source, the ions are directed toward the mass analyzer, where they are separated according to their m/z values under high-vacuum conditions (around 10^{-5} Torr). This vacuum prevents collisions with atmospheric gas molecules that could otherwise reduce ion transmission efficiency. At the entrance of the analyzer, two aligned conical steel plates, the curtain plate and the orifice plate, are positioned. A stream of curtain gas, typically nitrogen, flows between them to block neutral contaminants from entering the analyzer region. Different types of mass analyzers have been developed to separate ions based on their m/z ratio, each using a distinct operating principle. Some analyzers achieve separation spatially, while others do so temporally. For example, the time-of-flight (TOF) analyzer differentiates ions according to their velocities as they

traverse a field-free region, known as the flight tube. The quadrupole analyzer, instead, separates ions by exploiting the stability of their trajectories in oscillating electric fields. Another configuration, the ion trap analyzer, employs a radiofrequency (RF) quadrupolar field to confine ions in two or three dimensions, sequentially releasing them according to their mass-to-charge ratio to generate a spectrum. Likewise, a magnetic sector analyzer discriminates ions based on their momentum, given a defined magnetic field and circular path. Some advanced instruments combine multiple types of analysis to enhance resolution and analytical capability. In the context of ESI-based systems, the triple quadrupole analyzer is one of the most widely used configurations for quantitative MS/MS. It consists of three quadrupoles arranged in series: the first and third serve as mass filters, allowing only ions with selected m/z values to pass through, while the second functions as a collision cell, where controlled fragmentation of the selected ions occurs.

A quadrupole consists of four parallel metallic rods, with each opposing pair electrically connected (Figure 9).

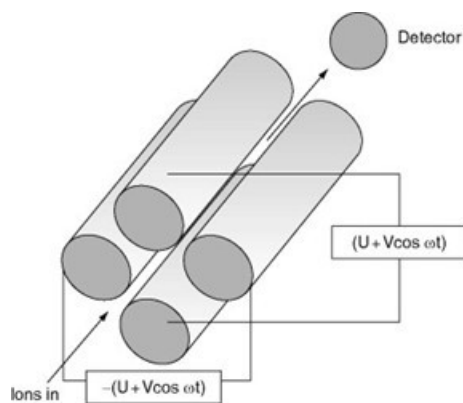


Figure 9. Graphic representation of a quadrupole analyzer.

Between adjacent rods, a combined voltage, comprising both a RF and a direct current (DC) component, is applied. When only the RF voltage is active, a broad range of ions with different m/z ratios can pass through the quadrupole, as the alternating field serves to focus the ion beam. However, to isolate ions of a specific m/z value, a DC potential is superimposed on the RF signal. Under these conditions, only ions with the selected m/z maintain stable trajectories through the quadrupole, while those with higher or lower m/z values become unstable and are deflected into the rods, resulting in their loss (Figure 10).

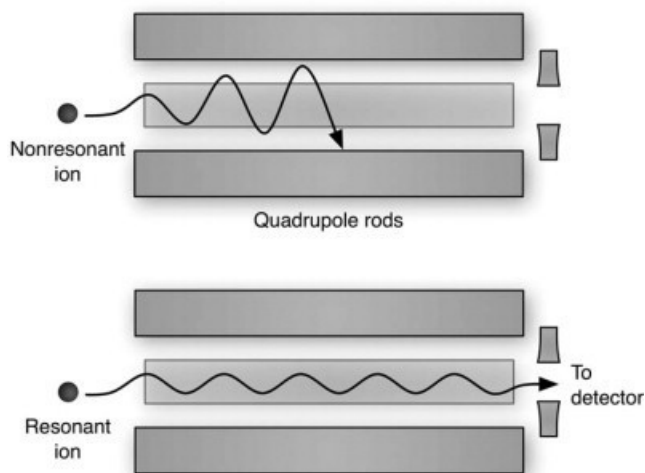


Figure 10, Representation of the operating principle of a quadrupole mass analyser.

Depending on the analytical objective, the first (Q1) and third (Q3) quadrupoles can operate in various modes to collect data. In MS/MS analysis, the instrument is configured to induce controlled fragmentation of the analyte, known as collision-induced dissociation (CID), within the second quadrupole (Q2), which serves as the collision cell. Positioned before Q1, there is an additional smaller quadrupole, referred to as Q0, which functions solely with an RF field (without DC) and is designed to focus and guide the ions efficiently into the mass filter. Through MS/MS analysis, it is possible to acquire information on both the mass of the analyte of interest (parent or precursor ion) and that of the fragments produced (product or daughter ions), which are generated by inducing fragmentation in Q2 using an appropriate collision energy. Generally, the m/z value of an analyte could be considered information about its identity yet, but, especially in the case of low-resolution MS, the highest specificity is obtained by also considering the analysis of its fragmentation pattern. In fact, for each substance, its fragmentation pattern is a sort of proper fingerprint.

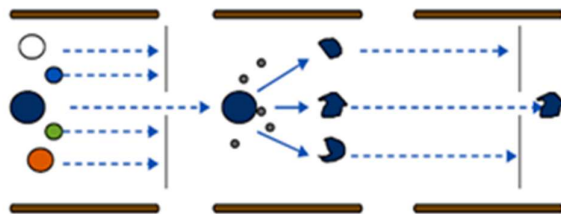


Figure 11, Schematic representation of the ion pathway during the select reaction monitoring mode.

The most common scanning mode for quantitative analysis is called selected reaction monitoring (SRM) (Figure 11); its application to more than one fragment ion is called multiple reaction monitoring (MRM), which consist in the following mechanism: Q1 act as

the first filter that selects the precursor ion of the analyte, which enters the Q2 where the presence of inert gas (argon or nitrogen) triggers the CID causing the precursor ion fragmentation and the creation of product ions, so the product ions exit from the Q2 and pass through the Q3 which act as the second filter that selects the product ions and sent them to the detector. In this way, a spectrum representing the fragmentation products of the selected ion is obtained. Thanks to the high specificity of this scanning mode, the analysis achieves an excellent signal-to-noise ratio (S/N), resulting in remarkable sensitivity. The coupling of MS/MS with LC has brought substantial advancements, enabling the analysis of samples across a wide range of concentrations. In particular, the enhanced sensitivity and selectivity provided by the SRM mode offer two major benefits:

- the ability to detect drugs and metabolites at extremely low concentration levels, thus requiring only minimal sample volumes;
- the capability to identify target analytes even within complex biological matrices, such as tissues or whole blood.

1.3.3 Validation of a LC-MS/MS method

To be used for the quantification of one or more substances in patients' biological samples, an LC-MS/MS method must be validated in accordance with the FDA¹²⁴ and EMA¹²⁵ guidelines for bioanalytical method validation. This process includes all the documented procedures required to demonstrate that the analytical method employed for the quantitative determination of the analyte in a specific biological matrix (e.g. plasma, serum, whole blood, or urine) is reliable, reproducible, and suitable for its intended purpose. Analytical determinations, regardless of the instrument used, must follow established scientific principles, and operators must adhere to standardized procedures to ensure that the results obtained are robust and trustworthy. The need for clear and harmonized validation standards emerged during the first AAPS/FDA Bioanalytical Workshop in 1990¹²⁶, which laid the foundation for the development of regulatory guidelines. These principles, resulting from collaboration between researchers and regulatory authorities, were first incorporated into Canadian health regulations in 1992, and subsequently, the FDA published its first Guidance on Bioanalytical Method Validation in May 2001. This document outlined the required workflow for validating analytical techniques such as GC, LC, GC-MS, LC-MS, ligand binding assays (LBA), immunoassays, and microbiological procedures. Following this, the discussion on method validation expanded internationally, and in 2011 the EMA released its own Guideline on Bioanalytical Method Validation in Europe. The most recent

updates of the bioanalytical method validation guidelines were published by the FDA in November 2022 and by the EMA in July 2022, reflecting current standards for ensuring reliable and reproducible analytical results. The validation of selective and sensitive analytical methods is fundamental for the successful execution of clinical and non-clinical pharmacological studies, as the quantitative determination of drugs, metabolites, and biomarkers provides crucial data to evaluate both safety and efficacy. In many phase I and II clinical trials, the measurement of analyte concentrations for PK analysis represents a primary or secondary objective; thus, the reliability and quality of analytical results are essential to ensure the scientific validity of the study outcomes¹²⁷. For a method to be considered validated, a detailed procedure must be established, clearly defining the instrumental conditions, materials, reagents, and the preparation of standards and samples. Preliminary experiments should also be performed to optimize the bioanalytical procedure and address all potential critical factors. Method validation can be classified as:

- complete, when all validation parameters are determined for a new method or when additional analytes are introduced into an existing one;
- partial, when minor modifications are applied to an already validated method (e.g. transfer to another laboratory, change of instrument, analytical range, sample matrix, or storage conditions);
- cross-validation, when comparing two or more bioanalytical methods used in the same study, or when results from different laboratories using the same method must be evaluated.

The key parameters for the validation of an LC-MS/MS analytical method include analyte recovery from the matrix, calibration curve linearity, sensitivity, precision, accuracy, selectivity, matrix effect, dilutional integrity, reproducibility, and analyte stability both in the biological matrix and in stock or working solutions.

The analytical method developed within this thesis was designed entirely from scratch; therefore, in compliance with EMA¹²⁵ and FDA¹²⁴ guidelines, a complete validation was carried out to ensure its robustness, reliability, and suitability for quantitative bioanalysis.

1.4 Precision study

The PRECISION study (Prostate cancer REsearch using Cross-validation of Innovative Sampling, Integrating LC-MS/MS for Optimized therapeutic drug monitoring study ID: CRO-2025-12) was conceived with the overarching goal of developing and validating innovative analytical strategies to optimize drug monitoring in patients with prostate cancer. The rationale behind the study lies in the increasing need for personalized therapeutic approaches, where treatment efficacy and safety can be maximized through accurate assessment of systemic drug exposure. Traditional PK evaluation, based on plasma sampling, is often limited by its invasiveness, logistical constraints, and the need for specialized handling; therefore, the PRECISION study explores the feasibility of alternative, less invasive, and more accessible sampling methods that can be integrated into routine clinical practice without compromising analytical accuracy. For the development of this study, dried blood spots (DBS) will be used as an alternative to conventional venous blood sampling, offering a minimally invasive and patient-friendly approach. This technique involves collecting small drops of capillary blood from a finger prick onto a specialized filter paper, where the samples are left to dry at room temperature and can then be stored and transported without refrigeration. Once dried, DBS samples provide stable conditions for analyte preservation, allowing reliable quantification of anticancer drugs through specific analytical methods. Sampling will be performed using the Capitainer®B10 device (formerly Capitainer®qDBS), which enables the collection of a precise and reproducible blood volume, enhancing sampling accuracy and supporting its application in remote TDM. The study has multiple specific aims. First, to compare the performance of novel sampling approaches with standard plasma-based methods in the quantification of selected anticancer agents (ABI, D4A, APA, N-desmethyl APA, DARO, keto-DARO, ENZA, N-desmethyl ENZA) using LC-MS/MS. Second, to assess the reproducibility, reliability, and potential clinical applicability of DBS matrixes for therapeutic monitoring. Third, to generate preliminary PK data in real-world patient populations, providing insights into inter- and intra-patient variability in drug exposure under steady-state conditions. Through these objectives, the study seeks to lay the groundwork for the future implementation of individualized dosing strategies supported by therapeutic drug monitoring in oncology.

As part of this project, we developed and fully validated a quantitative LC-MS/MS method in plasma, which currently serves as the reference analytical approach for drug quantification and PK evaluation. This plasma-based method was used as the comparator

for the assessment of alternative sampling techniques, (DBS) ensuring analytical robustness and clinical reliability.

Parallel to this, work is ongoing on the development of the analytical method DBS as a minimally invasive matrix. However, since the method is still under optimization and validation, no conclusive or relevant data are yet available to be included in this thesis.

2. AIMS

The main objective of this thesis was to develop, optimize, and analytically validate a new LC–MS/MS method for the simultaneous quantification of ABI, APA, DARO, ENZA, and their active metabolites in human plasma, within the framework of the PRECISION study. The goal was to explore the applicability of TDM to these second-generation hormonal agents, which represent key treatments for advanced prostate cancer.

Given the increasing clinical use of these oral agents and the growing evidence of substantial inter-patient variability in systemic exposure, the implementation of individualized dosing strategies based on TDM may represent a significant advancement toward precision pharmacotherapy in oncology.

This work focused on the development of a highly sensitive, selective, and reproducible LC–MS/MS method capable of accurately quantifying the selected drugs and metabolites in human plasma. Particular attention was devoted to ABI and its active metabolite, D4A, whose plasma concentrations are markedly lower compared to those of the other analytes, for which PK and pharmacodynamic data are already available in the literature. These data provide a valuable reference point for evaluating the analytical performance and potential clinical translation of the developed method.

Following the optimization of instrumental parameters, encompassing both chromatographic and mass spectrometric conditions, the method was fully validated in accordance with the current EMA and FDA bioanalytical guidelines. The validation process aimed to demonstrate the robustness, accuracy, precision, linearity, and stability of the method across clinically relevant concentration ranges, ensuring its suitability for quantitative applications in TDM.

Once validated, the method was applied to plasma samples obtained from prostate cancer patients enrolled in the PRECISION study. This step allowed the assessment of its applicability in a real clinical setting, providing preliminary PK data under steady-state conditions. The analysis of patient samples also offered an opportunity to explore inter-individual variability in systemic exposure, paving the way for future correlations between plasma concentrations, treatment efficacy, and safety outcomes.

Among the investigated compounds, ABI represents a particularly relevant model for TDM implementation since clear exposure–response relationships have already been established in the literature. Therefore, the method was evaluated against known PK thresholds to confirm its potential for dose optimization and personalized therapy management. For the other compounds, the present work provides a methodological foundation for future studies aimed at defining therapeutic reference ranges and evaluating exposure–response correlations.

Ultimately, this thesis demonstrate the integration of LC–MS/MS-based TDM into the clinical management of prostate cancer. The validated plasma method constitutes a reliable analytical platform and a reference tool for future development of alternative, minimally invasive matrices such as DBS, with the perspective of enabling decentralized and patient-friendly PK monitoring in oncology.

3. MATERIALS AND METHODS

3.1 LC-MS/MS method development of abiraterone, enzalutamide, darolutamide, apalutamide and their metabolites in human plasma

A bioanalytical method includes all the procedures necessary for the collection, storage, processing, and analysis of biological samples containing specific analytes of interest. In this thesis, the focus was on the quantitative determination of ABI, D4A, APA, N-desmethyl-APA, DARO, keto-DARO, ENZA, and N-desmethyl-ENZA in human plasma using an LC-MS/MS system.

The method development involved three main stages of instrumental optimization, all aimed at achieving the highest possible sensitivity and selectivity for these compounds:

Mass spectrometric optimization (see section 3.1.3) to maximize the signal-to-noise ratio (S/N) for each analyte.

Chromatographic optimization (see section 3.1.4) to obtain good separation, reduce potential interferences, and minimize matrix effects from endogenous plasma components such as salts and phospholipids.

Sample preparation optimization (see section 3.1.7), including the selection of an appropriate extraction method and the definition of calibration curve parameters, with the goal of achieving effective sample cleanup without overly complex or time-consuming procedures, while maintaining a calibration range suitable for accurate quantification.

The development of this method was particularly challenging, especially for ABI and its metabolite D4A, as their plasma concentrations are much lower than those of the other analytes. This required a significant reduction in the concentration range and ultimately led to the use of a more sensitive LC-MS/MS instrument to obtain detectable and reliable signals for these compounds.

3.1.1 Instrumentation

The LC-MS/MS analysis were performed using a Nexera LC-40 X3 composed by a SIL-40C X3 CL auto-sampler, three LC-40D X3 CL pumping modules, two DGU-405 CL degasser, a CBM-40 CL system controller and a CTO-40C CL column oven (Shimadzu Corporation, Tokyo, Japan). The LC system was coupled with a triple quadrupole mass spectrometer CITRINE 6500 QTrap, (SCIEX, Massachusetts, USA). The instrument was equipped with a Turbo Ion Spray source operating in positive ion mode. Data were processed using Analyst MD 1.7.3 and the chromatographic peaks were integrated with

MultiQuant MD 3.0.3 (SCIEX software package). Plasma separation from the whole blood samples was carried out with a 5810R centrifuge, while a 5427R bench-top centrifuge (Eppendorf, Hamburg, Germany) was adopted for the protein precipitation procedure. Analytical standard powders were weighted using a Mettler Toledo Delta Range XPE205 analytical balance (Columbus, Ohio, USA). Stock solutions (SS), working solutions (WS) and biological samples were handled exploiting a Pipetman L set (composed by P1000, P200, P100, P20, P10 and P2) and a Microman E set (composed by M1000, M100, M50, M25 and M10) of pipettes and tips, both purchased from Gilson (Villiers-le-Bel, France). Moreover, solutions and samples were prepared in Eppendorf polypropylene conical tubes (50 and 15 mL), in Eppendorf polypropylene safe-lock tubes (5, 2 and 1.5 mL) and in laboratory glassware (beakers, volumetric flasks, graduated cylinders etc) supplied by SciLabware (Stoke-on-Trent, UK), while for their high-speed mixing was adopted a Vortex-Genie 2 (Scientific Industries Inc., New York, USA). During the analysis, samples were kept in autosampler polypropylene vials with polytetrafluoroethylene (PTFE) caps, purchased from Agilent Technologies (Santa Clara, California, USA).

3.1.2 Standard and chemicals

The analytical reference standard of abiraterone (batch SVI-ALS-15-281, chemical purity 99,8%), apalutamide (batch SVI-ALS-18-075, chemical purity 97.3%), enzalutamide (batch SVI-ALS-17-214, chemical purity 99.7%), darolutamide (batch SVI-ALS-22-061, chemical purity 96,0%), N-desmethyl apalutamide (batch SVI-ALS-24-183, chemical purity 99%), desmethyl enzalutamide (batch MKU-ALS-25-007-P4, chemical purity 99%), keto darolutamide (batch JA-ALS-24-161-P6, chemical purity 96%), abiraterone-d7 (batch ES-ALS-16-204-P1, chemical purity 99%, isotopic purity) used as internal standard, apalutamide-13C-D3 (batch MJ-ALS-20-021-P1, chemical purity 99%) used as internal standard, darolutamide-d4 (batch NW-ALS-22-043-P1, chemical purity 99%) used as internal standard, enzalutamide-d6 (batch TM-ALS-13-028-P1, chemical purity 96.8%) used as internal standard, were supplied by Alsachim (Illkirch Graffenstaden, France). The analytical reference standard of abiraterone $\Delta 4$ metabolite (batch 0000132707, chemical purity 98%) was purchased from Sigma-Aldrich (Saint Louis, MO, USA). For the stock solution used for the quality controls the analytical reference standard of abiraterone (batch 114925, chemical purity 99,2%), apalutamide (batch 148628, chemical purity 99.9%), enzalutamide (batch 232304, chemical purity 100%), darolutamide (batch 150006, chemical purity 97,4%), N-desmethyl apalutamide (batch 154154, chemical purity 97,8%),

N-desmethyl enzalutamide (batch 146716, chemical purity 100%), ORM-15341 (batch 149327, chemical purity 98%) and abiraterone D4 metabolite (batch 247351, chemical purity 99.8%) were supplied by TargetMol (Boston, MA, USA). LC-MS grade methanol (MeOH), LC-MS grade acetonitrile (ACN) were provided by Carlo Erba Reagents (Cornaredo, Milano, Italy); formic acid (HCOOH) and HPLC grade dimethyl sulfoxide (DMSO) were supplied by Sigma-Aldrich (Saint Louis, MO, USA). 'Type 1' ultrapure water was obtained in-house through a Milli-Q IQ 7000 system from Merck (Milan, Italy). Control human plasma/K₂EDTA from healthy volunteers was provided by the Transfusion Unit of the National Cancer Institute of Aviano (CRO Aviano, PN, Italy). Pooled plasma was made by mixing the plasma of 16 healthy donors (8 males and 8 females) to prepare daily standard calibration curves and quality control samples. This reduces variability bias between different matrices. Plasma samples from individual donors were used for the selectivity test and matrix effect (see section 3.5.2).

3.1.3 Mass spectrometric conditions optimisation

Maximizing the signal-to-noise ratio (S/N) and sensitivity for the target compounds requires careful adjustment of two categories of parameters:

- Compound-dependent parameters, which are individually optimised for each analyte according to its ionization properties and fragmentation profile;
- Source-dependent parameters, which are influenced by factors such as the composition of the mobile phase and the applied flow rate.

3.1.3.1 Compound-dependent parameters optimisation

For the optimisation of compound-dependent parameters, individual solutions were prepared for each analyte. The solvent consisted of 50% H₂O and 50% MeCN with 0.1% HCOOH, in order to closely reproduce the conditions of the actual analysis. All solutions were prepared starting from the stock solution. A defined amount was first diluted to obtain an intermediate solution at 5000 ng/mL, which was then further diluted to 50 ng/mL using the solvent mixture described above. Through a syringe pump, each solution was directly infused to the TIS source at a flow rate of 10 μ L/min and, for each analyte, the following procedure was performed.

Declustering Potential (DP)	A parameter that controls the potential difference between Q0 and the orifice plate. It is used to minimise the cluster formation due to aggregation between ions and solvent droplets.
Entrance Potential (EP)	A parameter that controls the potential which guides and focuses ions through the high-pressure Q0 region.
Collision Energy (CE)	A parameter that controls the potential difference between Q0 and Q2, which represents the amount of energy that the precursor ion receives once accelerated into Q2, where it collides with the gas molecules and is fragmented.
Collision Cell Exit Potential (CXP)	A parameter that controls the potential which focuses and accelerates ions exiting Q2. It is the potential difference between Q2 and ST3 (a lens that separates Q2 and Q3).

Table 2, Definitions of each compound-dependent parameter.

With the HPLC disabled, the spectrometer configured in manual tuning mode and all source-dependent parameters set to default values, the first step consisted in the analyte presence confirmation by the identification of its pseudo-molecular ion $[M+H]^+$ knowing its monoisotopic mass M . To do that, a Q1 scan (Q1MS) in positive ion mode was performed: it worked as a single quadrupole scan because no energy was applied to Q2 which, together with Q3, worked in RF only and focused the positive ions from Q1 to the detector without filtering them. (Figure 12)

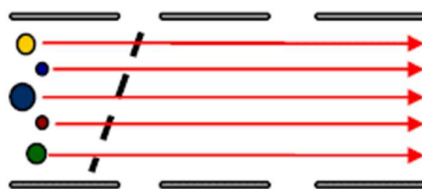


Figure 12, Schematic representation of the triple quadrupole analyzer in Q1MS configuration.

The scan was performed in an adequate range of m/z . In order to obtain an adequate number of duty cycles, the scan time was chosen adopting the following rule:

$$10 \text{ ms} \times \Delta_{\text{amu}}$$

where Δ_{amu} represents the range of m/z values analyzed. After the total ion current (TIC) stabilization, a spectrum was recorded activating the multiple count acquisition (MCA) mode, which summed all the events detected thus increasing the S/N and allowing a more

accurate read of the m/z value of the pseudo-molecular ion. For the consequent optimisation of the DP and EP parameters, the spectrometer was set in Q1 multiple ions mode (Q1MI), meaning that Q1 did not perform a scan anymore, but worked in selected ion monitoring (SIM) by selecting a specific m/z value (i.e. the one of the pseudo-molecular ions found in the previous test) while Q2 and Q3 worked in RF only. (Figure 13)



Figure 13, Schematic representation of the triple quadrupole analyzer in Q1MI configuration.

By ramping the DP from 0 to 250 V, the intensity trend of the extracted ion current (XIC) was monitored to choose the most correct DP value for the pseudo-molecular ion. Generally, the signal intensity in line with the DP increase has a trend similar to a Gaussian curve and the optimal DP value is the one at the apex of the curve. This because too low DP values will result in lower ion intensity due to interferences from clusters, while too high values might cause an in-source fragmentation. The optimal EP value (in a range of 1-15 V) was determined in the same way, even if it is often left at 10 V (i.e. the default value) without any impact on analyte detection limit because EP has a minor effect in compound optimisation. While the abovementioned experiments had been done in a single quadrupole configuration (only Q1 was working, while Q2 and Q3 were only focusing ions), to define the remaining compound-dependent parameters (i.e. CE and CXP), all the three quadrupoles were exploited in an MS/MS configuration. First, an analysis of the fragmentation pattern was carried out for each compound. The spectrometer was set in product ion mode (MS2), that means that Q1 filtered only the pseudo-molecular ions (also called precursor ions, in this kind of experiment), which were fragmented in Q2 and a scan of all fragments (also called product ions) was performed by Q3. (Figure 14)

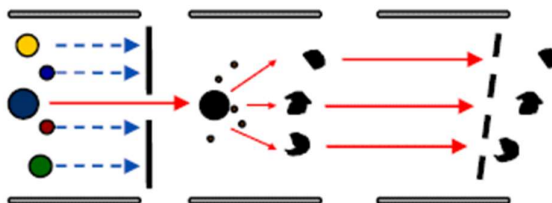


Figure 14, Schematic representation of the triple quadrupole analyzer in MS2 configuration.

Several spectra were recorded with different CE values (5, 10, 20, 30, 40, 50, 60 and 70 eV) activating the MCA mode and adopting the correct DP and EP values for the analyzed compound. The m/z range explored was 100-500 for all the three analytes because fragments lower than 100 are not informative. In this way, for each analyte, a first evaluation of the most representative fragments was carried out. Once the main fragments had been selected, the optimal CE value was simultaneously determined for each of them by setting the spectrometer in MRM mode. In this configuration, Q1 behave as a filter by selecting a precise precursor ion, which is fragmented in Q2 and, from the resultant product ions, a further selection is performed in Q3, which behave as a second filter. (Figure 15)

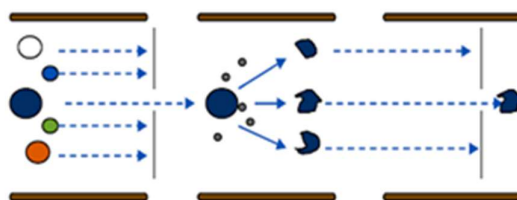


Figure 15, Schematic representation of the triple quadrupole analyzer in MRM configuration.

Depending on the number of transitions (fragmentation reactions from precursor to product ion), the dwell time was selected, and a spectrum was recorded by increasing the CE value during the time from 5 to 130 V. The resulting spectrum showed the XIC intensity for each transition in line with the rise of the CE values. The transition with the highest signal intensity was selected as the most suitable for the quantification, while the other two had the function of “qualifiers” to increase the specificity for the analyte of interest. The optimal CE value for each transition is the one at the apex of the XIC signal curve. A similar experiment was carried out by ramping the CXP value, while the CE was set at its optimum value for each transition. Once the correct values for all the compound-dependent parameter had been obtained, a complete MRM method for the simultaneous quantification of ABI, D4A, APA, N-desmethyl APA, DARO, keto-DARO, ENZA and N-desmethyl ENZA was built up.

3.1.3.2 Source-dependent parameters optimisation

Source-dependent parameters (Table 3) can be optimized using a single analyte, as they are common to all compounds analyzed within the same assay. In this method, tuning was initially carried out with the ABI solution and subsequently verified with the D4A solution, since both proved to be the most critical analytes in terms of signal intensity due to their

concentration range. First, a solution of ABI was prepared in a solvent mixture consisting of 50% MeCN and 50% H₂O with 0.1% HCOOH, at a concentration of 100 ng/mL. This solution was directly infused into the TIS source at a flow rate of 10 μ L/min, together with the mobile phase (MP) delivered by the HPLC pumps.

Curtain gas (CUR)	A parameter that controls the pressure of the curtain gas, which flows between the curtain plate and the orifice preventing the contamination of the ion optics by minimizing the entrance of solvent droplets.
CAD gas (CAD)	A parameter that controls the pressure of collision gas in Q2, which in MS/MS experiments has the function of fragment the precursor ions.
IonSpray Voltage (IS)	A parameter that controls the voltage applied to the needle that ionizes the sample, thus influencing the spray stability.
Temperature (TEM)	A parameter that controls the temperature of the turbo gas.
Gas 1 (GS1)	A parameter that controls the pressure of the nebulizer gas, which has the function of helping to generate small droplets of sample flow.
Gas 2 (GS2)	A parameter that controls the pressure of the turbo gas which has the function of helping the evaporation of the spray droplets and avoiding solvent entrance into the analyzer.

Table 3, Definitions of each source-dependent parameter.

The mobile phase composition was 50:50 (v/v) between A (MPA: H₂O with 0.1% HCOOH) and B (MPB: MeCN with 0.1% HCOOH), at a flow rate of 0.200 mL/min. The mixing with the ABI solution was achieved through a tee union, while another union was used to replace the chromatographic column, which was not required for this setup (Figure 16).

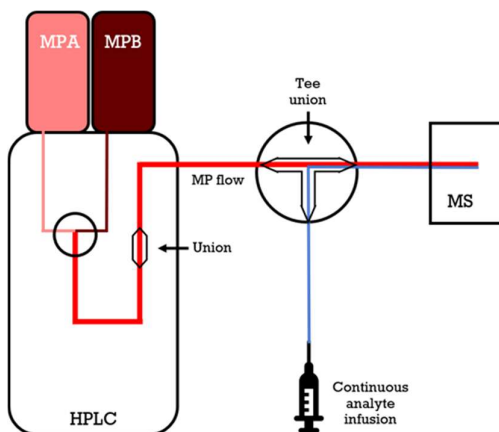


Figure 16, Schematic representation of the instrumental set up for the optimization of the source dependent parameters.

This configuration was designed to reproduce the actual operating conditions of the LC–MS/MS system.

With the LC enabled, the spectrometer configured in manual tuning mode and all the sourcedependent parameters set to default values (i.e. CUR= 10 psi, CAD= medium, IS= -4500 V, TEM= 0 °C, GS1= 10 psi and GS2= 0 psi), the first step consisted in a SRM experiment with all the compound-dependent parameters set at the optimal value to analyze the quantifier transition of ABI. In this way a XIC signal was obtained and, once stabilized, it was constant in intensity. By manually varying each source-dependent parameter, an increase or decrease in XIC intensity was observed. The goal of this optimisation was to reach the maximum signal intensity in order to achieve the greatest sensitivity for the quantification method. Once all the source-dependent parameters had been obtained with ABI, the same procedure was repeated with D4A: a 100 ng/mL solution of the analyte was directly infused to the TIS source, monitoring the signal intensity of its quantifier transition while each source parameter was manually tuned.

3.1.4 Chromatographic conditions optimisation

Developing the reversed-phase (RP) chromatographic method involved identifying the optimal conditions for effectively separating all analytes.

The first consideration was the selection of the analytical column, depending on the physicochemical characteristics of the analytes (i.e. the type of stationary phase), the number of compounds to be quantified (i.e. the column length) and the required level of resolution (i.e. the particle size). The use of a pre-column was also considered, taking into account the complexity of the biological matrix.

Once the stationary phase had been defined, attention turned to other critical parameters, such as column temperature, flow rate and the composition of the mobile phase. The temperature and flow rate were adjusted according to the properties of the mobile phase, as highly viscous solvents can generate excessive backpressure within the chromatographic system. This issue can be mitigated by reducing the flow rate or slightly increasing the column temperature, as this decreases solvent viscosity. Elevated temperatures within the stability limits of the stationary phase also promote better chromatographic resolution by enhancing the exchange kinetics of analytes between the stationary and mobile phases.

Method evaluation was based on peak symmetry, retention time consistency, carryover levels, and signal stability.

The most challenging and time-consuming part of the optimisation process was defining the chromatographic elution strategy, beginning with deciding between a fully isocratic approach and a multi-step gradient approach (Figure 17).

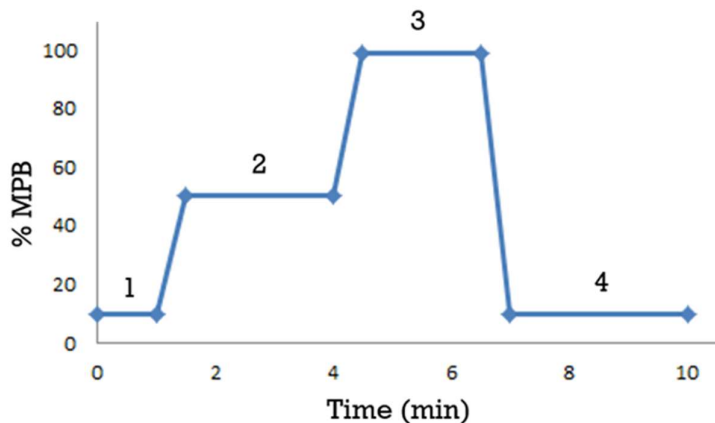


Figure 17, Schematic representation of a multi-step chromatographic method.

While in the former, the MP composition remains unchanged during the whole chromatographic run, in the latter the MPA/MPB ratio changes over time, ideally following a pattern like the one represented in figure 21 and described below:

- conditioning phase of the column characterised by a low percentage of MPB which helps the correct packing of the analytes at the head of the column. The initial conditions of the chromatographic run determine the environment encountered by the sample after its injection into the column. In an RP chromatography run, where analytes are eluted in increasing order of affinity for the organic phase, if the initial amount of MPB is too high, it could interfere with the interaction between the analytes and the functional groups on the column particles. This can lead, for example, to an undesired peak-split of the analyte. During the optimization, various percentages of MPB were tested and the possibility to omit this step to save time was considered too. The evaluation criteria were peak shape and the degree of separation between analytes.
- Elution phase of the analytes, which might follow an isocratic or a gradient regime. During the optimization, the choice between the two regimes was evaluated, by exploring both different slopes for the gradient approach and different percentages of MPB for the isocratic one; The evaluation criteria were peak shape, retention time and the degree of separation.
- Washing phase, in which the more lipophilic interferents in the matrix (e.g. phospholipids, peptide residuals, etc.) still bound to the SP, elute from the column

thanks to a high percentage of MPB. An adequate washing phase is important to lengthen the life of the column, so during the optimization, different durations of this step were considered by simultaneously monitoring three of the most abundant phospholipids (PLs) in human plasma: phosphatidyl choline (PC), lysophosphatidyl choline (LPC) and lysophosphatidyl ethanolamine (LPE). The goal was considered achieved when the elution of all three PLs occurred before the last step and in a reproducible manner during various chromatographic runs.

- Reconditioning phase of the column, in which the MP composition returns to the initial condition. The length of this last step depends on the MP flowrate and the column volume because the column is considered reconditioned only after 10-20 column volumes of MP. Failure to recondition can lead to alterations in retention times and therefore to the lack of reproducibility of repeated runs. In fact, if the analytes at the time of the injection were in a different condition compared to that present at T0, they could behave differently. During the optimization, the reconditioning conditions are kept fixed until the retention times of all the compounds remain constant after 3 consecutive runs.

By working on all these aspects, the purpose was to obtain a chromatographic method with the following features:

- an adequate degree of separation between all the analytes and the three metabolites.
- narrow chromatographic peaks with a good symmetry (nor tailing neither fronting phenomena were accepted) for all the compounds.
- reproducibility of consecutive analysis.
- good control over the carryover phenomenon.
- minimum analysis time.

For all the optimization steps, plasma samples containing all analytes and their metabolites were prepared at concentrations corresponding to point H of the calibration curve. In addition, different sample injection volumes (1, 2, 5 and 10 μL) to be introduced into the LC-MS/MS system were tested.

3.1.5 Calibration curve and quality controls preparation

In order to perform quantitative measurements, it is necessary to calibrate the instrument using a series of samples with known scalar concentrations, establishing the relationship between the detected signal and the analyte concentration. These samples are called calibrators. They must be prepared using the same matrix type as the real samples for which

the quantification method is designed. From measuring the signal intensities of these calibrators, a curve known as the calibration curve is identified. This curve is characterised by a linear trend if there is a direct proportionality between the analyte concentration and its signal. The Calibration curves should cover the expected drug concentration range of the patients' samples, ensuring the developed assay is fit for purpose. The calibration curve was generated using least-squares linear regression, which allows finding the line that minimises the sum of the squares of the distances between the experimental points and the extrapolated ones. Furthermore, a weighting factor of $1/x^2$ has been applied. This is particularly important when dealing with large calibration curves, such as that applied in the present method, which is characterised by a standard deviation of instrument responses that varies according to analyte concentrations¹²⁸. The weighting factor gives more importance to data points with low variance, and less weight to those with high variance. Therefore, it balances the regression line, generating an evenly distributed error throughout the calibration range. According to FDA¹²⁴ and EMA¹²⁵ guidelines, a calibration curve should include at least six calibrators, including the LLoQ. For the method discussed in this thesis, a nine-point calibration curve was used in order to cover all the drugs range that are very different. Each calibrator was indicated with a letter of the alphabet, from I, which corresponded to the LLoQ, to A, which corresponded to the ULoQ.

Quality controls (QCs) are samples designed to mimic the study samples. They are prepared from the same matrix as the real samples by spiking human plasma with a known amount of analyte. As their name suggests, they are used to ensure the quality of the analysis and the accuracy of quantification. In addition, these samples are employed to assess analyte stability under various stress conditions (e.g., freeze–thaw cycles or storage at room temperature). In each run, three replicates of low (QCL), medium (QCM) and high (QCH) concentration QCs were analyzed. The replicates are homogeneously distributed during the analytic run, in order to perform their function towards the entire series of the analyzed samples. As established by EMA guidelines, QCL represents the low concentration, which should be within three times the LLOQ; QCM corresponds to the medium concentration, falling in the middle of the linear range; and QCH indicates the high concentration, close to 75–85% of the ULOQ. All the concentrations must be different from the calibrators. QCs can be purchased or, like in this thesis method, self-prepared from different stock solutions.

As mentioned earlier, two separate stock solutions were prepared for ABI, D4A, APA, N-desmethyl APA, DARO, keto-DARO, ENZA, and N-desmethyl ENZA, at different

concentrations (Table 4): in DMSO for ABI and ENZA and their metabolites, and in MeOH for all the others.

	C (ng/mL) Stock calibrators	C (ng/mL) Stock QCs
ABI	101796	99993,6
D4A	95745	107730
APA	2915108	2943054
N-desmethyl APA	1580800	1916880
DARO	3029760	3011608
keto-DARO	1619520	2208920
ENZA	3010940	3550000
N-desmethyl ENZA	1855464	1631092

Table 4, Different concentrations of all the analytes used for both calibrators and QCs

By mixing appropriate amounts of the stock solutions for the calibrators and diluting the mixtures with MeOH, nine working solutions (WSs) were prepared with the following concentrations: 2, 20, 50, 200, 350, 500, 650, 850, and 1000 ng/mL for ABI and D4A; 400, 4000, 10000, 40000, 70000, 100000, 130000, 170000, and 200000 ng/mL for APA, N-desmethyl APA, DARO, and keto-DARO; and 800, 8000, 20000, 80000, 140,000, 200000, 260000, 340000, and 400000 ng/mL for ENZA and N-desmethyl ENZA.

For the QC set, the corresponding stock solutions were mixed and diluted with MeOH to obtain three WSs for QC preparation, with the following concentrations: 5, 375, and 750 ng/mL for ABI and D4A; 1005, 75000, and 150000 ng/mL for APA, N-desmethyl APA, and DARO; 1200, 84000, and 160000 ng/mL for keto-DARO; and 2010, 150000, and 300000 ng/mL for ENZA and N-desmethyl ENZA. All solutions were stored in polypropylene tubes at -80 °C. Each calibrator and QC was prepared by adding 5 μ L of the corresponding WS (with the concentration reported in table) to 95 μ L of pooled plasma in a 1.5 mL polypropylene tube.

Then, 500 μ L of IS WS (a MeCN solution containing 100 ng/mL of all internal standards, see section 3.1.6) were added to the tube for protein precipitation (Figure 18). The samples were centrifuged at 16,200 rcf for 10 minutes at 4 °C, and 200 μ L of the resulting supernatant were transferred into polypropylene vials for analysis.

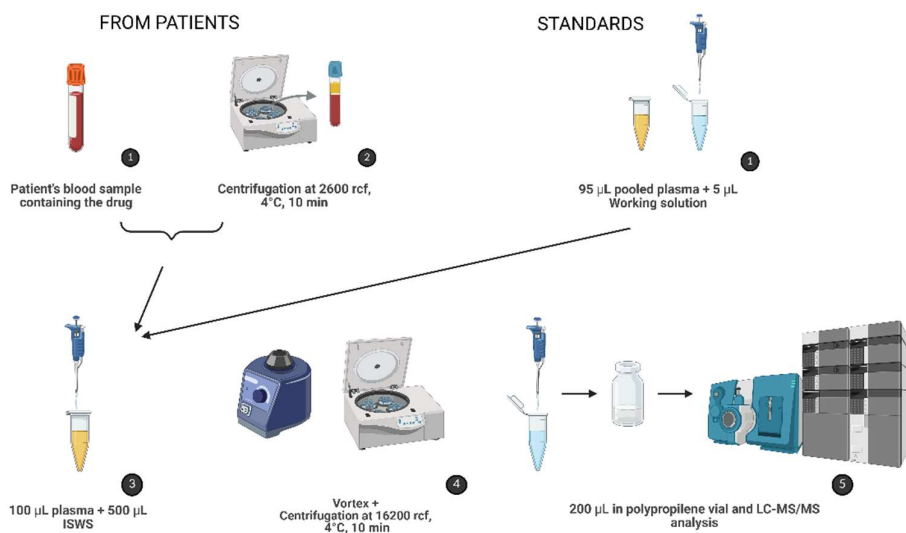


Figure 18, Schematic representation of calibrators, QCs (standards), and patient samples preparation

WS	ABI (ng/mL)	D4A (ng/mL)	APA (ng/mL)	N-desmethyl APA (ng/mL)	DARO (ng/mL)	keto-DARO (ng/mL)	ENZA (ng/mL)	N-desmethyl ENZA (ng/mL)
I	2	2	400	400	400	400	800	800
H	20	20	4000	4000	4000	4000	8000	8000
G	50	50	10000	10000	10000	10000	20000	20000
F	200	200	40000	40000	40000	40000	80000	80000
E	350	350	70000	70000	70000	70000	140000	140000
D	500	500	100000	100000	100000	100000	200000	200000
C	650	650	130000	130000	130000	130000	260000	260000
B	850	850	170000	170000	170000	170000	340000	340000
A	1000	1000	200000	200000	200000	200000	400000	400000
QCL	5	5	1005	1005	1005	1160	2010	2010
QCM	375	375	75000	75000	75000	86000	150000	150000
QCH	750	750	150000	150000	150000	172000	300000	300000

Table 5, concentrations of the WSs

3.1.6 Internal Standard

In this thesis, quantification was performed using the internal standard (IS) approach. During sample preparation, a fixed amount of an additional compound, the internal

standard, was added into every sample (including calibrators, quality controls, and study samples). Quantification was then based on the ratio between the peak areas of the analyte and the IS. For the method to be effective, the IS should share physicochemical properties similar to those of the target analyte, so that any variations arising from sample handling affect both compounds in a comparable way, allowing the analyte signal to be normalized. The use of an IS helps correct for fluctuations in extraction efficiency, injection volume, and ionization, thereby improving the robustness and reliability of the results. Stable isotope-labelled (SIL) analogs of the analyte (e.g., compounds labelled with deuterium or ^{13}C) are considered the gold standard as internal standards for LC-MS/MS analysis. They closely mimic the chromatographic behaviour of the target analyte but can still be clearly differentiated due to their distinct m/z values. Since the analyte and its SIL counterpart co-elute during the chromatographic run, both are equally affected by matrix effects, which significantly reduces their influence on quantification. In this thesis, the analytes and their active metabolites share the same IS, as described in the table.

[$^2\text{H}_7$]-Abiraterone	ABI
	D4A
[$^{13}\text{C}, ^2\text{H}_3$]-Apalutamide	APA
	N-desmethyl APA
[$^2\text{H}_4$]-Darolutamide	DARO
	keto-DARO
[$^2\text{H}_6$]-Enzalutamide	ENZA
	N-desmethyl ENZA

Table 6, Internal standards used for each corresponding analyte.

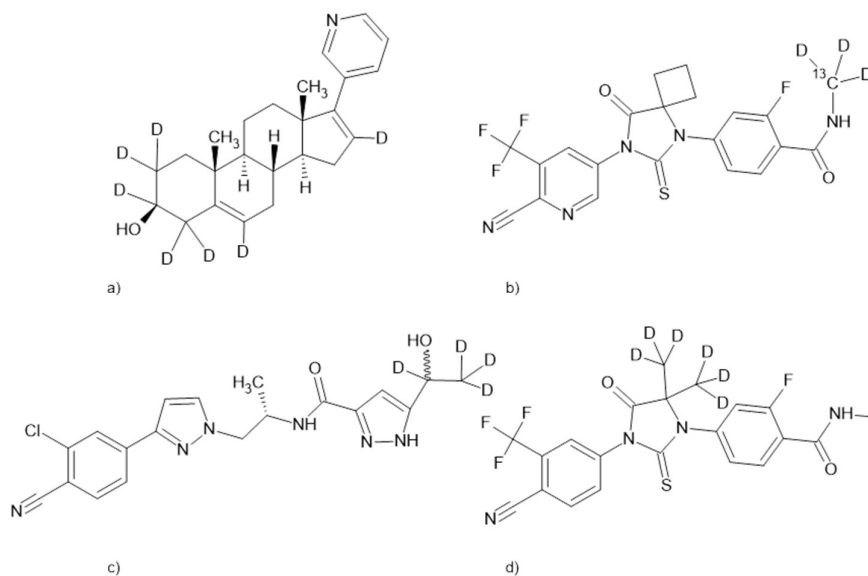


Figure 19, Molecular structures of the internal standards: a) [$^2\text{H}_7$]-Abiraterone, b) [$^{13}\text{C}, ^2\text{H}_3$]-Apalutamide, c) [$^2\text{H}_4$]-Darolutamide, and d) [$^2\text{H}_6$]-Enzalutamide.

in order to apply the internal standard method for the analytes quantification, a set of stock solutions for [²H₇]-Abiraterone, [¹³C,²H₃]-Apalutamide, [²H₄]-Darolutamide and [²H₆]-ENZA were prepared in DMSO at a concentration of 0.1mg/mL. By mixing appropriate amounts of the stock solutions and diluting the mixtures with ACN (in order to guarantee PP) the IS WS was obtained at a concentration of 100ng/mL. All the stock solutions were kept in polypropylene tubes and stored at -80 °C. Moreover, 50 mL aliquots of the IS WS were kept in 50 mL polypropylene conical tubes and stored at -20 °C.

3.1.7 Sample preparation

3.1.7.1 Sample extraction optimisation

Biological matrices are highly complex and contain endogenous components such as proteins and lipids, which may interfere with the detection and quantification of analytes. Optimising sample preparation is crucial, since these components can damage the chromatographic column and the spectrometric source. In addition, they may interfere with ionization, leading to matrix effects (3.2.2), which represents one of the major concerns during quantitative analysis. So, it is important to remove the interfering factors while simultaneously solubilizing the analytes in a suitable solvent for ionization. Several extraction methods are available. The most commonly used techniques are solid-phase extraction (SPE), liquid-liquid extraction (LLE) with immiscible solvents, and protein precipitation (PP) with organic solvents miscible in water. The less time-consuming and simplest technique for extraction from human plasma is PP. More specifically, when organic solvents miscible with water are added to an aqueous sample such as plasma, they displace water molecules from the protein surface. This displacement causes desolvation, which disrupts the weak interactions stabilizing the tertiary structure. As a result, proteins undergo aggregation driven by electrostatic and dipole–dipole interactions, ultimately leading to their precipitation. This extraction method matches with our analytes because the plasma protein binding is 99,8% for ABI³⁸, 96% for APA⁵⁵, 92% for DARO⁷¹, and 97-98% for ENZA⁸¹ in human plasma. The most common PP solvents are MeOH and MeCN, added in volumes at least three times greater than the sample.¹²⁹ To select the solvent to be used and determine the appropriate volume, tests were carried out using a plasma sample containing all the analytes at the concentration values of the corresponding LLOQ and ULOQ. Particular attention had to be paid to dilutions, since the ABI calibrators reach very low concentrations, while at the same time the signals of ENZA and APA risked saturating

MATERIALS AND METHODS

the instrument. Samples were extracted with both MeCN and MeOH, and several sample:solvent ratios (1:3, 1:4, 1:5) were tested, along with dilutions in MPA (1:4, 1:5, 1:6, 1:8, and 1:12) and different injection volumes (2, 3, 5, and 10 μL). After extraction with the solvent, samples were centrifuged at 16,200 rcf for 10 minutes at 4 °C, and the resulting supernatant was collected in polypropylene vials.

3.2 LC-MS/MS validation study

The analytical method object of this thesis project was developed from scratch and therefore, after its optimisation, a complete validation study was performed according to the FDA¹²⁴ and ICH¹²⁵ guidelines for the validation of a bioanalytical method. In particular, the validation was carried out by evaluating the following parameters: recovery of the analyte from the matrix, linearity of the calibration curve, intra-day and inter-day precision and accuracy, selectivity, matrix effect, dilution integrity, reproducibility and stability of the analyte in samples and solutions.

3.2.1 Selectivity

The selectivity identifies the ability of the assay to differentiate and quantify both the analyte of interest and the IS in presence of other interferents such as matrix components, metabolites, decomposition products or other drugs administered concurrently. To investigate the selectivity of the proposed bioanalytical method, six blank samples obtained by six individual sources of human plasma (i.e. from six different healthy donors) were analysed. The samples analysed should be free of interference at the retention times of the analytes and the ISs: the absence of interference was defined as a signal intensity $\leq 20\%$ of the LLoQ for the analytes and $\leq 5\%$ of the IS response in the LLOQ sample.

3.2.2 Matrix effect

The presence of endogenous substances within biological matrices can influence the ionization efficiency of both the analyte and its internal standard, a phenomenon known as the matrix effect. In an ESI source, the analyte in the liquid phase is transformed into gas-phase ions through processes of charging and desolvation before entering the mass analyzer. When endogenous compounds co-elute with the target analyte, they may interfere with these processes, leading to variations in ionization efficiency that manifest as either ion suppression or ion enhancement. Typically, matrix effects arise from endogenous components such as salts, amines, and phospholipids present in biological samples. However, exogenous contaminants, including certain plasticizers leached from containers or additives like anticoagulants, can also contribute to ionization disturbances. Negative impacts on the precision, accuracy, sensitivity and selectivity of an analytical method can

be caused by both ion suppression and ion enhancement, affecting the overall reliability of the generated data. For this reason, both the FDA and EMA strongly recommend evaluating matrix effects. According to their guidelines, this assessment should use plasma samples obtained from at least six individual donors to evaluate potential variability among different biological matrices, which could otherwise compromise the method's reproducibility. In this thesis, the matrix effect was evaluated using three replicates each of QCL and QCH prepared in six different plasma matrices, plus one additional haemolysed matrix. All plasma samples were obtained from male donors only, as the developed method is intended for drugs used in the treatment of prostate cancer. For each value obtained from every matrix, accuracy was required to be within $\pm 15\%$, and the coefficient of variation (CV%) had to be below 15%.

3.2.3 Recovery

The extraction recovery from a complex biological matrix is a crucial parameter for evaluating the efficiency of the sample preparation process. For each analyte the percentage recovery was determined at two quality control levels (QCL and QCH), prepared in triplicate using pooled human plasma.

Recovery was calculated by comparing the instrument response of two sets of samples with identical nominal concentrations but prepared through different workflows. In the first set, plasma samples from six different male donors, were spiked with the appropriate working solution (WS) before protein precipitation (PP), following the standard analytical procedure (see Section 3.1.5). In the second set, plasma was spiked after the PP step, representing a theoretical 100% recovery condition.

The percentage recovery (%REC) for each analyte and QC level was calculated.

$$\%REC = \frac{\text{analyte peak area (in matrix)}}{\text{mean analyte peak area (in extracted matrix)}} \times 100$$

Although recoveries do not necessarily need to reach 100%, they should be reproducible and consistent across the different concentration levels (QCL and QCH), ensuring the reliability of the extraction process.

3.2.4 Calibration curve and range

The calibration curve was established to define the relationship between the nominal concentration of each analyte and the corresponding analytical response obtained from the LC-MS/MS system. Calibration standards were prepared by spiking pooled-plasma with the Ws in order to achieve the target concentration, covering the entire expected concentration range. The calibration range was defined by the lower limit of quantification (LLOQ), representing the lowest standard with acceptable precision and accuracy, and the upper limit of quantification (ULOQ), corresponding to the highest standard within the validated range.

Each calibration curve included a blank sample (without analyte and IS), a zero sample (blank sample spiked only with the internal standard), and nine calibration levels, ranging from the LLOQ to the ULOQ. The calibration standards were analyzed in each analytical run to ensure the reliability of the quantification process.

A least-squares linear regression model was applied to describe the concentration-response relationship, using a weighting factor of $1/x^2$ to account for signal variability across the calibration range. Blank and zero samples were excluded from the regression analysis. The curve parameters (slope, intercept, and correlation coefficient) were recorded for each run.

The accuracy was required to be within $\pm 20\%$ of the nominal value at the LLOQ and within $\pm 15\%$ at all other levels. At least 75% of the calibration standards had to meet these acceptance criteria for the curve to be considered valid.

3.2.5 Accuracy and precision

Intra- and inter-day precision refer to the degree of variability observed among a series of repeated measurements, whereas intra- and inter-day accuracy indicate how close the measured mean value is to the true or nominal concentration. The precision of the analytical method was expressed as the coefficient of variation (CV%), calculated by dividing the standard deviation (SD) by the mean (\bar{X}) of the measured concentrations and multiplying by 100, according to the following formula:

$$CV\% = \frac{SD}{\bar{X}} \times 100$$

For each calibrator except the LLoQ, CV% must be $\leq 15\%$ while for LLoQ, CV% must be $\leq 20\%$. The precision was determined both within a single analysis session (intra-run), by determining the analyte in five replicates at four different nominal concentration (i.e. 5 x LLOQ, 5 x QCL, 5 x QCM and 5 x QCH) and within different analytical sessions (inter-run) through the analysis in five replicates in at least 3 analytical runs over at least two days. The calibration curve used to determine the real concentrations of the QCs was freshly prepared every day. The accuracy of the analytical method was reported as a percentage of the nominal concentration and it was determined both intra-run and inter-run in the same way as accuracy. Accuracy was calculated for calibrator using the following formula:

$$Accuracy\% = \frac{x_{ibc} - x_{in}}{x_{ibc}} \times 100$$

Where:

x_{ibc} = back-calculated concentration of the i^{th} analyte;

x_{in} = nominal concentration of the i^{th} analyte.

The accuracy was evaluated by comparing the mean measured concentration at each level with the corresponding nominal value. According to the acceptance criteria, accuracy had to be within $\pm 15\%$ of the nominal concentration for all levels, except for the LLOQ, where a deviation of up to $\pm 20\%$ was considered acceptable.

3.2.6 Carry-over

Carry-over was evaluated to verify the absence of residual analyte in the analytical system that could affect the quantification of subsequent samples. This phenomenon occurs when traces of the analyte from a previous injection remain within the chromatographic or ionization system, potentially leading to artificially elevated signals.

During method validation, carry-over was assessed by injecting blank samples immediately after the calibration standard at the ULOQ. The analytical response observed in these blanks was required to be no greater than 20% of the analyte signal at the LLOQ and no higher than 5% of the internal standard response.

3.2.7 Dilution integrity

Dilution integrity must be demonstrated in order to be sure that samples having concentrations out of the calibration range established for the method can be quantified after dilution. In particular, this should be evaluated by diluting a plasmatic sample at a known concentration value with blank matrix, at least in quintuplicate per dilution factor tested. Dilution integrity was assessed for two dilution factors 1:2 and 1:5 and only for ABI and D4A. The dilution integrity test was not performed for all analytes, as the validated calibration ranges were already well above the expected therapeutic plasma concentrations reported in the literature. Therefore, it was considered unnecessary to further assess dilution effects under these conditions. To simulate the occurrence of a sample with a concentration exceeding the validated calibration range, a spiked plasma sample at 80 ng/mL was prepared. For this purpose, a WS at 1600 ng/mL in MeOH was prepared from the stock solutions. The plasma was then spiked with this WS and subsequently diluted to evaluate dilution integrity. Specifically, 50 μ L of the spiked plasma were mixed with 50 μ L of blank plasma to obtain a 1:2 dilution factor, and 50 μ L of spiked plasma were mixed with 200 μ L of blank plasma to achieve a 1:5 dilution factor. Samples were then processed following the usual workflow, as reported in section 3.1.5. This test was considered accepted if both accuracy and precision were within 85-115% and $\leq 15\%$, respectively.

3.2.8 Stability and reinjection reproducibility

Reinjection reproducibility was evaluated to verify the stability and reliability of processed samples in case reinjection is necessary, for example due to instrument interruptions or technical issues. A complete analytical run, including calibration standards and at least five replicates of low, medium, and high QC levels, was reinjected after storage. The precision and accuracy of the reinjected QCs were assessed using the same acceptance criteria as the original analysis to confirm the viability of the samples. The results were recorded and included in the method validation documentation.

The analyte stability is a function of the matrix in which it is dispersed, of the conditions in which it is stored and of the chemical properties of the analyte itself. Evaluating the stability of the analyte in stock solutions, working solutions and in the matrix is essential to ensure the reliability of the results obtained from the analytical method. This assessment includes all the situations that can be encountered during the whole analytical procedure such as freeze-thaw stability, short- and long-term stability, stock stability and post-

processing stability. The stability of the analytes of interest was evaluated using only the low and high QC levels (QCL and QCH), each analyzed in triplicate.

Long-term stability in plasma was assessed by storing the QC samples at $-80\text{ }^{\circ}\text{C}$ for 15 days, 30 days, and 2 months, and comparing the results to freshly prepared calibration curves and QCs. Bench-top stability in plasma was evaluated by leaving the samples at room temperature for 2 and 4 hours prior to processing. The stability in whole blood was assessed at 30 minutes, 1 hour, 2 hours, and 4 hours, and the analytes were considered stable by comparing the analyte-to-internal standard area ratios. Post-processing stability in the autosampler, maintained at $4\text{ }^{\circ}\text{C}$, was determined by re-analyzing the extracted samples after 5 and 7 days. Freeze-thaw stability was tested over five cycles, where QC aliquots were frozen at $-80\text{ }^{\circ}\text{C}$, thawed, processed, and analyzed, repeating the cycle five times.

For all stability tests, each analyte was considered stable if the measured concentration of at least two out of three replicates per QC level was within 85–115% of the nominal value.

3.3 Patient enrolment

At the Oncology Reference Center in Aviano (PN), a phase IV clinical study protocol entitled " **PRECISION: Prostate cancer REsearch using Cross-validation of Innovative Sampling, Integrating LC-MS/MS for Optimized therapeutic drug moNitoring**" has been launched. The protocol for this clinical trial (EudraCT Code: CRO-2025-12) has been reviewed and approved by the Friuli Venezia Giulia Regional Ethics.

3.3.1 Patient characteristics

The eligibility criteria are:

- Patients treated with ABI, APA, DARO, and ENZA according to the routine clinical practice criteria. The dose and the treatment cycle do not matter but patients should be at the steady state.
- Patients aged 18 years or older
- Signed informed consent is required.

The exclusion criteria are uncooperative and/or unreliable patients and refusal to give informed consent.

3.3.2 Treatment and sampling

Patients will be offered additional blood samples that are not required by normal clinical practice. As per medical advice, these extra blood tests will be recommended for patients during each of their scheduled clinical check-ups. These samples will be collected alongside scheduled blood chemistry tests and accompanied by the completion of a brief questionnaire. Blood samples will be taken at specific times, where possible, to determine the C_{\min} of the drugs. Steady state, and consequently the correct C_{\min} value, is reached approximately five drug half-lives after treatment initiation. Information on when blood sampling should be performed during treatment is provided in Table 7 for each drug, according to its PK properties.

Drug	Half-life (t _{1/2})	Days treatment initiation to reach steady state	Hours from the last drug administration to reach C _{min}	References
Abiraterone	12 h	8 days	24 h	39,130
Enzalutamide	5.8 days (S,R) 9 h	28 days	24 h	82,131
Darolutamide	(S,S) 22 h	5 days	12 h	69,132
Apalutamide	3 days	28 days	24 h	55,133

Table 7, Timing for the correct collection of samples at C_{min}

Accurate estimation of the real C_{min} in a patient's plasma requires precise timing of pill intake. For this reason, the following information will be recorded during sample collection using the 'Patient Questionnaire' form:

- Time (date and hours) of drug intake the day before the clinical evaluation;
- Time (date and hours) of blood collection.

On the day of the clinical evaluation, patients will be asked not to take the drug until sampling has been performed. For each patient, two blood samples will be taken:

- A regular venous blood sample will be collected into a 4.9 mL K-EDTA-containing tube.
- At least two blood drops from a fingertip puncture (finger-prick) will be collected using Capitainer B device.

3.3.3 Patients' samples processing procedures

The 4.9 mL tube should be processed immediately by centrifugation at 2608 ref for 10 min at 4°C in order to obtain the plasma sample (stored at -80°C) for standard quantification. For the plasma of patients treated with ABI, extra care must be taken. In literature, it has been reported many times that the drug is very unstable in blood and at room temperature¹³⁴⁻¹³⁶, which is why the sample was kept on ice from the blood collection clinic to the analysis laboratory. After the validation of the analytical method, we can proceed to analyze patients' plasma. Each sample was thawed at room temperature and vortex-mixed for 10s and then processed as already explained in section 3.1.5. During the analysis, 2 µL of each sample were injected, together with the calibrators and QCs, into the LC-MS

system for the analysis. As required by guidelines^{125,137}, prior to each analysis, system suitability (SST) must be submitted, this is to verify the instrument performance (e.g. signal to noise ratio, peak shape and retention time). It is conducted by analysing: a blank sample, containing only the extracted matrix, a zero sample, which is a blank added with IS and a LLoQ sample. Both guidelines describe the criteria that must be met for an analysis to be considered accepted:

- The SST should guarantee the quantification of the LLoQ and the absence of a quantifiable signal of each analyte in the blank sample
- have a precision (CV%) of $\leq 15\%$ and an accuracy of 85-115%, except for the LLoQ, which should have a precision of $\leq 20\%$ and an accuracy of 80-120%
- have at least 75% of the calibration standard concentrations (except for the two extremes, which must always meet the criteria of accuracy) in the criteria.
- have a precision of $\leq 15\%$ and an accuracy of 85-115%, with no more than one QC excluded for each of the three concentration levels.

4. RESULTS AND DISCUSSION

4.1 LC-MS/MS method development of abiraterone, enzalutamide, darolutamide, apalutamide and their metabolites in human plasma

4.1.1 Mass spectrometric conditions optimisation

4.1.1.1 Compound-dependent parameters optimisation

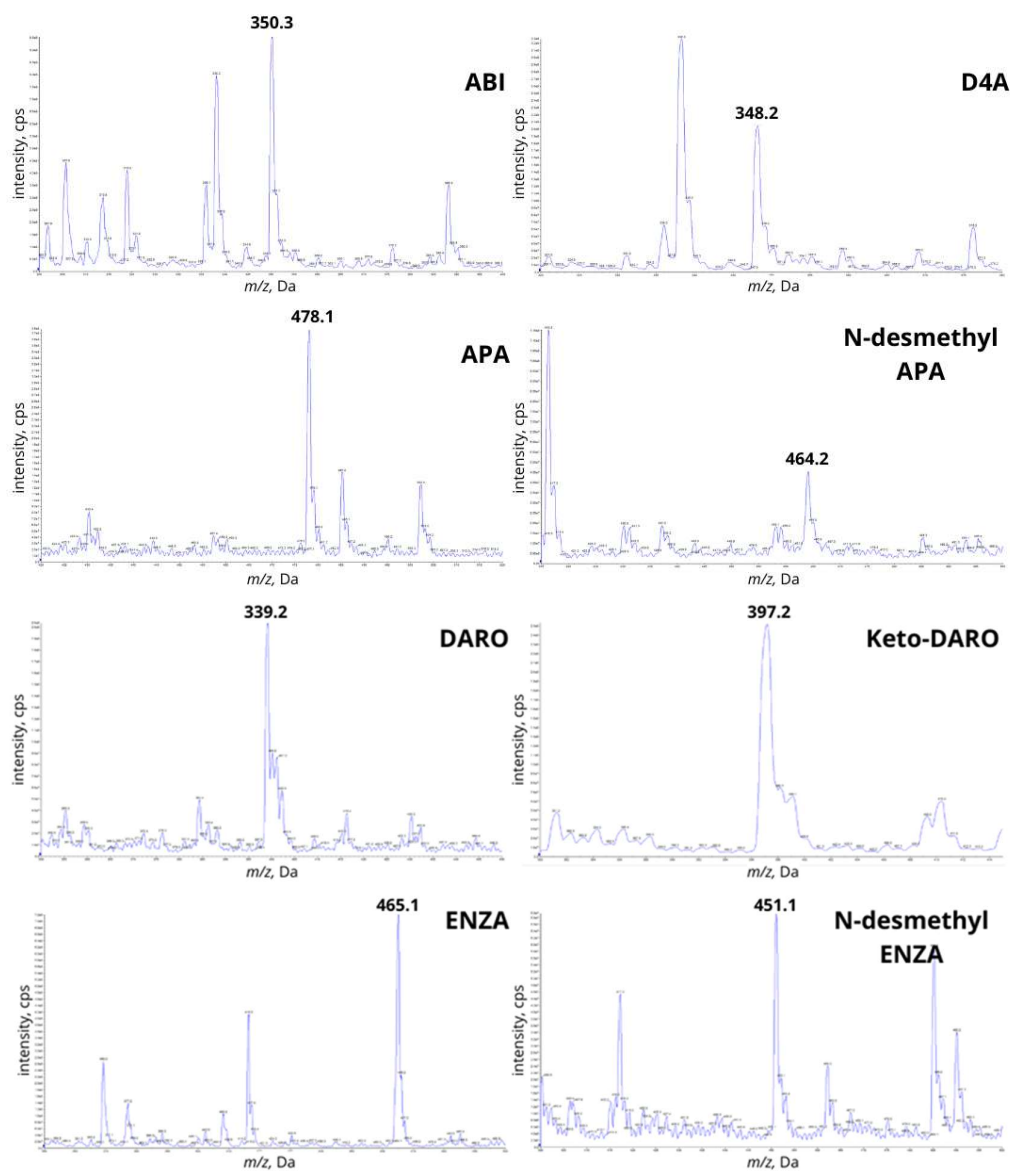
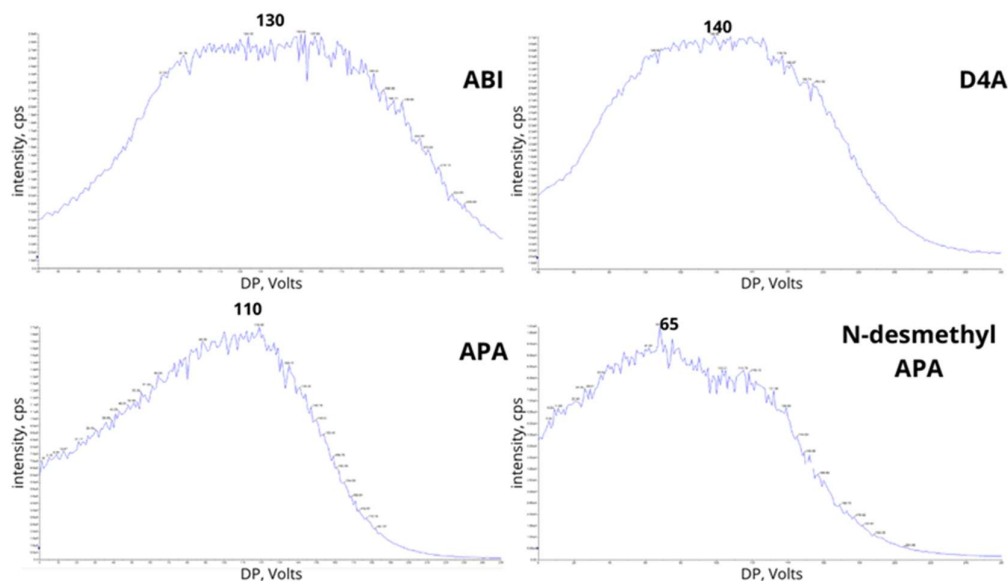


Figure 20, Spectra obtained in positive ion mode showing the presence of all the compound and the isotopic pattern of each protonated molecule.

The monoisotopic mass of ABI, D4A, APA, N-desmethyl APA, DARO, keto-DARO, ENZA, and N-desmethyl ENZA is equal to 349.5, 347.4, 477.4, 463.4, 398.9, 396.8, 464.4, and 450.4 Da, respectively. During each Q1 full scan, performed with the TIS source operating in positive mode and scanning from 100 to 600 Da (dwell time = 5 s), the presence of the analyte of interest was confirmed by the detection of the corresponding protonated molecule $[M+H]^+$ at 350.3, 348.2, 478.1, 464.2, 399.2, 397.2, 465.1, and 451.1 m/z respectively. (Figure 20).

Then, through Q1MI scan mode, the XIC of each protonated molecule was monitored by ramping the DP value from 0 to 400 V. The XIC with highest intensity was reached with DP set at 130, 140, 110, 65, 75, 70, 200, 100, 150 and 155 V for ABI, D4A, APA, N-desmethyl APA, DARO, keto-DARO, ENZA, and N-desmethyl ENZA, respectively (Figure 21). This represented the ideal values for preventing the ions from clustering together. In the same way, the value of 10 V was defined as optimal for the EP of each protonated molecule, by ramping from 2 to 15 V.



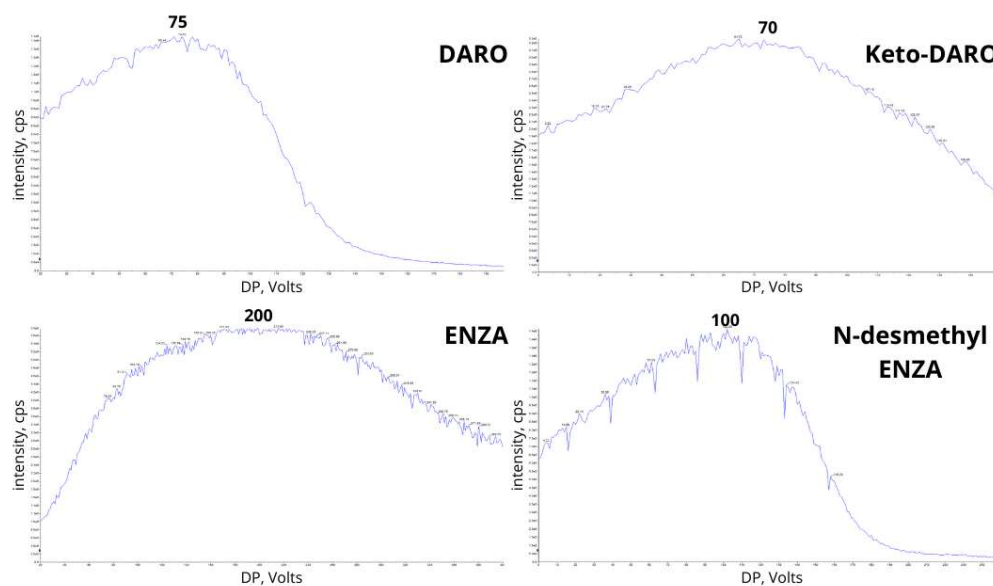
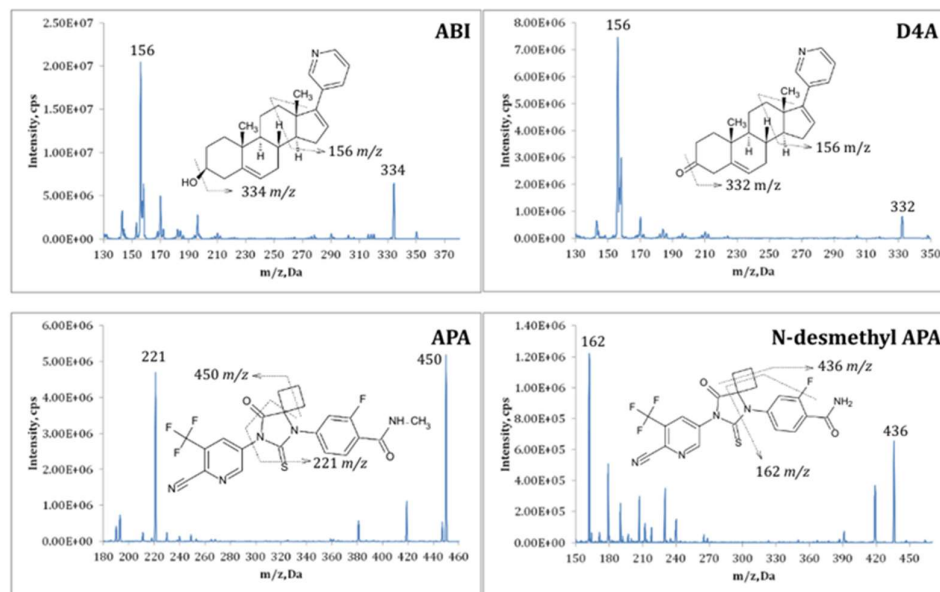


Figure 21, Spectra representing the variation of all the compounds signal intensity versus the DP increase, obtained in positive ion mode

In product ions (MS2) mode, the fragmentation pattern of each precursor ion was evaluated by slowly ramping the CE values (from 5 to 45 V) in the collision cell. As reported in Figure 22, two product ions were found and identified for each protonated molecule.



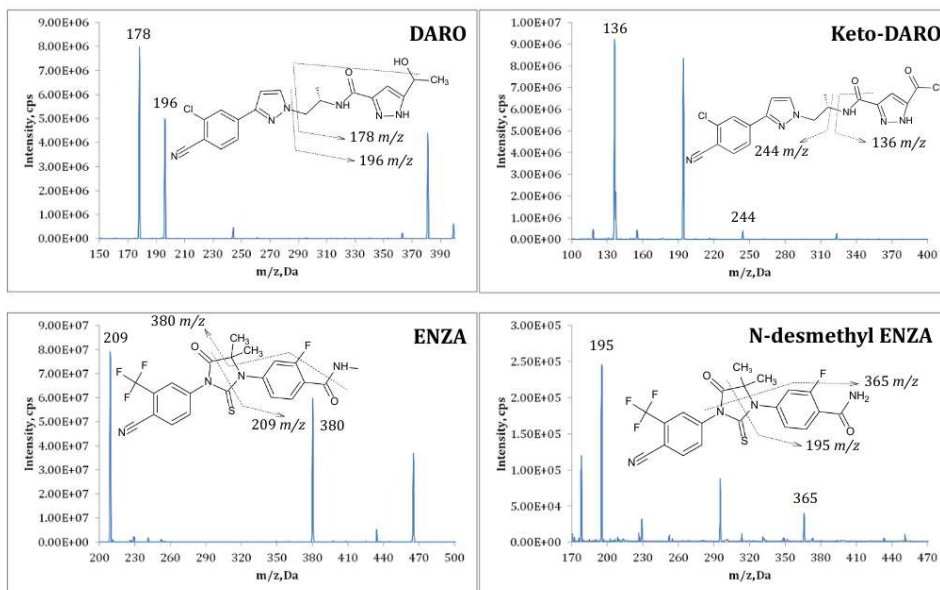
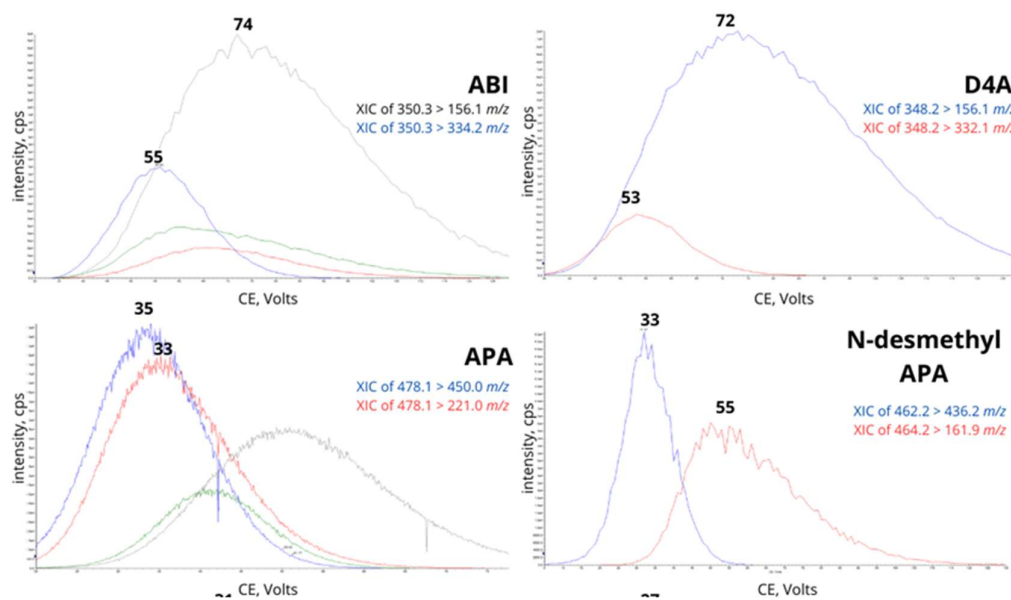


Figure 22, Spectra recorded in product ions mode, showing the fragmentation pattern of all the compounds, showing the fragmentation pattern.

For each analyte, the signal intensity for both transitions was monitored through an MRM scan by ramping the CE value from 5 to 130V, valuating the optimal CE value to generate each fragment.



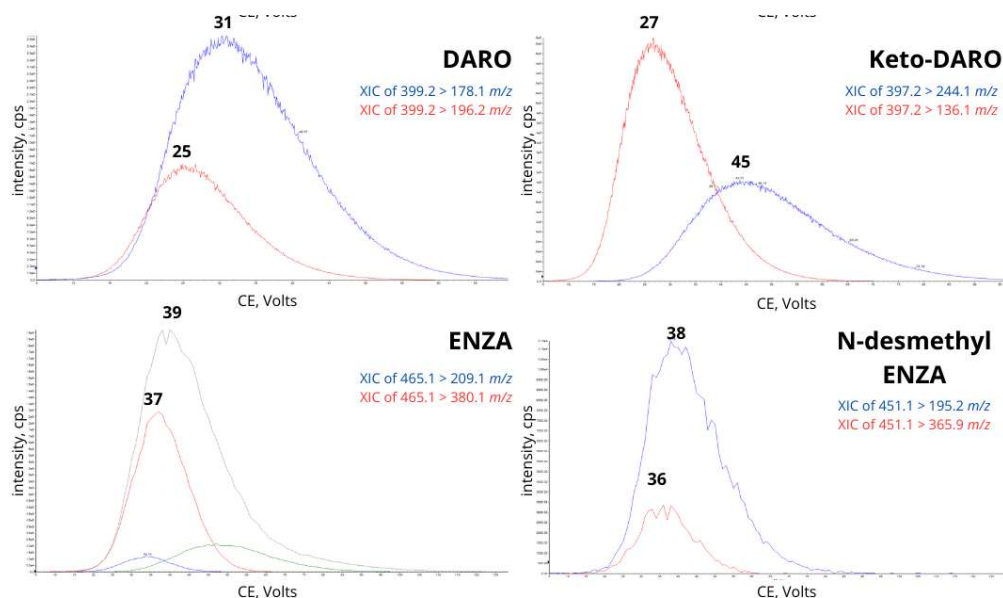


Figure 23, Spectra representing the variations in signals intensity of the two selected fragments.

In Table 8 all the transitions are reported. The daughter ions that had reached the highest signal intensity were selected as quantifiers and are reported as the first transition for every analyte. Thanks to a similar experiment, ramping from 0 to 55V, the optimal CXP for every fragment was evaluated.

Lastly, with the mass spectrometer in precursor ion scan mode, it was possible to confirm the direct derivation of the two selected product ions from their precursor ion, for each analyte.

The compound-dependent parameters for the internal standards were determined with the same experiments described for the other analytes.

The optimized compound-dependent parameters, particularly CE and DP, required slight detuning for all analytes except ABI, D4A, and keto-DARO, to prevent detector saturation in the mass spectrometer. The final optimized and adjusted parameter values applied in the MS method are listed in Table 8. A reduction in analyte concentration during sample preparation or at the final dilution stage was not considered viable, as it would have negatively impacted the sensitivity for ABI and D4A detection.

Precursor Ion				Product Ion		
Analyte	Q1 (amu)	DP (volts)	EP (volts)	Q3 (amu)	CE (volts)	CXP (volts)
ABI	350.3	130	10	156.1	74	26
				334.2	55	18
D4A	348.2	140	10	156.1	72	25
				332.1	53	18

APA	478.1	160 (110)	10	450.0	42 (35)	12
				221.0	35	38
N-desmethyl APA	464.2	160 (65)	10	436.2	33	11
				161.9	55	27
DARO	399.2	115 (75)	10	178.1	23 (31)	30
				196.2	25	33
keto-DARO	397.2	70	10	244.1	45	20
				136.1	27	22
ENZA	465.1	40 (200)	10	209.1	29 (39)	35
				380.1	37	9
N-desmethyl ENZA	451.1	160 (100)	10	195.2	60 (38)	15
				365.9	36	9
[² H ₇]-ABI	357.4	150	10	157.1	75	26
				341.3	56	18
[¹³ C, ² H ₃]-APA	482.2	155	10	225.2	35	39
				454.4	34	12
[² H ₄]-DARO	403.3	85	10	182.0	31	31
				200.0	27	30
[² H ₆]-ENZA	471.2	160	10	215.2	40	37
				380.1	36	9

Table 8, Optimal values of the compound-dependent parameters for each analyte and IS. Values in parentheses are the optimized ones; those in the table are the values used in the method and are detuned.

4.1.1.2 Source-dependent parameters optimisation

The objective of this experiment was to maximize signal intensity to achieve the highest possible sensitivity. As detailed in section 3.1.3.2, the XIC trend of the ABI quantifier transition ($350.3 > 156.1$ m/z) was monitored in SRM mode while each source-dependent parameter was manually optimized to enhance the signal response.

Initially, TEM was determined by gradually ramping it from 50 °C to 550 °C in increments of approximately 1 minute per step, allowing sufficient time for both temperature stabilization and signal equilibration. As illustrated in Figure 24, the maximum signal intensity was obtained at 550 °C, which was therefore selected as the optimal TEM value for further analyses.

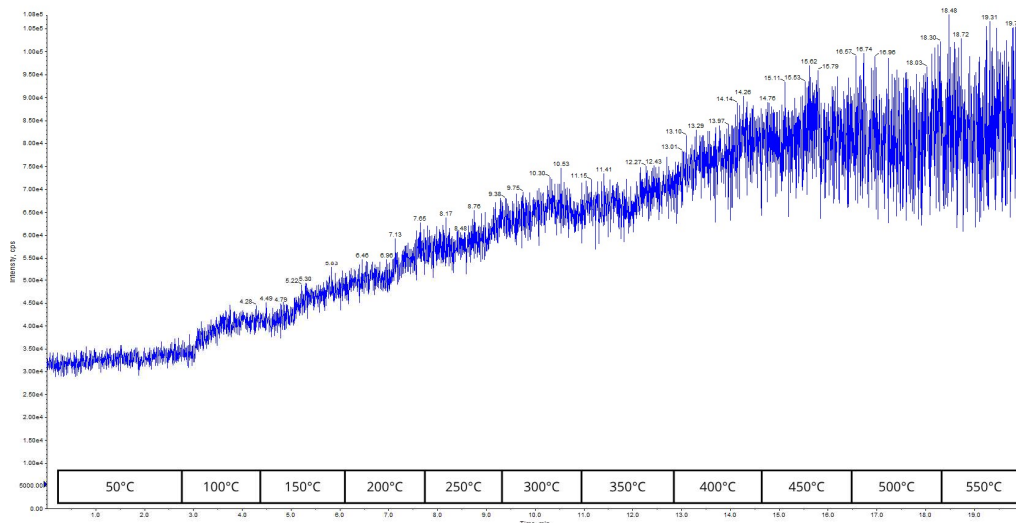


Figure 24, Spectrum representing the XIC trend of ABI versus TEM.

A similar experiment was conducted to determine the optimal IS. The IS value, typically set to a default of 5500 V, was progressively reduced to 4500 V in 500 V increments while simultaneously testing different TEM settings. This combined evaluation allowed assessment of how both parameters influenced signal intensity. The highest and most stable signal was obtained with a TEM of 550 °C and an IS of 5500 V, which were therefore selected as the optimal conditions for subsequent analyses.

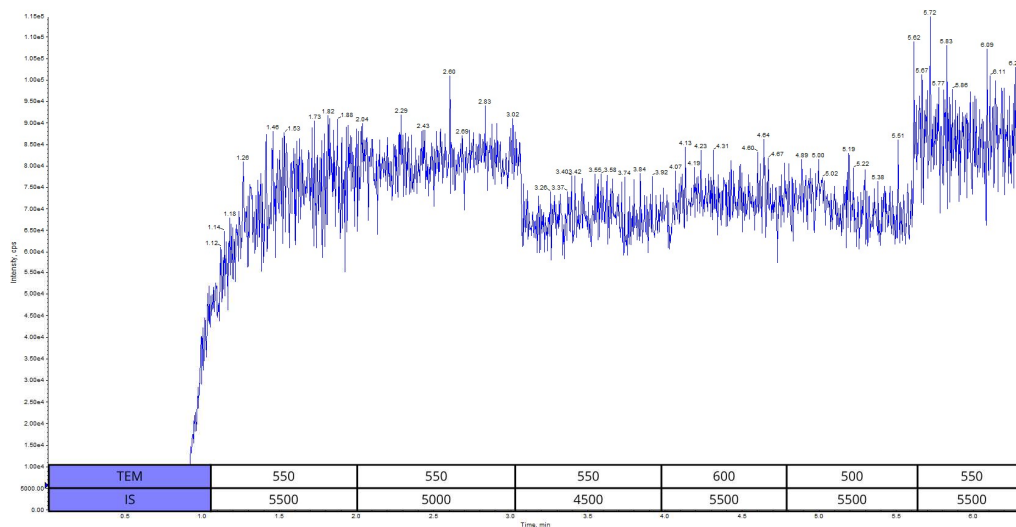


Figure 25, Spectrum representing the XIC trend of ABI versus the IS and TEM.

The CUR parameter, which is typically set around 35 and generally not lower than 20, was also optimized. Starting from the standard value of 35, it was gradually increased up to 39

in steps of 1 to evaluate its effect on signal intensity and stability. Since no significant variation in the signal was observed across this range, the CUR value of 35 was confirmed as optimal and retained for the final method.

The final optimization step involved adjusting the nebulizer gas (GS1) and heater gas (GS2) pressures. Since GS2 generally operates at a higher pressure than GS1, the two parameters were tuned together while ensuring that their combined value did not exceed 100 psi, the maximum output of the nitrogen generator. Various GS1/GS2 settings were tested, including 10/50, 20/50, 30/50, 30/40, 20/40, 20/60, 50/50, 40/50, 30/60, and 40/60. The most stable and intense signal in the XIC trace was obtained with GS1 set to 50 psi and GS2 to 50 psi, which was therefore selected as the optimal condition.

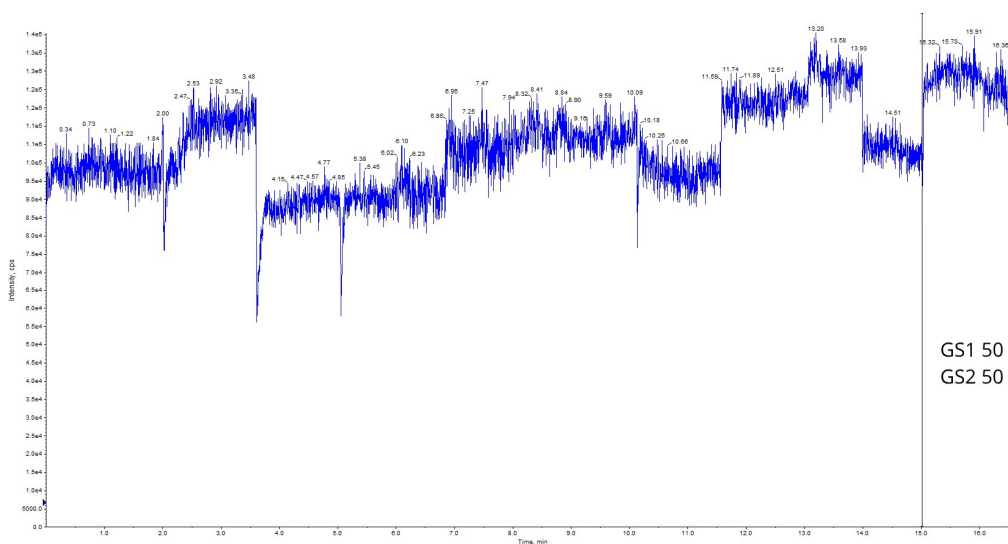


Figure 26, Spectrum representing the XIC trend of ABI versus GS1 and GS2.

Once all the source-dependent parameters had been optimized using ABI, the same procedure was repeated by monitoring the quantifier transition of D4A ($348.2 > 156.1$ m/z), confirming the previously established parameter settings.

All the source-dependent parameters obtained through the optimisation process are reported in Table 9.

CUR	35
CAD	Medium
ION SPRAY	5500
TEM	550
GS1	50
GS2	50

Table 9, Source-dependent parameter.

4.1.2 Chromatographic conditions optimisation

In this method, a high degree of chromatographic separation between analytes was not strictly required, since detection was performed using a triple quadrupole mass spectrometer, which provides excellent selectivity based on specific mass transitions. However, unwanted interferences may still occur when analytes coelute, making the choice of an appropriate stationary phase crucial.

To achieve optimal separation, several C18 columns were evaluated due to their ability to distinguish subtle hydrophobic differences, such as the presence of methyl groups or fluorine atoms. The initial tests were performed using a Kinetex® EVO C18 core-shell column (2.6 μm , 100 \times 2.1 mm), which allowed effective analyte separation in gradient mode; however, the total chromatographic runtime was relatively long because of the column length.

To shorten the analysis, a shorter Kinetex® EVO C18 column (5 μm , 50 \times 2.1 mm) was tested, but the resulting peaks showed poor resolution, likely due to the larger particle size. A subsequent trial with a Kinetex® C18 column (2.6 μm , 50 \times 2.1 mm) provided improved separation and peak shape, proving to be a more suitable compromise between efficiency and runtime.

For comparison, a Synergi™ Fusion-RP 80 column (4 μm , 50 \times 2 mm) was also evaluated, but its enhanced polarity led to suboptimal performance, with broad and tailing peaks, particularly for ABI. Based on these observations, the Kinetex® C18 (2.6 μm , 50 \times 2.1 mm) was selected as the optimal column for further optimization of the chromatographic method. The use of a guard column was also evaluated; however, it led to a noticeable deterioration in peak shape, likely due to increased dead volume and dispersion effects. Consequently, the guard column was excluded from the final chromatographic setup to preserve optimal resolution and maintain sharp, symmetrical peaks.

The selection of the mobile phase was initially guided by a literature review of previously published analytical methods. Most of these studies employed MeCN as the strong solvent and Type 1 ultrapure H₂O as the weak solvent. Both mobile phases were commonly modified with 0.1% formic acid (HCOOH) to enhance ionization efficiency and peak shape. Considering the simplicity of this composition and after performing preliminary tests confirming satisfactory chromatographic performance, this mobile phase system was selected for the final method. Considering the composition of the mobile phases, a column temperature of 30 °C was deemed sufficient to balance the backpressure generated during chromatographic runs, ensuring stable flow conditions and consistent peak performance.

With respect to the elution strategy, a fully isocratic approach was ruled out because of the complexity and impurity of the analysed samples. To ensure effective column cleaning from potential matrix interferences introduced during injections, a multi-step gradient elution method was therefore selected.

Based on literature data, the initial chromatographic conditions were set using a gradient method starting from 20% of the organic phase and reaching 90%. To determine the total run time, the column volume was calculated and multiplied by a factor of 10 for both the equilibration and washing phases. In the preliminary runs, a shorter washing step equivalent to 5 column volumes was occasionally applied to better evaluate the overall chromatographic behaviour. The initial flow rate was maintained at 0.3 mL/min. Subsequently, different conditions were tested by increasing the initial percentage of the organic phase to 30% and adjusting the gradient slope to optimize peak resolution and elution time. The main goal was to achieve sharp, symmetrical peaks without tailing, ensuring that all analytes eluted properly during the gradient phase rather than in the washing phase. A note should be added specifying that N-desmethyl ENZA was not included in the initial experiments due to issues with the shipment of the reference material, which delayed its availability for analysis.

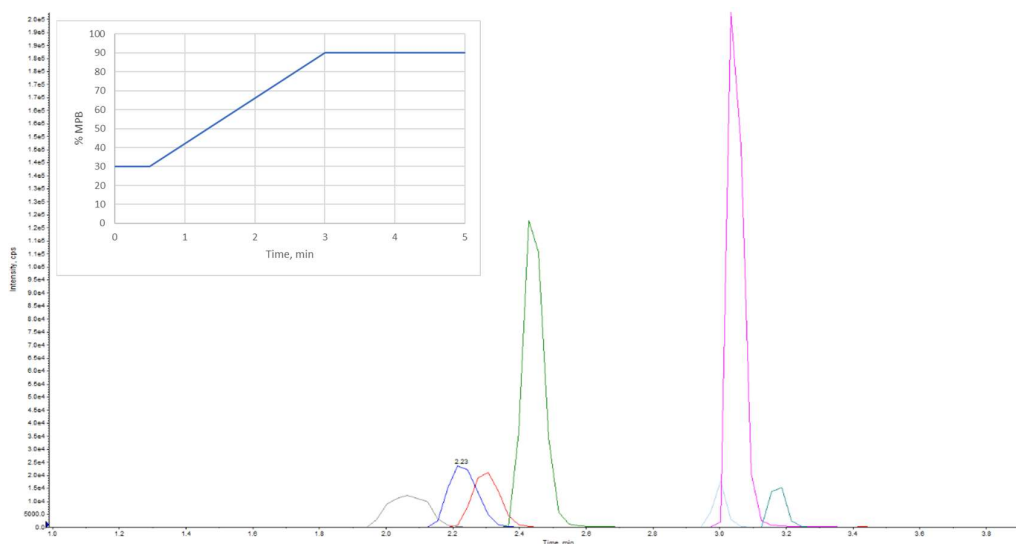


Figure 27, MRM chromatographic profile of all analytes except N-desmethyl ENZA, acquired with an initial mobile-phase organic content of 30% and a shallow gradient.

Four chromatographic methods were tested, starting with an initial FMB percentage of 20% and then 30%, each evaluated with different gradient slopes. Specifically, the gradient ramp was progressively reduced from 58% to 28% per minute to improve separation efficiency.

Comparative analysis of the chromatograms revealed that the best peak shape was obtained with a 30% initial FMB, while optimal separation was achieved with the gentler gradient slope. As shown in the figure, the peaks were fairly narrow (with a maximum width of approximately 6 seconds) but defined by a limited number of data points (Figure 27). For this reason, in the following analyses, the dwell time was adjusted to provide a more accurate peak profile. It was estimated that to obtain at least 15 data points per peak, a cycle time of 0.2 seconds would be required.

Although the obtained peak shapes with the 30% initial organic phase and the reduced gradient slope were satisfactory, with well-defined, narrow peaks, the elution of the analytes occurred too late in the chromatographic run, in some cases extending into the washing phase. This behavior prevented the analytes from eluting entirely within the gradient, which is preferably to ensure consistent chromatographic performance. Consequently, even though the peak morphology met the desired criteria, the method could not yet be considered optimal, as it would not allow a substantial reduction in chromatographic time or efficient elution of the analytes during the programmed gradient phase.

To address this issue, the initial percentage of organic phase was increased, and the isocratic segment preceding the gradient was removed to initiate the elution immediately.

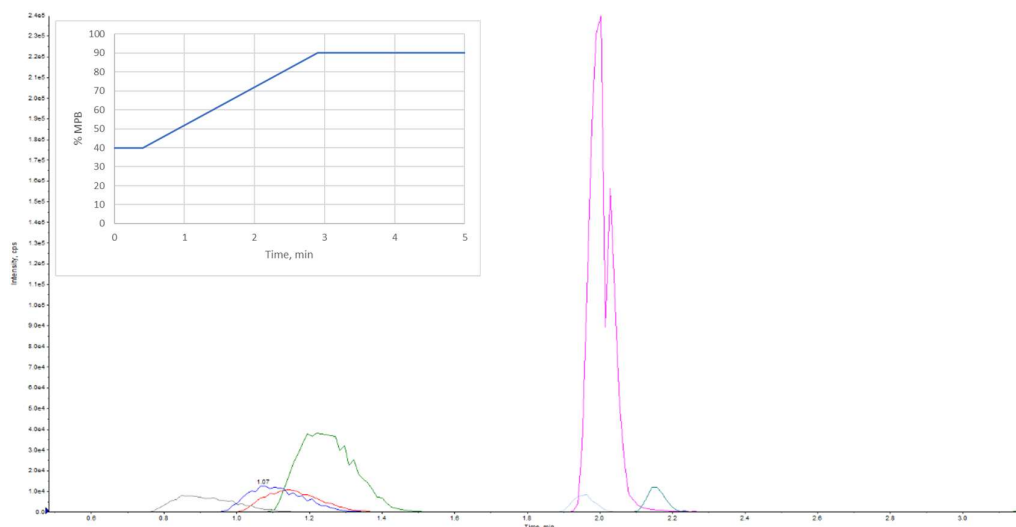


Figure 28, MRM chromatographic profile of all analytes except *N*-desmethyl ENZA, acquired with an initial mobile-phase organic content of 40% and a shallow gradient.

As shown in the figure, the peaks are now better defined thanks to the adjustment of the dwell time. However, the 40% starting organic phase did not result in optimal peak shapes, so the initial condition was reverted to 30%. To further improve the elution time, the initial isocratic segment was removed, and the flow rate was increased to 0.4 and 0.5 mL/min.

At a flow rate of 0.5 mL/min, the peaks appeared tailing and poorly shaped, whereas at 0.4 mL/min they maintained good symmetry and definition. By removing the initial isocratic phase and increasing the flow rate, the retention times shifted earlier, allowing all analytes to elute within the gradient. Therefore, this chromatographic setup was selected as the final working method.

After optimizing analyte elution, it was essential to include a washing phase in the chromatographic method. The aim was to ensure the elution of the most lipophilic interferences typically found in plasma, such as protein residues and phospholipids (PLs). To determine the appropriate duration of this step, a dedicated method was developed to monitor the phospholipid elution profile (see Section 3.1.4). Different washing times were tested: 3.5, 2, 1.5, 1, and 0.5 minutes. The washing phase was considered efficient when the phospholipid chromatographic profiles showed consistent and reproducible patterns across consecutive analyses.

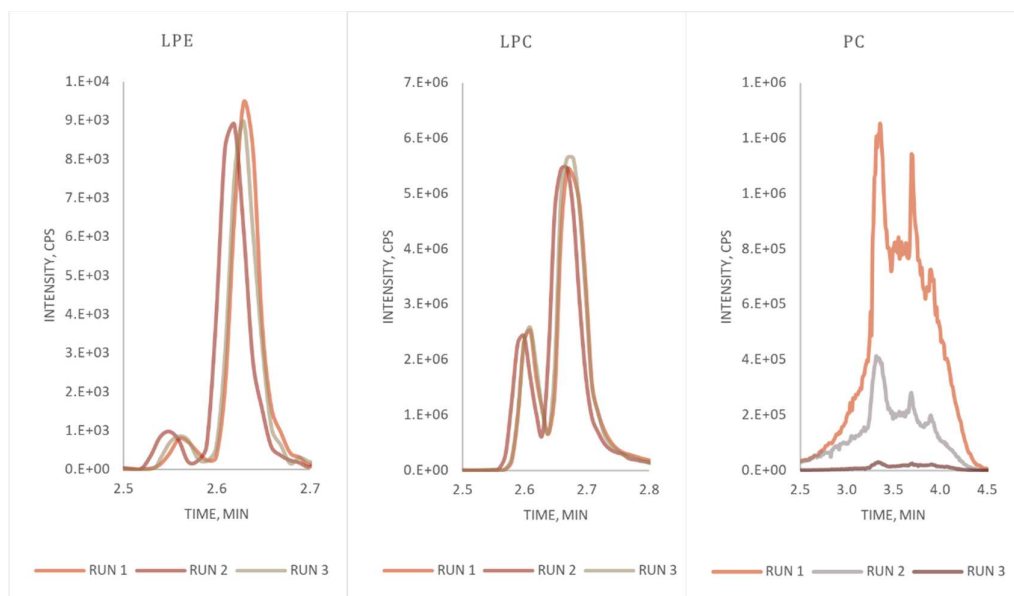


Figure 29, MRM chromatograms of three of the most abundant PLs in human plasma during 0.5 min of wash step from three consecutive injections. LPE is lysophosphatidyl ethanolamine, LPC is lysophosphatidyl choline and PC is phosphatidyl choline.

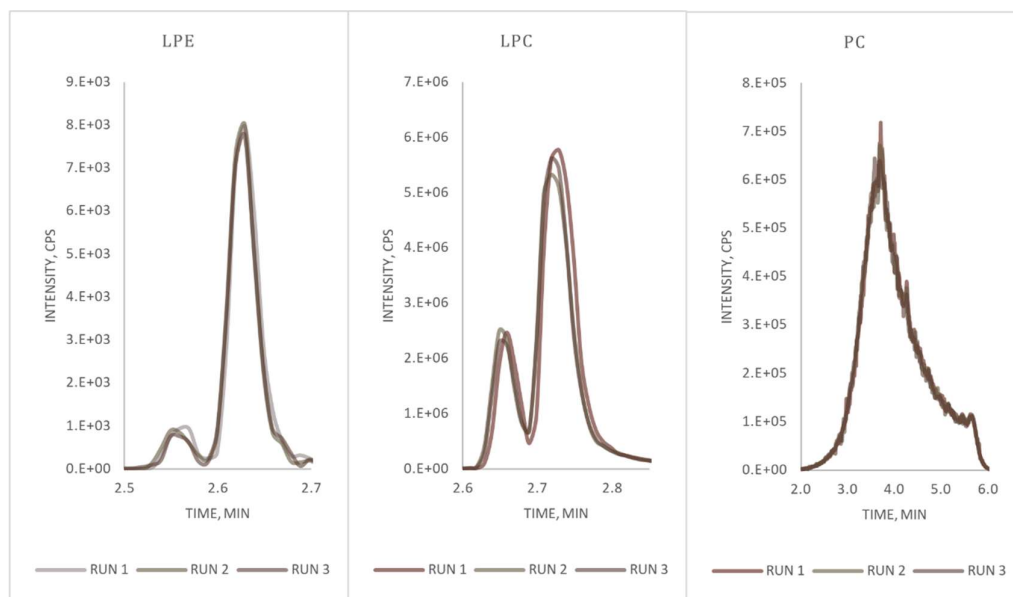


Figure 30, MRM chromatograms of three of the most abundant PLs in human plasma during 1.5 min of wash step from three consecutive injections. LPE is lysophosphatidyl ethanolamine, LPC is lysophosphatidyl choline and PC is phosphatidyl choline.

As shown in Figure 29 and Figure 30, a 0.5 min washing phase proved insufficient to achieve reproducible phospholipid elution patterns, indicating inadequate column cleaning. Conversely, with a 1.5 min washing step, the phospholipid profiles from three consecutive runs were perfectly superimposable, demonstrating that this duration was adequate to ensure efficient phospholipid elution and consistent signal repeatability. Regarding the re-equilibration phase, we aimed to minimize its duration, testing progressively shorter times down to one minute. To assess feasibility, LLOQ peaks were compared to verify the reproducibility of retention times. Based on these results, a washing time of 1.5 minutes and a re-equilibration time of 2 minutes were selected as optimal conditions.

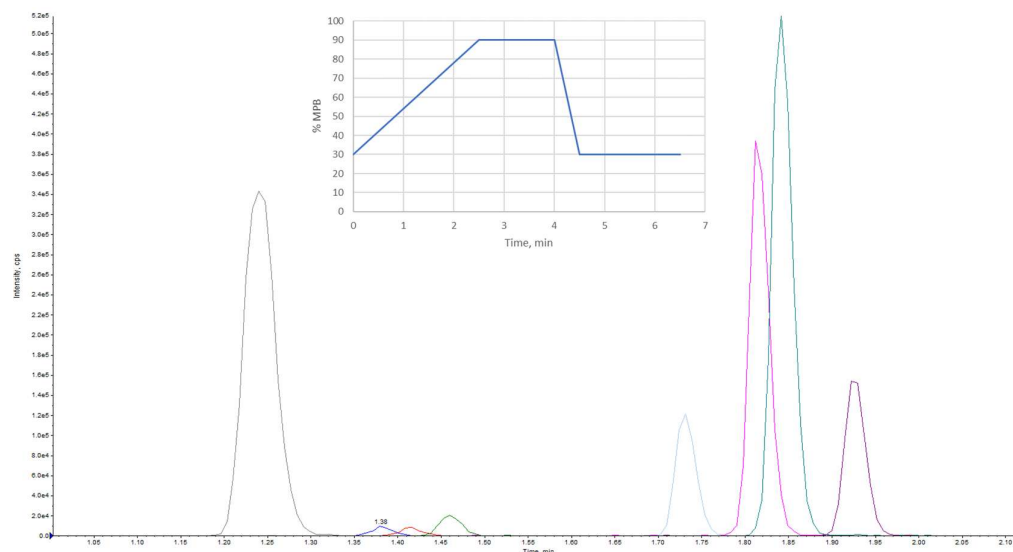


Figure 31, MRM chromatographic profile of all analytes, acquired with an initial mobile-phase organic content of 30%, a shallow gradient, and a flow rate of 0.4 mL/min. The injection corresponds to a calibration-curve point, so the analytes are present at different concentrations.

4.1.3 Sample preparation

4.1.3.1 Sample extraction optimisation

PP was selected as the sample extraction technique due to its simplicity and rapid execution. This approach allows for quick sample handling while minimizing preparation errors, making it particularly suitable for the practical requirements of TDM applications.

The sample preparation process proved to be one of the most challenging aspects of method development. Since each analyte required calibration curves with different concentration ranges, it was particularly difficult to balance adequate signal-to-noise ratios for ABI and its metabolite at the LLoQ while avoiding detector saturation for the other analytes at the ULoQ. To address this, several injection volumes and dilution strategies were tested.

Initially, MeCN was selected as the protein-precipitating solvent after comparison with MeOH, as it provided superior performance. Different volumes of precipitating solvent were then evaluated, maintaining a minimum plasma-to-solvent ratio of 1:3, testing 200, 300, and 400 μ L, as well as various post-precipitation dilution volumes using either mobile phase or organic solvent. Dilutions performed with the mobile phase yielded poor chromatographic peak shapes, particularly for ABI, and were therefore discarded. Dilution with MeCN also proved unsuitable due to ABI instability during analysis. As reported in the literature¹³⁵, ABI undergoes degradation in ACN, a trend confirmed by a progressive

decrease in signal intensity when plasma-to-solvent ratios exceeded 1:6. Subsequent attempts to dilute with MeOH also produced unsatisfactory results, mainly due to poor signal-to-noise ratios that rendered LLOQ samples for ABI unquantifiable. Consequently, the dilution step was omitted, and attention shifted toward optimizing the precipitation volume. Tests with 400 and 500 μL of ISWS in ACN showed that 500 μL achieved the best compromise, ensuring strong signal intensity for ABI and D4A while avoiding signal saturation for ENZA and its metabolite. Ultimately, the optimized procedure consisted of precipitating plasma samples with 500 μL of ISWS in ACN and directly transferring the supernatant into vials without any dilution step.

4.1.3.2 Calibration curve and quality controls preparation

A seven-point calibration curve and, at least, three replicates of each QC concentration level were freshly prepared every day during the validation study and for patients' samples analysis. For each calibrator and QC, 5 μL of the respective WS were added to 95 μL of human pooled plasma, then samples were processed as presented in section 3.1.5. The final concentration obtained are reported in Table 10.

	ABI (ng/mL)	D4A (ng/mL)	APA (ng/mL)	N-desmethyl APA (ng/mL)	DARO (ng/mL)	Keto- DARO (ng/mL)	ENZA (ng/mL)	N-desmethyl ENZA (ng/mL)
I	0,1	0,1	20	20	20	20	40	40
H	1	1	200	200	200	200	400	400
G	2,5	2,5	500	500	500	500	1000	1000
F	10	10	2000	2000	2000	2000	4000	4000
E	17,5	17,5	3500	3500	3500	3500	7000	7000
D	25	25	5000	5000	5000	5000	10000	10000
C	32,5	32,5	6500	6500	6500	6500	13000	13000
B	42,5	42,5	8500	8500	8500	8500	17000	17000
A	50	50	10000	10000	10000	10000	20000	20000
QCL	0,25	0,25	50,25	50,25	50,25	60	100,5	100,5
QCM	18,75	18,75	3750	3750	3750	4200	7500	7500
QCH	37,5	37,5	7500	7500	7500	8500	15000	15000

Table 10, Final concentrations of calibrators and QCs.

4.2 LC-MS/MS validation study

According to the FDA and EMA guidelines, the parameters considered for the validation of the developed LC-MS/MS method were selectivity, matrix effect, analytes recovery from the matrix, calibration curve linearity and range, intra-day and inter-day precision and accuracy, carry-over, dilution integrity, analytes stability in samples and solutions and reinjection reproducibility.

4.2.1 Selectivity

The method demonstrated a good selectivity: no significant interferences were detected from the analysis of six blank plasma samples, especially at the retention times of the analytes. The area of the interference at the same retention time of the analytes, compared with the analyte response at the LLOQ, is on average: 1.5% for ABI, 4.6% for D4A, 1.4% for APA, 2.3% for N-desmethyl APA, 1.1% for DARO, 4.9% for keto-DARO, 0.8% for ENZA, and 1.9% for N-desmethyl ENZA. The area of the interfering components compared with the response of the IS at the LLOQ for all analytes is less than 0.1%, with a maximum of 0.1% for N-desmethyl APA and a minimum of 0.001% for ABI.

4.2.2 Matrix effect

As part of the matrix effect assessment, quantification of the analytes using plasma samples from seven healthy donors demonstrated satisfactory precision and accuracy, with CV% values $\leq 14.0\%$ and accuracy ranging from 86% to 112%. When ABI and D4A were excluded from the analysis, variability further decreased, with CV% $\leq 9.3\%$ and accuracy between 91% and 112%. Moreover, the presence of haemolysed plasma did not significantly affect quantification, as accuracy remained within 85–109% and CV% $\leq 9.3\%$. Comprehensive accuracy and precision data for each analyte across all tested matrices are reported in the following tables.

Analyte	Nominal conc. (ng/mL)	M1			M2		
		mean \pm SD (ng/mL)	Acc %	CV %	mean \pm SD (ng/mL)	Acc %	CV %
ABI	0,25	0,26 \pm 0,02	104	5,9	0,26 \pm 0,01	105	4,6
	37,5	37,2 \pm 1,9	99	5,1	36,90 \pm 0,10	98	0,3

RESULTS AND DISCUSSION

D4A	0,25	0,27±0,01	106	5,5	0,24±0,02	98	6,4
	37,5	35,10±1,60	94	4,6	34,90±0,50	93	1,5
APA	50,25	53,6±3,1	107	5,8	51,7±3,3	103	6,4
	7500	7984,0±223,2	106	2,8	7910,7±198,8	105	2,5
N-desmethyl APA	50,25	56,2±3,2	112	5,7	54,5±3,5	108	6,5
	7500	7628,3±167,7	102	2,2	7647,3±167,5	102	2,2
DARO	50,25	55,7±2,5	111	4,5	54,0±2,6	107	4,7
	7500	7603,0±131,0	101	1,7	7614,7±59,7	102	0,8
keto-DARO	58	63,9±1,4	110	2,2	62,2±3,5	107	5,7
	8600	8481,0±22,6	99	0,3	8385,0±47,6	98	0,6
ENZA	100,5	102,0±5,4	101	5,3	98,4±6,2	98	6,3
	15000	14540,0±78,1	97	0,5	14483,3±355,6	97	2,5
N-desmethyl ENZA	100,5	103,7±5,6	103	5,4	102,8±7,6	102	7,4
	15000	15370,0±204,2	102	1,3	15133,3±305,3	101	2,0

Analyte	Nominal conc. (ng/mL)	M3			M4		
		mean ±SD (ng/mL)	Acc%	CV%	mean ±SD (ng/mL)	Acc %	CV%
ABI	0,25	0,25±0,02	99	7,4	0,26±0,02	104	8,6
	37,5	37,20±1,60	99	4,3	37,30±2,10	99	5,7
D4A	0,25	0,24±0,03	96	11,1	0,26±0,02	104	7,5
	37,5	35,20±1,20	94	3,3	35,60±1,30	95	3,6
APA	50,25	49,3±1,4	98	2,9	51,8±2,6	103	5,0
	7500	7966,0±346,5	106	4,4	8131,7±418,3	108	5,1
N-desmethyl APA	50,25	55,6±2,0	111	3,6	56,3±2,6	112	4,6
	7500	7897,7±300,9	105	3,8	7906,3±232,8	105	2,9
DARO	50,25	55,5±1,3	111	2,3	54,9±2,3	109	4,1
	7500	7902,7±392,1	105	5,0	7911,7±182,1	105	2,3
keto-DARO	58	59,3±4,7	102	7,8	63,4±3,6	109	5,6
	8600	8837,0±344,4	103	3,9	8663,0±108,6	101	1,3
ENZA	100,5	101,4±3,9	101	3,8	100,5±3,1	100	3,1
	15000	14713,3±225,0	98	1,5	14833,3±353,6	99	2,4
N-desmethyl ENZA	100,5	97,9±1,8	97	1,8	101,6±5,4	101	5,3
	15000	15510,0±252,4	103	1,6	15650,0±304,1	104	1,9

Analyte	Nominal conc. (ng/mL)	M5			M6		
		mean ±SD (ng/mL)	Acc%	CV%	mean ±SD (ng/mL)	Acc%	CV%
ABI	0,25	0,25±0,03	99	10,3	0,27±0,04	107	14,0
	37,5	36,70±1,10	98	2,9	34,60±0,90	92	2,5
D4A	0,25	0,24±0,01	96	4,5	0,24±0,01	96	9,7
	37,5	33,50±0,80	89	2,4	32,20±0,40	86	1,3
APA	50,25	52,0±2,1	103	4,0	50,0±0,6	100	1,2

	7500	7396,7±173,5	99	2,3	7313,3±140,9	98	1,9
N-desmethyl APA	50,25	56,2±0,8	112	1,4	54,8±3,6	109	6,6
	7500	7346,7±128,8	98	1,8	7232,3±72,5	96	1,0
DARO	50,25	52,2±1,2	104	2,3	53,6±2,4	107	4,6
	7500	7495,0±263,3	100	3,5	7246,7±147,5	97	2,0
keto-DARO	58	62,1±3,4	107	5,5	59,3±0,4	102	0,7
	8600	8196,3±244,7	95	3,0	7848,3±140,1	91	1,8
ENZA	100,5	97,2±2,7	97	2,7	96,3±6,0	96	6,2
	15000	14080,0±427,6	94	3,0	13733,3±162,6	92	1,2
N-desmethyl ENZA	100,5	96,3±6,3	96	6,6	92,9±3,2	92	3,4
	15000	14953,3±706,0	100	4,7	14070,0±170,9	94	1,2

Analyte	Nominal conc. (ng/mL)	Haemolysed		
		mean ±SD (ng/mL)	Acc%	CV%
ABI	0,25	0,24±0,01	97	3,3
	37,5	34,90±0,60	93	1,8
D4A	0,25	0,23±0,01	92	3,4
	37,5	32,00±0,70	85	2,0
APA	50,25	51,0±2,6	102	5,0
	7500	7422,7±393,2	99	5,3
N-desmethyl APA	50,25	54,5±5,1	109	9,3
	7500	7387,0±283,9	98	3,8
DARO	50,25	52,5±3,8	104	7,2
	7500	7358,0±130,6	98	1,8
keto-DARO	58	58,4±3,2	100	5,5
	8600	8183,7±77,6	95	0,9
ENZA	100,5	95,1±5,4	95	5,7
	15000	14006,7±140,1	93	1,0
N-desmethyl ENZA	100,5	95,8±0,8	95	0,9
	15000	14810,0±625,1	99	4,2

Table 11, Matrix effect estimation for all the analytes

4.2.3 Recovery

The recovery was evaluated in three replicates for each QC concentration level (L, H), prepared as reported in section 3.2.3, and was calculated by employing the equation described in the same section. Protein precipitation provided excellent extraction efficiency for all analytes from the plasma matrix, with recovery values ranging between 94% and 103%. For APA, ENZA, DARO, and their respective metabolites, recovery results were consistent across both QCL and QCH levels, showing SD values ≤ 10 ng/mL and CV% \leq

9%. Slightly higher variability was observed for ABI and D4A; however, results remained within the established acceptance limits, with SD values ≤ 14 ng/mL and CV% $\leq 13.8\%$. A summary of the recovery data for all analytes is presented in the following table.

Analyte	Nominal conc. (ng/mL)	Recovery (%) \pm SD	Recovery CV%
ABI	0,25	101 \pm 13	13,2
	37,5	100 \pm 4	4,2
D4A	0,25	103 \pm 14	13,8
	37,5	99 \pm 4	4,4
APA	50,25	94 \pm 8	9,0
	7500	95 \pm 6	6,0
N-desmethyl APA	50,25	95 \pm 7	7,2
	7500	94 \pm 6	6,3
DARO	50,25	103 \pm 7	6,6
	7500	100 \pm 4	4,2
keto-DARO	58	103 \pm 9	8,4
	8600	100 \pm 5	4,6
ENZA	100,5	103 \pm 10	9,5
	15000	102 \pm 5	4,6
N-desmethyl ENZA	100,5	98 \pm 6	5,9
	15000	99 \pm 4	4,3

Table 12, Analytes recovery from human plasma.

4.2.4 Calibration curve and range

Calibration curves for ABI, APA, ENZA, DARO, and their respective active metabolites were freshly prepared each day throughout the validation process. For each curve the peak area ratios of the analytes to the IS were plotted against their nominal concentrations, and a weighted linear regression model ($1/x^2$) was applied to obtain the calibration equation. The good linearity was evidenced by the correlation coefficients obtained for each analyte, which were always ≥ 0.997 . This result was also confirmed by the data on the accuracy and precision of the calibration curves: accuracy ranged from 91 to 107% for all compounds, while precision was $\leq 7.8\%$, excluding LLOQ of ABI which has a mean CV of 19%. All the results are in the following table.

Analyte	Nominal conc. (ng/mL)	Mean (ng/mL) \pm SD	CV%	Acc%
ABI (N=3) $R^2=0,9980\pm 0,0004$	0,1	0,10 \pm 0,02	19,0	100
	1	1,00 \pm 0,04	3,9	100
	2,5	2,50 \pm 0,10	4,0	99

RESULTS AND DISCUSSION

	10	10,10±0,31	3,1	101
	17,5	17,70±0,52	3,0	101
	25	24,90±0,69	2,8	100
	32,5	33,00±0,85	2,6	101
	42,5	42,10±1,77	4,2	99
	50	49,40±1,62	3,3	99
D4A (N=3) R ² = 0,9994±0,0005	0,1	0,10±0,01	6,3	100
	1	1,00±0,03	3,3	100
	2,5	2,50±0,06	2,4	99
	10	9,90±0,23	2,3	99
	17,5	17,70±0,49	2,7	101
	25	25,10±0,80	3,2	100
	32,5	33,00±0,86	2,6	101
	42,5	42,40±1,25	2,9	100
	50	49,5±1,38	2,8	99
APA (N=3) R ² = 0,9991±0,0006	20	20,0±0,5	2,5	100
	200	196,7±7,8	4,0	98
	500	495,2±17,3	3,5	99
	2000	2043,5±98,1	4,8	102
	3500	3491,0±109,8	3,1	100
	5000	4939,3±385,3	7,8	99
	6500	6739,3±283,8	4,2	104
	8500	8373,0±202,9	2,4	99
	10000	9755,8±567,3	5,8	98
N-desmethyl APA (N=3) R ² = 0,9975±0,0012	20	19,8±1,0	5,2	99
	200	213,6±6,4	3,0	107
	500	524,7±25,2	4,8	105
	2000	1829,5±65,9	3,1	107
	3500	3559,8±164,8	4,6	102
	5000	4967±112,8	2,3	99
	6500	6370,5±220,3	3,5	98
	8500	7862,2±326,1	4,1	92
	10000	9080,7±427,7	4,7	91
DARO (N=3) R ² = 0,9992±0,0006	20	19,9±0,41	2,0	100
	200	204,7±3,2	1,6	102
	500	517,2±11,9	2,3	103
	2000	2064,0±40,5	2,0	103
	3500	3546,7±125,2	3,5	101
	5000	5005,8±122,5	2,4	100
	6500	6456,8±86,9	1,3	99
	8500	8115,2±272,6	3,4	95
	10000	9511,5±348,2	3,7	95
keto-DARO (N=3)	20	19,9±1,3	6,5	99
	200	208,6±5,4	2,6	104

R ² = 0,9989±0,0004	500	520,5±17,2	3,3	104
	2000	2037,3±62,7	3,1	102
	3500	3487,8±98,2	2,8	100
	5000	4931,8±141,5	2,9	99
	6500	6476,2±145,4	2,2	100
	8500	8119,3±237,3	2,9	96
	10000	9687,8±428,8	4,4	97
ENZA (N=3) R ² = 0,9987±0,0005	40	39,9±0,5	1,1	100
	400	408,2±11,3	2,8	102
	1000	1006,5±17,8	1,8	101
	4000	4277,5±80,8	1,9	107
	7000	7174,7±159,0	2,2	102
	10000	10147,3±338,9	3,3	101
	13000	13023,3±234,6	1,8	100
	17000	15950,0±451,5	2,8	94
N-desmethyl ENZA (N=3) R ² = 0,9995±0,0001	20000	18535,0±448,2	2,4	93
	40	40,0±1,3	3,4	100
	400	404,6±10,2	2,5	101
	1000	974,8±17,0	1,7	97
	4000	4077,8±98,3	2,4	102
	7000	6988,7±194,1	2,8	100
	10000	10032,7±192,4	1,9	100
	13000	13161,7±248,6	2,2	101
	17000	16541,7±463,1	2,8	97
20000	20150,0±673,1	3,3	101	

Table 13. Linearity, accuracy and precision data for calibration curves of all the compounds.

4.2.5 Accuracy and precision

Method precision and accuracy were assessed by analysing five replicates for each QC concentration level. Both intra-day and inter-day evaluations were performed using this approach, with inter-day analyses conducted over three separate working days to ensure reproducibility and consistency of the results. For all compounds, intra-day accuracy ranged from 85% (84% for ABI at LLOQ level) to 110%, while precision was $\leq 12.9\%$ (16.1% for ABI at LLOQ level), and for the inter-day, considering all the analytes, accuracy ranged from 90% to 106%, while precision was $\leq 11.6\%$.

RESULTS AND DISCUSSION

Analyte	Nominal conc. (ng/mL)	Run 1		
		mean \pm SD (ng/mL)	Acc%	CV%
ABI	0,1	0,09 \pm 0,01	92	16,1
	0,25	0,24 \pm 0,02	94	9,4
	18,75	17,94 \pm 0,88	101	1,0
	37,5	35,95 \pm 1,46	98	2,0
D4A	0,1	0,10 \pm 0,01	104	12,9
	0,25	0,21 \pm 0,02	85	8,4
	18,75	17,63 \pm 0,36	94	2,0
	37,5	34,80 \pm 0,87	93	2,5
APA	20	20,8 \pm 1,0	104	4,6
	50,25	48,2 \pm 3,0	96	6,1
	3750	3895,2 \pm 127,4	104	3,3
	7500	7442,6 \pm 355,4	99	4,8
N-desmethyl APA	20	19,3 \pm 1,3	97	6,7
	50,25	51,0 \pm 1,6	101	3,1
	3750	4140,0 \pm 203,3	110	4,9
	7500	7368,8 \pm 447,9	98	6,1
DARO	20	20,0 \pm 0,5	100	2,4
	50,25	49,9 \pm 2,1	99	4,3
	3750	4030,4 \pm 70,5	107	1,7
	7500	7530,0 \pm 138,4	100	1,8
keto-DARO	20	18,2 \pm 2,3	91	12,5
	58	57,2 \pm 3,3	99	5,8
	4300	4417,8 \pm 124,8	103	2,8
	8600	8293,2 \pm 228,1	96	2,8
ENZA	40	39,3 \pm 0,9	98	2,2
	100,5	92,5 \pm 2,5	92	2,7
	7500	7835,0 \pm 123,3	104	1,6
	15000	14200,0 \pm 270,6	95	1,9
N-desmethyl ENZA	40	41,0 \pm 0,7	102	1,6
	100,5	94,7 \pm 4,1	94	4,3
	7500	7847,6 \pm 206,0	105	2,6
	15000	14798,0 \pm 540,2	99	3,7
Analyte	Nominal conc. (ng/mL)	Run 2		
		mean \pm SD (ng/mL)	Acc%	CV%
ABI	0,1	0,09 \pm 0,01	95	9,2
	0,25	0,24 \pm 0,02	95	6,9
	18,75	17,03 \pm 0,29	91	1,7
	37,5	34,29 \pm 0,87	91	2,5
D4A	0,1	0,11 \pm 0,01	108	11,0
	0,25	0,25 \pm 0,01	100	3,8

RESULTS AND DISCUSSION

	18,75	16,43±0,33	88	2,0
	37,5	32,84±0,14	88	0,4
APA	20	20,8±0,8	104	3,9
	50,25	50,2±2,3	100	4,6
	3750	3666,6±105,3	98	2,9
	7500	7305,4±70,7	97	1,0
N-desmethyl APA	20	19,1±0,8	95	4,3
	50,25	53,1±2,9	106	5,5
	3750	3960,0±64,0	106	1,6
	7500	7545,8±236,4	101	3,1
DARO	20	20,2±0,5	101	2,3
	50,25	49,7±1,7	99	3,3
	3750	3726,6±98,2	99	2,6
	7500	7377,0±120,0	98	1,6
keto-DARO	20	21,6±1,1	108	5,1
	58	56,2±3,7	97	6,6
	4300	4051,0±125,9	94	3,1
	8600	8073,6±77,8	94	1,0
ENZA	40	41,6±2,0	104	4,7
	100,5	99,1±2,8	99	2,8
	7500	7268,2±204,6	97	2,8
	15000	13858,0±258,2	92	1,9
N-desmethyl ENZA	40	39,1±1,5	98	3,8
	100,5	97,1±3,2	97	3,3
	7500	7174,4±284,1	96	4,0
	15000	1448,0±405,2	97	2,8
			Run 3	
Analyte	Nominal conc. (ng/mL)	mean ±SD (ng/mL)	Acc%	CV%
ABI	0,1	0,08±0,00	84	2,9
	0,25	0,24±0,01	97	4,8
	18,75	17,80±0,36	95	2,0
	37,5	36,76±0,89	98	2,4
D4A	0,1	0,11±0,004	106	3,6
	0,25	0,24±0,02	89	8,2
	18,75	16,64±0,36	89	2,2
	37,5	34,55±0,55	92	1,6
APA	20	19,2±0,8	96	4,1
	50,25	49,3±2,8	98	5,8
	3750	3608,6±84,3	96	2,3
	7500	7337,2±221,0	98	3,0
N-desmethyl APA	20	18,1±1,1	91	6,2
	50,25	54,5±2,0	108	3,6
	3750	3853,8±111,0	108	2,9
	7500	7423,4±111,7	99	1,5

RESULTS AND DISCUSSION

DARO	20	20,3±1,1	101	5,4
	50,25	54,0±1,2	108	2,3
	3750	3877,4±93,4	103	2,4
	7500	7423,8±160,2	99	2,2
keto-DARO	20	21,0±1,0	105	4,5
	58	59,9±1,6	103	2,7
	4300	4217,0±64,9	98	1,5
	8600	8199,2±122,6	95	1,5
ENZA	40	38,1±1,8	95	4,7
	100,5	101,4±3,8	101	3,7
	7500	7435,4±271,1	99	3,6
	15000	14066,0±343,1	94	2,4
N-desmethyl ENZA	40	40,9±2,7	102	6,6
	100,5	107,5±5,0	107	4,6
	7500	7435,2±249,8	99	3,4
	15000	14958,0±185,0	100	1,2

Table 14, intraday accuracy and precision.

Analyte	Nominal conc. (ng/mL)	mean ±SD (ng/mL)	Acc%	CV%
ABI	0,1	0,09±0,01	90	11,6
	0,25	0,24±0,02	95	6,8
	18,75	17,94±0,88	96	4,9
	37,5	35,98±1,46	96	4,1
D4A	0,1	0,11±0,01	106	9,4
	0,25	0,23±0,02	94	9,6
	18,75	16,90±0,63	90	3,7
	37,5	34,07±1,06	91	3,1
APA	20	20,3±1,1	101	5,4
	50,25	49,2±2,7	98	5,4
	3750	3726,5±162,0	99	4,4
	7500	7361,7±234,9	98	3,2
N-desmethyl APA	20	18,9±1,2	94	6,1
	50,25	52,9±2,6	105	4,8
	3750	3984,6±177,3	106	4,5
	7500	7446,0±287,6	99	3,9
DARO	20	20,2±0,7	101	3,5
	50,25	51,2±2,6	102	5,1
	3750	3878,1±152,2	103	3,9
	7500	7443,6±146,0	99	2,0

keto-DARO	20	20,3±2,1	101	10,3
	58	57,8±3,2	100	5,6
	4300	4228,6±185,1	98	4,4
	8600	8188,7±171,9	95	2,1
ENZA	40	39,7±2,1	99	5,3
	100,5	97,7±4,8	97	4,9
	7500	7513,1±313,2	100	4,2
	15000	14041,3±307,9	94	2,2
N-desmethyl ENZA	40	40,3±1,9	101	4,7
	100,5	99,8±6,9	99	6,9
	7500	7485,7±367,9	100	4,9
	15000	14745,3±427,0	98	2,9

Table 15, interday accuracy and precision

4.2.6 Carry-over

Carry-over was evaluated in one of the accuracy and precision analysis. Initially, a non-negligible carry-over was observed for ABI and DARO, despite the use of a standard needle-wash solution consisting of 70% MeCN, 30% H₂O, and 1% formic acid. Considering the chemical properties of these molecules, the needle wash was subsequently replaced with a slightly basic mixture, 80% MeCN, 20% H₂O, and 0.05% NH₃, which improved residue removal and effectively reduced carry-over. The area of the carry-over in the blank sample after the ULoQ compared with the analyte response at the LLOQ, is 1.1% for ABI, 7.3% for D4A, 6.6% for APA, 5.4% for N-desmethyl APA, 1.6% for DARO, 6.2% for keto-DARO, 4.1% for ENZA, and 8.0% for N-desmethyl ENZA. The area of the interfering components compared with the response of the IS at the LLOQ for all analytes is less than 0.3%, with a maximum of 0.3% for N-desmethyl APA and a minimum of 0.001% for ABI.

4.2.7 Dilution integrity

The dilution integrity for ABI and D4A was evaluated at two dilution factors, 1:5 and 1:2 by diluting a plasma sample at a concentration value higher than the ULoQ, prepared in pooled plasma. As reported in Table 16, the accuracy and CV% resulted in being within 98%-104% and ≤4.2% for all analytes, demonstrating that samples having a concentration

out of the range established by the method can be quantified after appropriate dilution without affecting precision and accuracy of the analysis.

4.2.8 Stability and reinjection reproducibility

Table 16 reports the results of analyte stability testing under various storage and handling conditions across different biological matrices. In human plasma, all analytes demonstrated good stability following five freeze–thaw cycles at -80°C . After sample preparation, all compounds also remained stable in the autosampler at 4°C for up to five days.

Bench-top stability was evaluated in both plasma and whole blood. In plasma, all analytes were stable for up to 4 hours at room temperature (RT), except APA, which showed stability for only 2 hours. Based on the observed accuracy values for ABI, D4A, APA, and N-desmethyl APA (ranging from 87% to 92%), plasma samples should not be left at RT for extended periods to prevent underestimation of analyte concentrations.

The stability of analytes in whole blood was assessed at RT and 4°C after 0.5, 1, 2, and 4 hours. ENZA, N-desmethyl ENZA, APA, and N-desmethyl APA remained stable for up to 4 hours under both conditions (accuracy 91–105%, $\text{CV}\% \leq 10.4\%$), while ABI and D4A were stable for 2 hours at both RT and 4°C (accuracy 100–109%, $\text{CV}\% \leq 7.9\%$).

	(% to concentration at the initial point)			
	QC Low		QC High	
	acc%	CV%	acc%	CV%
ABI				
<i>RT in plasma (4 h)</i>	87	6,2	87	4,4
<i>5 freeze/thaw cycles</i>	97	1,4	93	2
<i>processed sample (T=4°C, 5 days)</i>	93	8,5	101	1,5
<i>RT in blood (2h)</i>	106	7,0	100	0,9
<i>4 °C in blood (2h)</i>	106	2,8	100	4,2
<i>dilution integrity</i>	<i>factor 2</i>		<i>factor 5</i>	
	100	4,2	98	0,9
D4A				
<i>RT in plasma (4 h)</i>	90	3,7	88	4,4
<i>5 freeze/thaw cycles</i>	99	8,2	92	0,7
<i>processed sample (T=4°C, 5 days)</i>	99	7,3	102	1,6
<i>RT in blood (2h)</i>	106	7,9	106	2,6
<i>4 °C in blood (2h)</i>	109	7,6	101	3,3
<i>dilution integrity</i>	<i>factor 2</i>		<i>factor 5</i>	
	104	2,4	102	2,2
APA				
<i>RT in plasma (2 h)</i>	87	0,5	90	1,7

<i>5 freeze/thaw cycles</i>	91	3,7	97	2,8
<i>processed sample (T=4°C, 5 days)</i>	108	3,4	110	2,2
<i>RT in blood (4h)</i>	96	10,4	104	2,9
<i>4 °C in blood (4h)</i>	91	8,1	98	1,8
N-desmethyl APA				
<i>RT in plasma (4 h)</i>	92	6,4	87	2,4
<i>5 freeze/thaw cycles</i>	103	3,2	97	3,1
<i>processed sample (T=4°C, 5 days)</i>	113	1,4	104	1,2
<i>RT in blood (4h)</i>	97	9,8	101	3,9
<i>4 °C in blood (4h)</i>	95	10,3	100	1,5
DARO				
<i>RT in plasma (4 h)</i>	107	0,8	97	4,7
<i>5 freeze/thaw cycles</i>	107	1,3	104	3,5
<i>processed sample (T=4°C, 5 days)</i>	103	4	99	1,1
keto-DARO				
<i>RT in plasma (4 h)</i>	109	8,3	94	4,5
<i>5 freeze/thaw cycles</i>	104	2,1	99	5,0
<i>processed sample (T=4°C, 5 days)</i>	108	8	99	1,6
ENZA				
<i>RT in plasma (4 h)</i>	101	2,8	92	3,3
<i>5 freeze/thaw cycles</i>	100	0,9	98	3,8
<i>processed sample (T=4°C, 5 days)</i>	104	3,2	104	1,8
<i>RT in blood (4h)</i>	97	12,3	101	1,4
<i>4 °C in blood (4h)</i>	96	9,9	102	2,4
N-desmethyl ENZA				
<i>RT in plasma (4 h)</i>	104	1,6	99	3,6
<i>5 freeze/thaw cycles</i>	100	2,7	107	2,1
<i>processed sample (T=4°C, 5 days)</i>	105	3,1	105	1,8
<i>RT in blood (4h)</i>	100	8,0	105	2,5
<i>4 °C in blood (4h)</i>	99	6,4	102	4,8

Table 16, Stability at 4 °C and room temperature in plasma and whole blood, extracted-sample stability at 4 °C, freeze and thaw cycles, and dilution integrity for ABI and D4A.

DARO and its metabolite keto-DARO showed a different behaviour. At lower concentrations, DARO levels increased rapidly, reaching up to 153% of the initial value after 4 hours at RT (Table 17). Concurrently, keto-DARO concentrations decreased to approximately 35% of the baseline value after 4 hours at RT, with a less pronounced effect at 4°C. This pattern suggests a partial back-conversion of keto-DARO to DARO, as previously described, at low concentrations¹³⁸. Supporting this hypothesis, the combined concentration of DARO and keto-DARO remained nearly unchanged over time (Figure 32). Conversely, at higher concentrations, both compounds maintained stability for 4 hours under all tested conditions.

RESULTS AND DISCUSSION

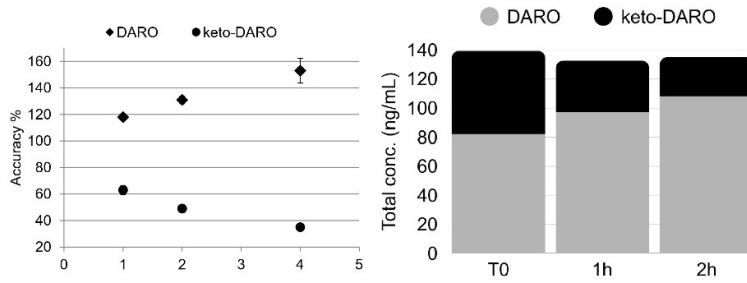


Figure 32, Trend of DARO and keto-DARO accuracies over time (left), and summed concentrations of DARO and keto-DARO shown in the columns on the right.

	DARO				keto-DARO			
	QC Low		QC High		QC Low		QC High	
	acc%	CV%	acc%	CV%	acc%	CV%	acc%	CV%
<i>RT in blood (0.5h)</i>	112	7,7	100	1,2	99	11,3	99	2,0
<i>RT in blood (1h)</i>	118	2,1	109	1,5	63	3,4	102	2,5
<i>RT in blood (2h)</i>	131	2,9	111	2,9	49	2,1	97	3,0
<i>RT in blood (4h)</i>	153	9,3	114	5,5	35	1,4	89	3,1
<i>4 °C in blood (0.5h)</i>	113	8,5	101	1,2	101	11,1	100	1,1
<i>4 °C in blood (1h)</i>	119	4,0	107	2,1	81	2,5	105	1,7
<i>4 °C in blood (2h)</i>	121	2,3	106	1,8	69	3,9	101	2,6
<i>4 °C in blood (4h)</i>	115	7,5	101	3,9	78	13,9	97	2,9

Table 17, Stability of DARO and keto-DARO at multiple time points in whole blood and plasma.

As shown in the table, both DARO and keto-DARO were found to be stable up to 0.5 hours at both RT and 4 °C. This information was crucial for defining the conditions for patient sample collection. Similarly to ABI, it was therefore decided to keep the blood collection tubes on ice immediately after sampling and to process the plasma within 30 minutes from collection to ensure the integrity of the analytes and prevent potential degradation or interconversion phenomena.

4.3 Application of the method in human plasma samples

After validation, the developed method was applied to quantify ABI, APA, DARO, ENZA, and their active metabolites in 157 plasma samples collected from 68 prostate cancer patients enrolled in the above-mentioned clinical study (protocol code: CRO-2025-12). Patients' demographic characteristics are reported in Table 18, along with the number of patients and sample collected per drug. As listed in Table 18, patients were receiving ABI at the doses of 500 and 100 mg/die, APA at the doses of 60, 120, 180, and 240 mg/die, DARO at the doses of 300, 600, and 1200 mg/die, and ENZA at the doses of 80, 120, and 160 mg/die.

Patients' characteristics	N	
		ABI
	APA	73 (60-81)
	DARO	65 (53-76)
Age (range)	ENZA	77 (63-84)
Therapy	ABI (13 patients, 32 samples)	5 samples at 500 mg/die
		26 samples at 1000 mg/die
	APA (21 patients, 53 samples)	1 sample at 60 mg/die
		15 samples at 120 mg/die
		4 samples at 180 mg/die
		33 samples at 240 mg/die
	DARO (10 patients, 27 samples)	1 sample at 300 mg/die
		3 samples at 600 mg/die
		23 samples at 1200 mg/die
	ENZA (17 patients, 46 samples)	14 samples at 80 mg/die
		4 samples at 120 mg/die
		28 samples at 160 mg/die

Table 18, Principal demographic and clinical characteristics of the enrolled patients.

Not all patient samples were collected precisely at the expected C_{\min} (see section 3.3.2), and for this reason, a conversion formula, widely applied in previous PK studies, such as those on imatinib¹³⁹, was used to recalculate concentrations. The log-linear extrapolation was performed using the following established algorithm:

$$C_{\min,SS} = C_{\text{measured}} \times 0.5^{\frac{TAD}{t_1/2}}$$

where TAD is the time elapsed since the last administered dose, and $t_{1/2}$ represents the reported elimination half-life of the drug.

To apply this formula accurately, it was essential to record both the exact time of the last drug intake and the time of venous blood sampling. These data, together with the known half-life of each analyte, allowed for reliable recalculation of the predicted trough concentrations.

Particular attention was required for ABI, since, as reported in literature¹⁴⁰, the use of this formula may not ideally estimate C_{\min} when dealing with compounds that exhibit high variability or complex PKs. In such cases, an alternative approach has been suggested, which approximates C_{\min} by taking the ratio of the observed concentration to the population-predicted concentration from a population PK model, and then multiplying this ratio by the simulated population.

Although the development of a population PK model for ABI would allow for a more accurate estimation of trough levels, this was not feasible within the current study due to time constraints. However, the implementation of such a model is planned for future investigations.

4.3.1 Abiraterone

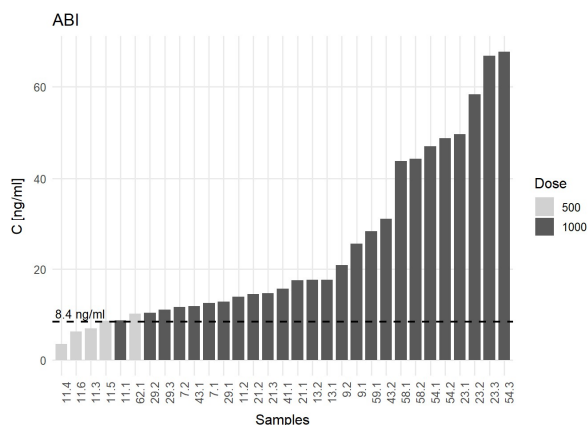


Figure 33, C_{\min} values for all ABI samples analyzed; the dashed line indicates the efficacy target established in previous studies. Different colors represent different doses, as detailed in the legend.

As previously described, the reported concentrations were normalized to the theoretical trough level using the correction formula (see Section 4.3). In the figure, each bar represents the calculated ABI C_{\min} for each collected sample, while the horizontal line at 8.4 ng/mL marks the efficacy threshold proposed in literature (see section 1.1.1.1). Samples are color-coded according to the administered dose, as indicated in the legend. Each sample label reports the progressive patient identifier followed by a second progressive number

indicating the specific draw, allowing each measurement to be uniquely traced to both the subject and the corresponding sampling occasion. Overall, most concentrations are above the therapeutic threshold, with only a few samples falling below it. A total of 13 patients with 31 samples were included in the analysis of ABI trough concentrations. The global mean C_{\min} across patients (mean of patient means) was 24.65 ± 16.96 ng/mL, corresponding to a between-subject coefficient of variation (CV%) of 68.8%, indicating pronounced inter-individual variability in systemic exposure. This high variability is consistent with what is already reported for ABI PKs and reflects substantial differences among patients in terms of absorption, adherence, and metabolic profile.^{45,48}

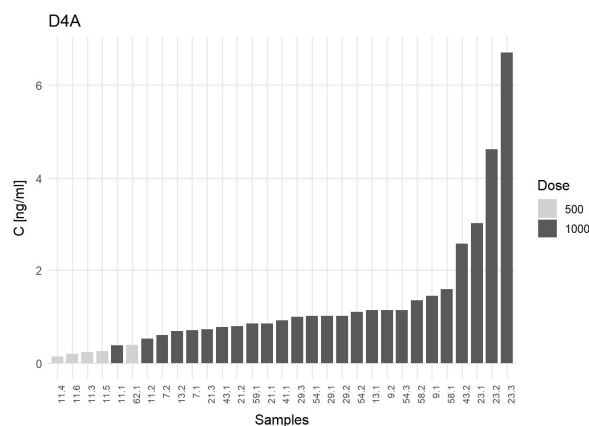


Figure 34, C_{\min} values for all D4A samples analyzed. Different colors represent different doses, as detailed in the legend.

Variability analysis was also extended to the active metabolite D4A. The figure reports the calculated C_{\min} for each sample, ordered from the lowest to the highest value. As for ABI, samples are colour-coded according to the administered dose at the time of collection. D4A concentrations show a wide dispersion, with several samples close to zero and a progressive increase in the upper tail of the distribution. Across the 13 patients included in this analysis, the global mean D4A C_{\min} (mean of patient means) was 1.24 ± 1.13 ng/mL, corresponding to a between-subject coefficient of variation of 91.1%. This confirms a very pronounced inter-individual variability, even higher than that observed for the parent compound. The distribution in the graph reflects this pattern, with values spanning more than one order of magnitude across subjects.

Intra-patient variability was also assessed for ABI. For this analysis, only patients with at least two available samples were included; three patients had a single blood draw and were therefore excluded from the calculation.

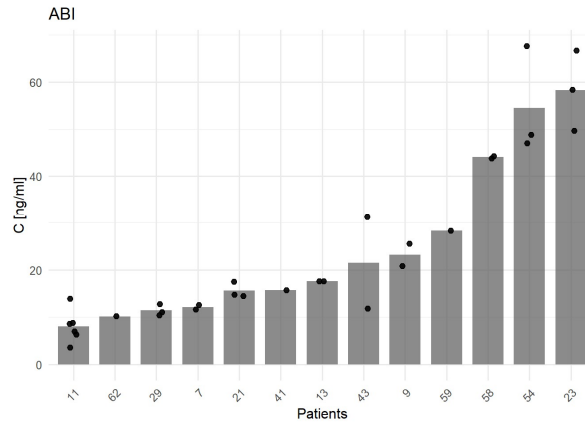


Figure 35, C_{min} values shown as black points for each ABI patient, with the bar representing the mean calculated C_{min} .

For ABI, the bar-and-dot plot displays for each patient the mean C_{min} (bar) together with all individual sampling points (dots). The dispersion of measurements around the mean highlights a clear intra-individual variability, with patients showing fluctuations across different sampling times. Quantitatively, the intra-patient coefficient of variation showed a median of 12.7%, and values spanning from 0.2% to 63.7%. This confirms that, although intra-individual variability is generally moderate, some patients exhibit pronounced fluctuations.

For the metabolite D4A, the same visualization reveals a broader spread of values within several patients, consistent with the higher variability observed globally for this analyte. However, the most clinically relevant factor is the variation in the inter- and intra-patient metabolic ratio, as discussed in Section 1.1.1.1. Previous studies reported that a higher

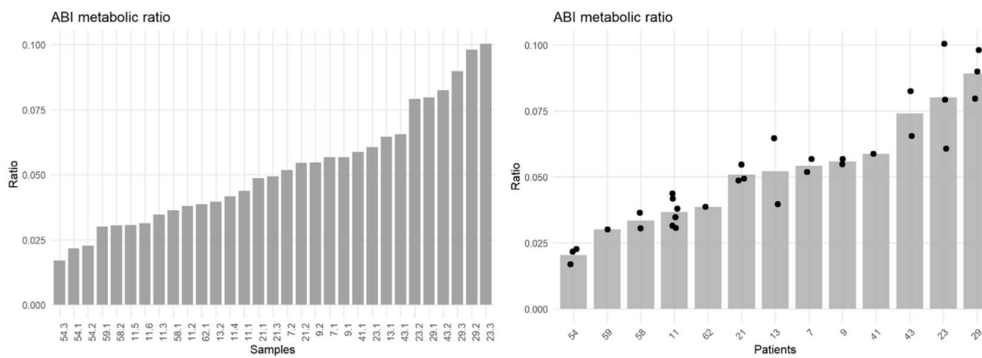


Figure 36, Metabolic ratio D4A/ABI values displayed on the left for individual samples and on the right grouped by patient.

D4A/ABI ratio is associated with shorter PFS and overall survival, suggesting that interindividual differences in the conversion rate from ABI to D4A can influence treatment efficacy.⁴⁶

Conversely, most cohorts did not show a consistent association between this ratio and clinically significant adverse events.

For these reasons, we also investigated the D4A/ABI ratio in our cohort. Figure 36 displays on the right, the metabolic ratio for each patient, calculated as the mean D4A concentration divided by the mean ABI concentration, and on the left the metabolic ratio for each sample. The mean ratio was 0.05 ± 0.02 , ranging from 0.02 to 0.09 corresponding to a between-subject CV of 39.2%. The metabolic ratio showed notable intra-patient heterogeneity. Among the ten patients with more than one sample, the mean intra-patient CV% was 14.3, ranging from 2.5% to 34.0%, indicating that some subjects displayed minimal fluctuations across repeated measurements while others showed substantial variability.

Published data provide useful reference points for contextualising the metabolic ratio observed in our cohort. One study reported a median D4A/ABI ratio of 0.047 (IQR 0.018–0.079)⁴⁷, while another described a mean D4A/ABI ratio of 0.18 ± 0.25 ⁴⁶. Compared with these values, the metabolic ratio measured in our population (mean 0.0518 ± 0.0203 , CV 39.2%) is closer to the lower range of previously published distributions and more consistent with the median-based estimate than with the markedly higher mean reported by the second study, which reflects a substantially more dispersed dataset.

A comparison of absolute metabolite concentrations is also informative. Literature reports D4A plasma levels (median \pm SD) of 1.0 ± 0.9 ng/mL⁴⁵, whereas in our dataset the pooled mean concentration was 1.24 ± 1.13 ng/mL. Thus, our measurements align with the expected magnitude of circulating D4A but show slightly higher dispersion, consistent with the broader inter-individual variability observed for both the parent drug and metabolite in our cohort.

Clinical data collection in our cohort is ongoing, and these observations will allow us to evaluate whether similar or divergent exposure–toxicity relationships emerge in our population.

4.3.2 Apalutamide

Also for APA the concentrations were normalized as described in section 4.3. The first graph report, for each patient, the mean APA concentration (bar) together with all

individual sampling points (dots). The distribution of individual points around the bar highlights the intra-individual fluctuations, with few patients showing noticeable dispersion between repeated measures.

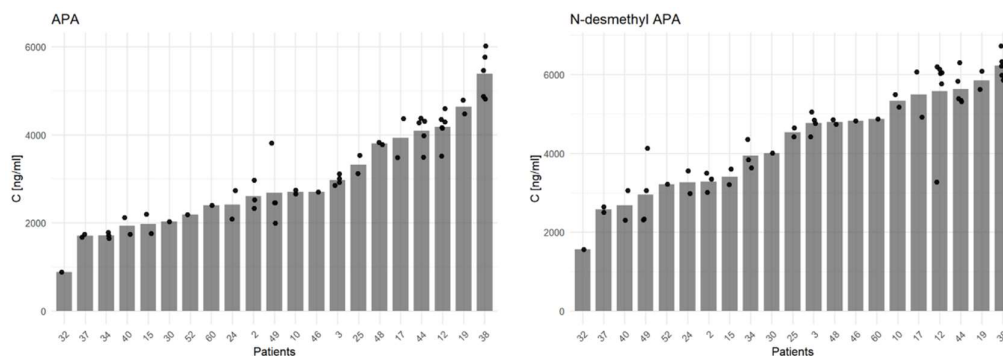


Figure 37, C_{min} values shown as black points for each APA patient, with the bar representing the mean calculated C_{min} . On the left the C_{min} of APA, on the right the C_{min} of N-desmethyl APA.

Across all patients with at least two samples ($n = 16$), the intra-patient CV% showed a mean of 10.1% (range 0.9% to 29.2%). This indicates that APA exposure is generally stable within the same individual, with only a minority of patients showing marked fluctuations. For the metabolite N-desmethyl-APA, intra-patient variability was comparable, with a mean CV of 10.0% (range 1.8–28.9%). These findings demonstrate that both analytes exhibit low-to-moderate within-subject variability at steady state. Between-patient variability was quantified by averaging concentrations within each subject and comparing these means across the cohort. The resulting mean APA concentration was 2868 ± 1116 ng/mL (CV% of 38.9%) for the parent drug and 4228 ± 1270 ng/mL (CV% of 30.0%) for N-desmethyl APA, confirming a substantial inter-individual variability in systemic exposure. This pattern aligns with the broad range of values visible in the bar-and-dot plots, where patient means vary from approximately 1500 ng/mL to more than 5000 ng/mL for both analytes.

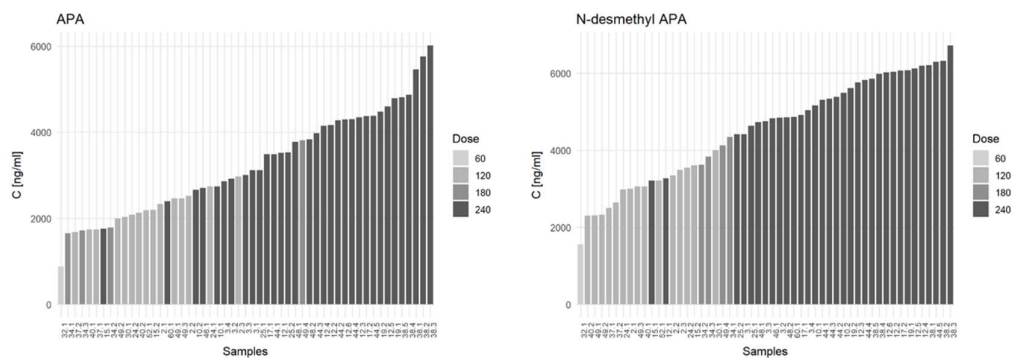


Figure 38, C_{min} values for all APA samples analyzed. Different colours represent different doses, as detailed in the legend. On the left the C_{min} of APA, on the right the C_{min} of N-desmethyl APA.

Part of the intra-individual variability can be ascribed to the different drug dose assumed by patients (60, 120, 180, and 240 mg). For this reason, to further explore the relationship between exposure and clinical dosing, an additional set of graphs displays individual concentrations stratified by dose level (60, 120, 180, and 240 mg). For each dose group, all measurements are shown as points, and the horizontal bar represents the mean concentration at that dose. The figures reveal the expected monotonic increase in both parent and metabolite concentrations across ascending dose tiers. The dispersion around the dose-specific means remains moderate, in line with the intra-patient variability described above.

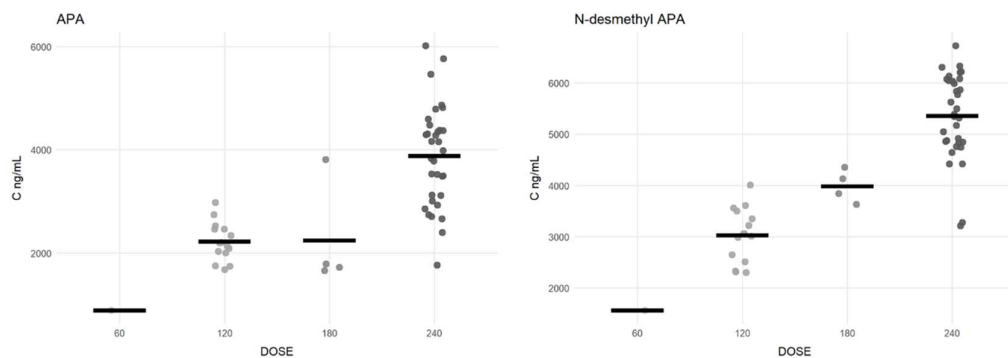


Figure 39, C_{min} values shown as individual points divided by patient dose, with APA on the left and N-desmethyl APA on the right.

For APA, the metabolic ratio was assessed with a descriptive approach. The between-patient mean metabolic ratio was 1.6 ± 0.5 , with a CV of 31.9%, indicating heterogeneity across subjects. Intra-patient variability was moderate instead: among 9 patients with repeated measurements, the mean intra-patient CV was 14.2% (range from 3.2% to 24.1%).

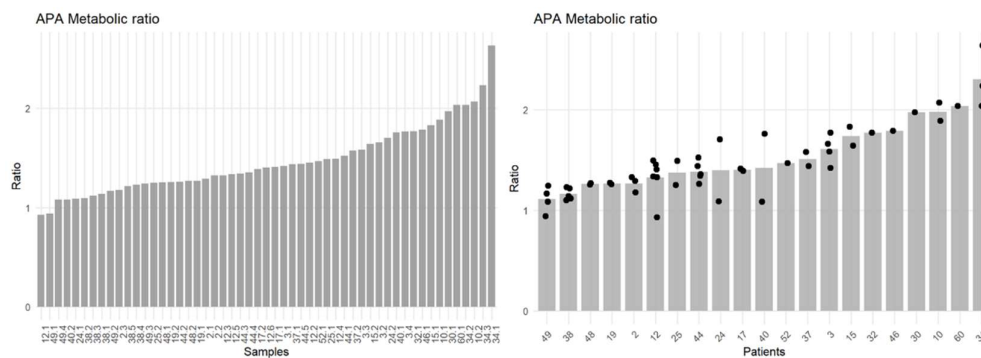


Figure 40, Metabolic ratio APA/N-desmethyl APA values displayed on the left for individual samples and on the right grouped by patient.

4.3.3 Darolutamide

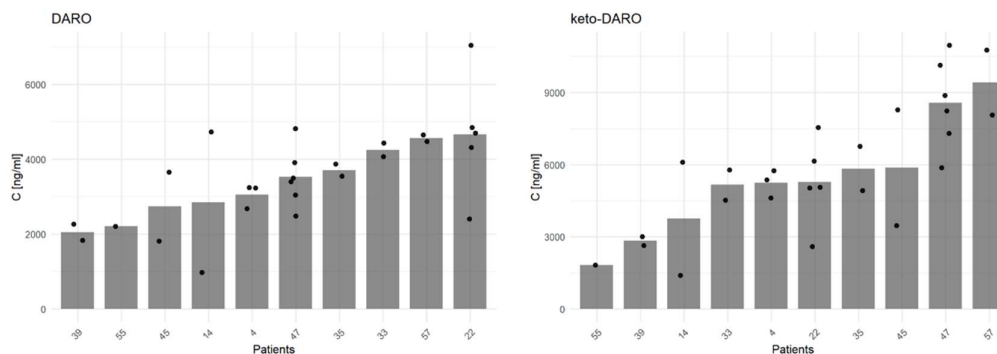


Figure 41, C_{min} values shown as black points for each DARO patient, with the bar representing the mean calculated C_{min} . On the left the C_{min} of DARO, on the right the C_{min} of keto-DARO.

The first set of graphs displays, for each patient, the mean DARO concentration (bars) together with all individual sampling points (dots). DARO concentrations showed marked variability both between and within subjects. Across the analysed cohort, samples spanned from approximately 1800 to more than 7000 ng/mL, with several patients showing tight clustering of replicates and others showing wide dispersion. This qualitative inspection already highlights substantial PK heterogeneity. Patients with at least two available samples were included in the intra-patient variability assessment. For DARO, 9 patients met this requirement. Intra-individual CV% was 28.0% (range from 0.7% to 90.3%). These data indicate that, while several patients maintained relatively stable concentrations across repeated measurements, others exhibited extremely large fluctuations, consistent with variable PK behaviour on different dosing days. keto-DARO, showed comparable variability patterns within individuals. Among the ten patients with more than one sample, the mean intra-patient CV was 31.4% (range from 9.5% to 88.4%) comparable with the

parent compound. Between-patient variability was quantified by averaging the concentration of each analyte per patient and comparing these means across the cohort. For DARO, the global mean was 8735 ± 3034 ng/mL, (CV% of 34.7%). For keto-DARO, the mean concentration across subjects was 5376 ± 2324 ng/mL (CV of 43.6%).

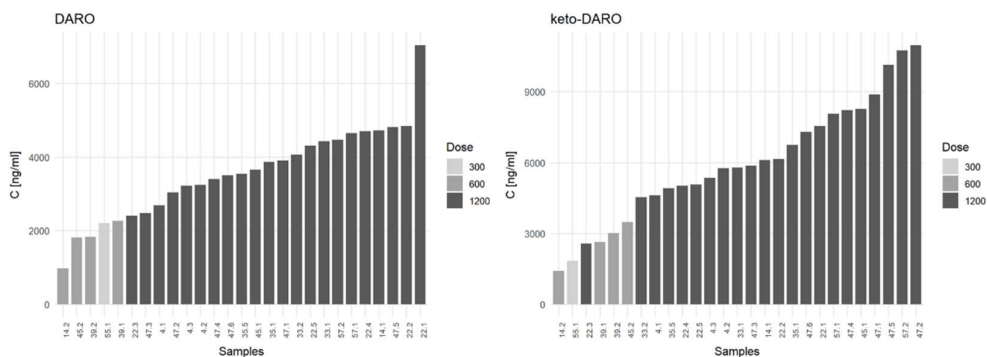


Figure 42, C_{min} values for all DARO samples analyzed. Different colours represent different doses, as detailed in the legend. On the left the C_{min} of DARO, on the right the C_{min} of keto-DARO.

These figures were generated to verify the consistency between clinical dosing information and expected systemic exposure. The dose–concentration relationship was further illustrated in dedicated scatter plots showing individual measurements for each dose group together with a horizontal bar marking the group mean. As expected, samples from patients receiving 1200 mg displayed the highest systemic levels, while 600mg groups showed correspondingly lower concentrations. Despite this overall coherence, the 1200mg group exhibited a wider spread, suggesting the presence of additional modulators such as adherence, timing of administration, or individual absorption differences.

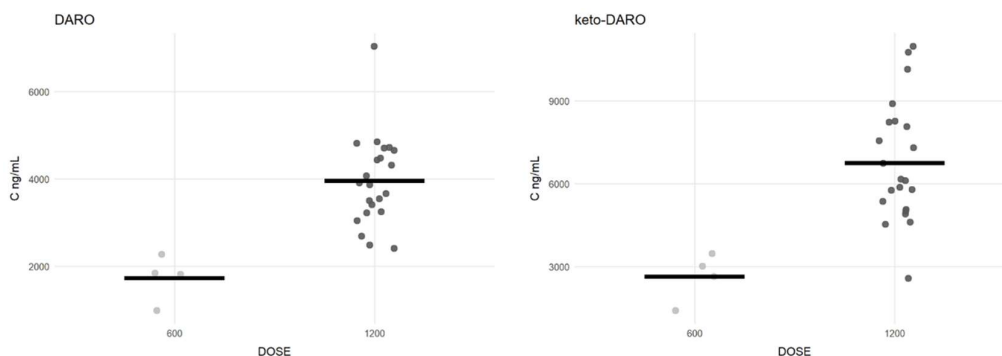


Figure 43, C_{min} values shown as individual points divided by patient dose, with DARO on the left and keto-DARO on the right.

Because keto-DARO can partially reconvert to DARO in whole blood, total exposure may be better represented by the sum of the parent drug and metabolite. To evaluate this possibility, variability analyses were repeated on the combined concentration (DARO + keto-DARO).

The intra-patient CV for the summed analyte had a mean of 28.0% (median 16.0%), with values spanning from 0.7% to 90.3%, closely paralleling the variability observed for DARO alone. At the inter-patient level, the mean total concentration was 8735 ± 3034 ng/mL (CV 34.7%), almost identical to the variability of DARO alone and lower than the variability observed for keto-DARO. To explore inter-patient differences in drug metabolism, the metabolic ratio was evaluated as a descriptive parameter. Only the variability between patients and within patients was considered, without deriving any clinical interpretation since clinical data collection is ongoing.

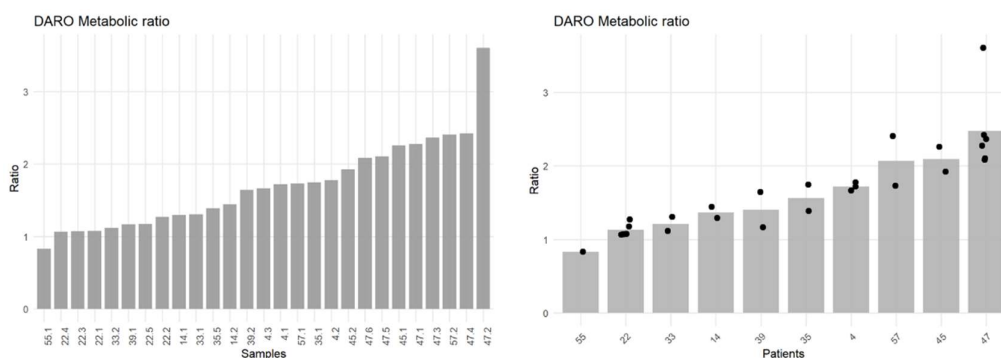


Figure 44, Metabolic ratio DARO/keto-DARO values displayed on the left for individual samples and on the right grouped by patient.

Across patients, the metabolic ratio showed a mean of 1.6 ± 0.3 , corresponding to a between-patient CV of 20.8%. Within-patient variability was modest: among the 16 patients with repeated samples, the mean intra-patient CV was 10.5% (range from 0.8% to 33.6%).

4.3.4 Enzalutamide

The bar-and-dot plots show, for each patient, the mean concentration (bar) together with all individual sampling points (dots). This representation allows direct visual assessment of intra-individual fluctuations as well as the systematic differences in exposure across patients.

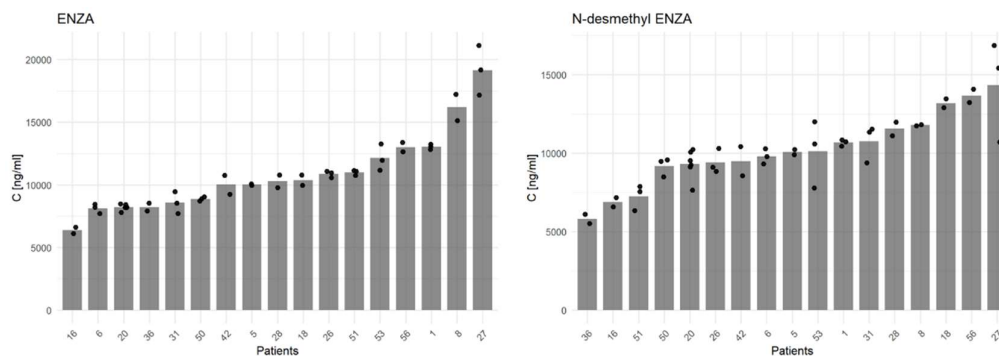


Figure 45, C_{min} values shown as black points for each ENZA patient, with the bar representing the mean calculated C_{min} . On the left the C_{min} of APA, on the right the C_{min} of N-desmethyl APA.

Across the cohort, ENZA exposure demonstrated a wide inter-patient variability. The mean C_{min} (mean of patient means) in our study population was 10850 ± 3172 ng/mL (CV% of 29.7%). Concentrations spanned from values around 6000 ng/mL in the lowest-exposed subjects to over 19000 ng/mL in the highest-exposed patients. Intra-patient variability was quantified for the 17 patients with at least two measurements. The intra-patient CV showed a mean of 5.46% (range 0.82% to 10.8%). These values confirm that ENZA displays limited variability within the same subject, consistent with its long half-life and minimal peak–trough oscillation at steady state. The plotted points for each patient also illustrate this behaviour, with most subjects showing tight clustering of concentrations around their individual mean. The active metabolite N-desmethyl-ENZA exhibited a similar but slightly higher degree of dispersion.

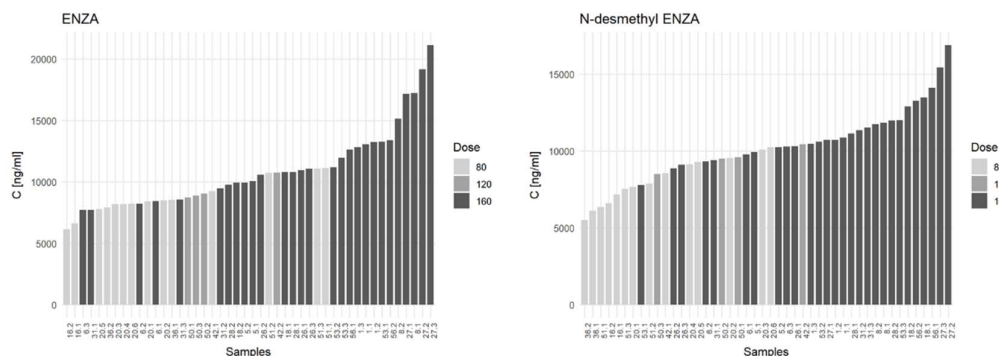


Figure 46, C_{min} values for all ENZA samples analyzed. Different colours represent different doses, as detailed in the legend. On the left the C_{min} of ENZA, on the right the C_{min} of N-desmethyl ENZA.

The global mean C_{min} across subjects was 10199 ± 2366 ng/mL, (CV% of 23.3%). The intra-patient CV for the metabolite averaged 8.25%, (range 0.51%–22.5%). This confirms that N-desmethyl-ENZA displays somewhat larger within-subject fluctuations than ENZA, although still within a narrow and pharmacologically consistent range.

Dose-stratified plots were generated for both the parent compound and its metabolite. Bars represent the individual concentration at each sampling time, coloured according to the administered dose (80, 120, or 160 mg), while the overlaid black line denotes the mean concentration for that dose group. As expected, patients receiving 160 mg showed the highest concentrations, followed by those on 120 mg and 80 mg. Overlap between groups was present but limited, and remained consistent with known inter-individual variability in ENZA PKs.

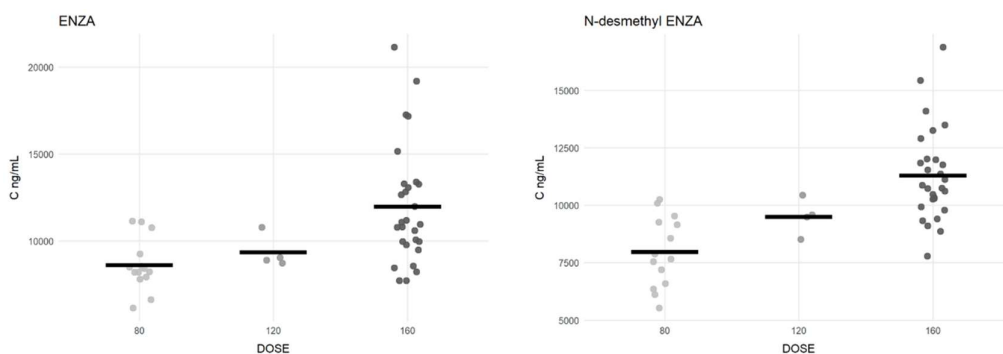


Figure 47, *C_{min}* values shown as individual points divided by patient dose, with ENZA on the left and N-desmethyl ENZA on the right.

Taken together, the variability analyses demonstrate that ENZA shows moderate between-patient dispersion and low within-patient fluctuation, with the metabolite N-desmethyl-ENZA following a nearly parallel behaviour. The consistency between dose levels and measured concentrations further supports the robustness of the analytical measurements and their alignment with clinical dosing information. The metabolic ratio was also examined for ENZA to provide a descriptive picture of metabolic variability. As with the other agents, interpretation is limited to statistical characterization, while clinical correlations will be evaluated once patient data collection is complete. Across the cohort, the metabolic ratio showed a mean of 1.0 ± 0.2 , corresponding to a between-patient CV of 20.5%. Intra-patient variability was generally moderate: among 17 evaluable patients, the mean intra-patient CV was 8.2%, (range from 0.8% to 26.7%). Overall, variability in the ENZA metabolic ratio appears low.

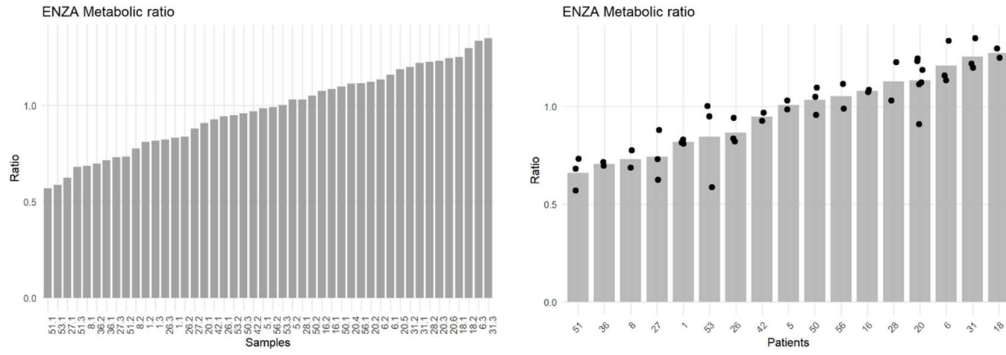


Figure 48, Metabolic ratio ENZA/N-desmethyl ENZA values displayed on the left for individual samples and on the right grouped by patient.

5. CONCLUSIONS

In conclusion, a robust LC–MS/MS method was successfully developed for the simultaneous quantification of ABI, APA, DARO, ENZA, and their active metabolites in human plasma, and it was fully validated according to EMA and FDA guidelines. The assay demonstrated excellent linearity over wide concentration ranges (from low ng/mL levels up to tens of µg/mL, depending on the analyte, e.g. 0.1–50 ng/mL for ABI, 20–10000 ng/mL for APA and 40–20000 ng/mL for ENZA) with correlation coefficients $R^2 \geq 0.997$. Accuracy and precision met all acceptance criteria: intra-day accuracy was ~85–110% (down to 84% at the LLOQ) with precision $\leq 12.9\%$ (CV% up to 16.1% at LLOQ), and inter-day accuracy was 90–106% with precision $\leq 11.6\%$. The simple protein-precipitation sample prep yielded high extraction recovery (94–103%) with low variability (CV% typically $\leq 9\%$, maximally ~13.8% for abiraterone and its metabolite). Matrix effects were negligible: across plasma from seven donors, accuracy remained 86–112% (CV% $\leq 14\%$, improving to $\leq 9.3\%$ when excluding abiraterone/D4A) and even haemolyzed samples gave 85–109% accuracy (CV% $\leq 9.3\%$). All validation parameters (selectivity, carry-over, dilution integrity, stability under various conditions, etc.) were within regulatory guidelines, confirming the method's reliability for accurate and precise quantification of the target drugs and metabolites.

Following the activation of the clinical study protocol PRECISION, a total of 157 plasma samples from 68 prostate cancer patients were collected and analysed. Among these, 13 patients were treated with ABI, showing a mean exposure of 24.65 ± 16.96 ng/mL with an inter-patient variability of 69%. For its metabolite, the average concentration was 1.24 ± 1.13 ng/mL, with 91% variability. 21 patients were on APA, with a mean exposure of 2868 ± 1116 ng/mL (CV% 39%), while its metabolite reached 4228 ± 1270 ng/mL (CV% 30%). For DARO, data from 10 patients revealed an average exposure of 8735 ± 3034 ng/mL (CV% 35%) and 5376 ± 2324 ng/mL for its metabolite (CV% 43.6%). 17 patients were treated with ENZA, with mean concentrations of $10,850 \pm 3172$ ng/mL (CV% 29.7%) and $10,199 \pm 2366$ ng/mL for its metabolite (CV% 23.3%).

Among all drugs, ABI showed the highest inter-patient variability, a finding consistent with previous literature (see Section 1.1.1.1), supporting the potential clinical relevance of TDM for this agent.

The method is potentially suitable for diagnostic application, as it is fast, simple, and allows the simultaneous quantification of multiple drugs in patients undergoing different hormonal therapies. It is also compatible with routine laboratory workflows. Clinical data collection regarding treatment toxicity and efficacy is currently ongoing to explore correlations between C_{\min} values, therapeutic outcomes, and side effects.

CONCLUSIONS

The next step will be the development and cross-validation of the method using an alternative matrix, specifically DBS, to further expand its applicability in TDM.

REFERENCES

1. Bray F, Laversanne M, Sung H, et al. Global cancer statistics 2022: GLOBOCAN estimates of incidence and mortality worldwide for 36 cancers in 185 countries. *CA Cancer J Clin.* 2024;74(3):229-263. doi:10.3322/caac.21834
2. Sandhu S, Moore CM, Chiong E, Beltran H, Bristow RG, Williams SG. Prostate cancer. *The Lancet.* 2021;398(10305):1075-1090. doi:10.1016/S0140-6736(21)00950-8
3. Attard G, Parker C, Eeles RA, et al. Prostate cancer. *The Lancet.* 2016;387(10013):70-82. doi:10.1016/S0140-6736(14)61947-4
4. Cancer Today. Accessed June 10, 2025. <https://gco.iarc.fr/today/en>
5. I numeri del cancro in Italia. AIOM. Accessed June 10, 2025. <https://www.aiom.it/i-numeri-del-cancro-in-italia/>
6. Rebello RJ, Pearson RB, Hannan RD, Furic L. Therapeutic Approaches Targeting MYC-Driven Prostate Cancer. *Genes.* 2017;8(2):71. doi:10.3390/genes8020071
7. Wasim S, Lee SY, Kim J. Complexities of Prostate Cancer. *Int J Mol Sci.* 2022;23(22):14257. doi:10.3390/ijms232214257
8. Abate-Shen C, Shen MM. Molecular genetics of prostate cancer. *Genes Dev.* 2000;14(19):2410-2434. doi:10.1101/gad.819500
9. Sekhoacha M, Riet K, Motlounq P, Gumenku L, Adegoke A, Mashele S. Prostate Cancer Review: Genetics, Diagnosis, Treatment Options, and Alternative Approaches. *Mol Basel Switz.* 2022;27(17):5730. doi:10.3390/molecules27175730
10. Wilson TK, Zishiri OT. Prostate Cancer: A Review of Genetics, Current Biomarkers and Personalised Treatments. *Cancer Rep Hoboken NJ.* 2024;7(10):e70016. doi:10.1002/cnr2.70016
11. Hjelmborg JB, Scheike T, Holst K, et al. The heritability of prostate cancer in the Nordic Twin Study of Cancer. *Cancer Epidemiol Biomark Prev Publ Am Assoc Cancer Res Cosponsored Am Soc Prev Oncol.* 2014;23(11):2303-2310. doi:10.1158/1055-9965.EPI-13-0568
12. Rebbeck TR. Prostate Cancer Genetics: Variation by Race, Ethnicity, and Geography. *Semin Radiat Oncol.* 2017;27(1):3-10. doi:10.1016/j.semradonc.2016.08.002
13. Gnanapragasam VJ, Greenberg D, Burnet N. Urinary symptoms and prostate cancer-the misconception that may be preventing earlier presentation and better survival outcomes. *BMC Med.* 2022;20(1):264. doi:10.1186/s12916-022-02453-7
14. Merriel SWD, Funston G, Hamilton W. Prostate Cancer in Primary Care. *Adv Ther.* 2018;35(9):1285-1294. doi:10.1007/s12325-018-0766-1
15. Diagnostic and Therapeutic Strategies for Prostate Cancer - PubMed. Accessed June 3, 2025. <https://pubmed.ncbi.nlm.nih.gov/27825428/>

16. Raychaudhuri R, Lin DW, Montgomery RB. Prostate Cancer: A Review. *JAMA*. 2025;333(16):1433-1446. doi:10.1001/jama.2025.0228
17. Munjal A, Leslie SW. Gleason Score. In: *StatPearls*. StatPearls Publishing; 2025. Accessed October 23, 2025. <http://www.ncbi.nlm.nih.gov/books/NBK553178/>
18. Humphrey PA. Histopathology of Prostate Cancer. *Cold Spring Harb Perspect Med*. 2017;7(10):a030411. doi:10.1101/cshperspect.a030411
19. Siegel RL, Giaquinto AN, Jemal A. Cancer statistics, 2024. *CA Cancer J Clin*. 2024;74(1):12-49. doi:10.3322/caac.21820
20. LINEE GUIDA CARCINOMA DELLA PROSTATA | AIOM. Accessed October 16, 2025. <https://www.aiom.it/linee-guida-aiom-2024-carcinoma-della-prostata/>
21. Fizazi K, Gillessen S, ESMO Guidelines Committee. Electronic address: clinicalguidelines@esmo.org. Updated treatment recommendations for prostate cancer from the ESMO Clinical Practice Guideline considering treatment intensification and use of novel systemic agents. *Ann Oncol Off J Eur Soc Med Oncol*. 2023;34(6):557-563. doi:10.1016/j.annonc.2023.02.015
22. Swami U, McFarland TR, Nussenzveig R, Agarwal N. Advanced Prostate Cancer: Treatment Advances and Future Directions. *Trends Cancer*. 2020;6(8):702-715. doi:10.1016/j.trecan.2020.04.010
23. Ryan CJ, Ke X, Lafeuille MH, et al. Management of Patients with Metastatic Castration-Sensitive Prostate Cancer in the Real-World Setting in the United States. *J Urol*. 2021;206(6):1420-1429. doi:10.1097/JU.0000000000002121
24. Prostate cancer: ESMO Clinical Practice Guidelines for diagnosis, treatment and follow-up† - *Annals of Oncology*. Accessed October 23, 2025. [https://www.annalsofoncology.org/article/S0923-7534\(20\)39898-7/fulltext](https://www.annalsofoncology.org/article/S0923-7534(20)39898-7/fulltext)
25. Martínez-Breijo S, Chantada-Abal V, Aller-Rodríguez M, et al. [Castration resistance mechanisms in prostate cancer.]. *Arch Esp Urol*. 2018;71(8):628-638.
26. Hormonal Therapy for Prostate Cancer - PubMed. Accessed July 31, 2025. <https://pubmed.ncbi.nlm.nih.gov/33480983/>
27. Hamilou Z. The evolving options in metastatic castration-sensitive prostate cancer. *Curr Opin Support Palliat Care*. 2020;14(3):270-275. doi:10.1097/SPC.0000000000000507
28. Hoy SM. Apalutamide: A Review in Metastatic Castration-Sensitive Prostate Cancer. *Drugs*. 2020;80(15):1579-1585. doi:10.1007/s40265-020-01401-0
29. Hussain M, Fizazi K, Shore ND, et al. Metastatic Hormone-Sensitive Prostate Cancer and Combination Treatment Outcomes: A Review. *JAMA Oncol*. 2024;10(6):807-820. doi:10.1001/jamaoncol.2024.0591
30. Rathkopf DE, Scher HI. Apalutamide for the treatment of prostate cancer. *Expert Rev Anticancer Ther*. 2018;18(9):823-836. doi:10.1080/14737140.2018.1503954

31. Wenzel M, Nocera L, Collà Ruvolo C, et al. Overall survival and adverse events after treatment with darolutamide vs. apalutamide vs. enzalutamide for high-risk non-metastatic castration-resistant prostate cancer: a systematic review and network meta-analysis. *Prostate Cancer Prostatic Dis.* 2022;25(2):139-148. doi:10.1038/s41391-021-00395-4
32. Markham A, Duggan S. Darolutamide: First Approval. *Drugs.* 2019;79(16):1813-1818. doi:10.1007/s40265-019-01212-y
33. Castro E, Wang D, Walsh S, et al. Matching-adjusted indirect comparison of talazoparib plus enzalutamide versus abiraterone acetate and docetaxel in mCRPC. *Future Oncol Lond Engl.* 2025;21(9):1075-1084. doi:10.1080/14796694.2025.2471200
34. Bhattacharya S, Hirmand M, Phung D, van Os S. Development of enzalutamide for metastatic castration-resistant prostate cancer. *Ann N Y Acad Sci.* 2015;1358:13-27. doi:10.1111/nyas.12846
35. Scher HI, Fizazi K, Saad F, et al. Increased survival with enzalutamide in prostate cancer after chemotherapy. *N Engl J Med.* 2012;367(13):1187-1197. doi:10.1056/NEJMoa1207506
36. Khalaf DJ, Annala M, Taavitsainen S, et al. Optimal sequencing of enzalutamide and abiraterone acetate plus prednisone in metastatic castration-resistant prostate cancer: a multicentre, randomised, open-label, phase 2, crossover trial. *Lancet Oncol.* 2019;20(12):1730-1739. doi:10.1016/S1470-2045(19)30688-6
37. da Silva IP, de Amorim LGCR, Piredda GV, et al. Cabazitaxel versus abiraterone or enzalutamide for metastatic castration-resistant prostate cancer following docetaxel failure: a systematic review and meta-analysis. *Clin Transl Oncol Off Publ Fed Span Oncol Soc Natl Cancer Inst Mex.* 2025;27(8):3465-3476. doi:10.1007/s12094-025-03851-y
38. Abiraterone, INN-abiraterone acetate. Accessed August 6, 2025. https://www.ema.europa.eu/en/documents/product-information/abiraterone-accord-epar-product-information_en.pdf
39. “Abiraterone”-EMA. Zytiga- summary of product characteristics. Published online 2022. https://www.ema.europa.eu/en/documents/product-information/zytiga-epar-product-information_en.pdf
40. Thakur A, Roy A, Ghosh A, Chhabra M, Banerjee S. Abiraterone acetate in the treatment of prostate cancer. *Biomed Pharmacother Biomedecine Pharmacother.* 2018;101:211-218. doi:10.1016/j.biopha.2018.02.067
41. Li Z, Bishop AC, Alyamani M, et al. Conversion of abiraterone to D4A drives anti-tumour activity in prostate cancer. *Nature.* 2015;523(7560):347-351. doi:10.1038/nature14406
42. Han CS, Patel R, Kim IY. Pharmacokinetics, pharmacodynamics and clinical efficacy of abiraterone acetate for treating metastatic castration-resistant prostate cancer. *Expert Opin Drug Metab Toxicol.* 2015;11(6):967-975. doi:10.1517/17425255.2015.1041918

43. Arasaratnam M, Crumbaker M, Bhatnagar A, McKay MJ, Molloy MP, Gurney H. Inter- and intra-patient variability in pharmacokinetics of abiraterone acetate in metastatic prostate cancer. *Cancer Chemother Pharmacol*. 2019;84(1):139-146. doi:10.1007/s00280-019-03862-x
44. Carton E, Noe G, Huillard O, et al. Relation between plasma trough concentration of abiraterone and prostate-specific antigen response in metastatic castration-resistant prostate cancer patients. *Eur J Cancer Oxf Engl 1990*. 2017;72:54-61. doi:10.1016/j.ejca.2016.11.027
45. van Nuland M, Groenland SL, Bergman AM, et al. Exposure-response analyses of abiraterone and its metabolites in real-world patients with metastatic castration-resistant prostate cancer. *Prostate Cancer Prostatic Dis*. 2020;23(2):244-251. doi:10.1038/s41391-019-0179-5
46. Blanchet B, Carton E, Alyamani M, et al. A PK/PD study of Delta-4 abiraterone metabolite in metastatic castration-resistant prostate cancer patients. *Pharmacol Res*. 2018;136:56-61. doi:10.1016/j.phrs.2018.08.016
47. Takahashi Y, Narita S, Shiota M, et al. Impact of trough abiraterone level on adverse events in patients with prostate cancer treated with abiraterone acetate. *Eur J Clin Pharmacol*. 2023;79(1):89-98. doi:10.1007/s00228-022-03420-0
48. van der Kleij MBA, Meertens M, Groenland SL, et al. Feasibility and efficacy of therapeutic drug monitoring of abiraterone in metastatic castration resistant prostate cancer patients. *Br J Cancer*. 2025;132(7):635-642. doi:10.1038/s41416-025-02954-1
49. Benoist GE, Hendriks RJ, Mulders PFA, et al. Pharmacokinetic Aspects of the Two Novel Oral Drugs Used for Metastatic Castration-Resistant Prostate Cancer: Abiraterone Acetate and Enzalutamide. *Clin Pharmacokinet*. 2016;55(11):1369-1380. doi:10.1007/s40262-016-0403-6
50. Del Re M, Fogli S, Derosa L, et al. The role of drug-drug interactions in prostate cancer treatment: Focus on abiraterone acetate/prednisone and enzalutamide. *Cancer Treat Rev*. 2017;55:71-82. doi:10.1016/j.ctrv.2017.03.001
51. Fekete B, Bársony L, Biró K, et al. A new method to quantify the effect of co-medication on the efficacy of abiraterone in metastatic castration-resistant prostate cancer patients. *Front Pharmacol*. 2023;14:1220457. doi:10.3389/fphar.2023.1220457
52. Clegg NJ, Wongvipat J, Joseph JD, et al. ARN-509: A Novel Antiandrogen for Prostate Cancer Treatment. *Cancer Res*. 2012;72(6):1494-1503. doi:10.1158/0008-5472.CAN-11-3948
53. Alkhudair NA. Apalutamide: Emerging Therapy for Non-Metastatic Castration-Resistant Prostate Cancer. *Saudi Pharm J SPJ Off Publ Saudi Pharm Soc*. 2019;27(3):368-372. doi:10.1016/j.jsps.2018.12.005
54. Smith MR, Saad F, Chowdhury S, et al. Apalutamide Treatment and Metastasis-free Survival in Prostate Cancer. *N Engl J Med*. 2018;378(15):1408-1418. doi:10.1056/NEJMoa1715546

55. “Apalutamide”- EMA E. Erleada- summary of product characteristics. Published online 2024. https://www.ema.europa.eu/en/documents/product-information/erleada-epar-product-information_en.pdf
56. May MB, Glode AE. Apalutamide: A new agent in the management of prostate cancer. *J Oncol Pharm Pract Off Publ Int Soc Oncol Pharm Pract*. 2019;25(8):1968-1978. doi:10.1177/1078155219864424
57. de Vries R, Jacobs F, Mannens G, et al. Apalutamide Absorption, Metabolism, and Excretion in Healthy Men, and Enzyme Reaction in Human Hepatocytes. *Drug Metab Dispos Biol Fate Chem*. 2019;47(5):453-464. doi:10.1124/dmd.118.084517
58. Small EJ, Saad F, Chowdhury S, et al. Apalutamide and overall survival in non-metastatic castration-resistant prostate cancer. *Ann Oncol Off J Eur Soc Med Oncol*. 2019;30(11):1813-1820. doi:10.1093/annonc/mdz397
59. Boujonnier F, Lemaitre F, Scailteux LM. Pharmacokinetic Interactions Between Abiraterone, Apalutamide, Darolutamide or Enzalutamide and Antithrombotic Drugs: Prediction of Clinical Events and Review of Pharmacological Information. *Cardiovasc Drugs Ther*. 2024;38(4):757-767. doi:10.1007/s10557-023-07453-0
60. 210951orig1s000multidiscipliner.pdf. Accessed October 28, 2025. https://www.accessdata.fda.gov/drugsatfda_docs/nda/2018/210951orig1s000multidiscipliner.pdf
61. Perez-Ruixo C, Ackaert O, Ouellet D, et al. Efficacy and Safety Exposure-Response Relationships of Apalutamide in Patients with Nonmetastatic Castration-Resistant Prostate Cancer. *Clin Cancer Res Off J Am Assoc Cancer Res*. 2020;26(17):4460-4467. doi:10.1158/1078-0432.CCR-20-1041
62. T’jollyn H, Ackaert O, Chien C, et al. Efficacy and safety exposure-response relationships of apalutamide in patients with metastatic castration-sensitive prostate cancer: results from the phase 3 TITAN study. *Cancer Chemother Pharmacol*. 2022;89(5):629-641. doi:10.1007/s00280-022-04427-1
63. Appukkuttan S, Ko G, Fu C, et al. Drug-drug interaction potential among patients with nonmetastatic castration-resistant prostate cancer (nmCRPC) treated with novel androgen receptor inhibitors. *Expert Rev Anticancer Ther*. 2024;24(5):325-333. doi:10.1080/14737140.2024.2328778
64. Shore ND. Darolutamide (ODM-201) for the treatment of prostate cancer. *Expert Opin Pharmacother*. 2017;18(9):945-952. doi:10.1080/14656566.2017.1329820
65. Podgoršek E, Mehra N, van Oort IM, Somford DM, Boerrigter E, van Erp NP. Clinical Pharmacokinetics and Pharmacodynamics of the Next Generation Androgen Receptor Inhibitor-Darolutamide. *Clin Pharmacokinet*. 2023;62(8):1049-1061. doi:10.1007/s40262-023-01268-w
66. Moilanen AM, Riikonen R, Oksala R, et al. Discovery of ODM-201, a new-generation androgen receptor inhibitor targeting resistance mechanisms to androgen signaling-directed prostate cancer therapies. *Sci Rep*. 2015;5:12007. doi:10.1038/srep12007

67. T'jollyn H, Ackaert O, Chien C, et al. Efficacy and safety exposure–response relationships of apalutamide in patients with metastatic castration-sensitive prostate cancer: results from the phase 3 TITAN study. *Cancer Chemother Pharmacol*. 2022;89(5):629-641. doi:10.1007/s00280-022-04427-1
68. Fizazi K, Shore N, Tammela TL, et al. Darolutamide in Nonmetastatic, Castration-Resistant Prostate Cancer. *N Engl J Med*. 2019;380(13):1235-1246. doi:10.1056/NEJMoa1815671
69. “Darolutamide”-EMA. Nubeqa- summary of product characteristics. Published online 2024. https://www.ema.europa.eu/en/documents/product-information/nubeqa-epar-product-information_en.pdf
70. Taavitsainen P, Prien O, Kähkönen M, et al. Metabolism and Mass Balance of the Novel Nonsteroidal Androgen Receptor Inhibitor Darolutamide in Humans. *Drug Metab Dispos Biol Fate Chem*. 2021;49(6):420-433. doi:10.1124/dmd.120.000309
71. Nubeqa, INN-darolutamide. Accessed August 6, 2025. https://ec.europa.eu/health/documents/community-register/2020/20200327147390/anx_147390_it.pdf
72. Multi-Discipline Review. Published online 2018.
73. Shore N, Zurth C, Fricke R, et al. Evaluation of Clinically Relevant Drug-Drug Interactions and Population Pharmacokinetics of Darolutamide in Patients with Nonmetastatic Castration-Resistant Prostate Cancer: Results of Pre-Specified and Post Hoc Analyses of the Phase III ARAMIS Trial. *Target Oncol*. 2019;14(5):527-539. doi:10.1007/s11523-019-00674-0
74. Zurth C, Koskinen M, Fricke R, et al. Drug-Drug Interaction Potential of Darolutamide: In Vitro and Clinical Studies. *Eur J Drug Metab Pharmacokinet*. 2019;44(6):747-759. doi:10.1007/s13318-019-00577-5
75. Davis ID, Martin AJ, Stockler MR, et al. Enzalutamide with Standard First-Line Therapy in Metastatic Prostate Cancer. *N Engl J Med*. 2019;381(2):121-131. doi:10.1056/NEJMoa1903835
76. Hussain M, Fizazi K, Saad F, et al. Enzalutamide in Men with Nonmetastatic, Castration-Resistant Prostate Cancer. *N Engl J Med*. 2018;378(26):2465-2474. doi:10.1056/NEJMoa1800536
77. Hong JH. Pharmacokinetic/pharmacodynamic drug evaluation of enzalutamide for treating prostate cancer. *Expert Opin Drug Metab Toxicol*. 2018;14(3):361-369. doi:10.1080/17425255.2018.1440288
78. Gibbons JA, Ouatas T, Krauwinkel W, et al. Clinical Pharmacokinetic Studies of Enzalutamide. *Clin Pharmacokinet*. 2015;54(10):1043-1055. doi:10.1007/s40262-015-0271-5
79. 203415Orig1s000ClinPharmR.pdf. Accessed October 28, 2025. https://www.accessdata.fda.gov/drugsatfda_docs/nda/2012/203415Orig1s000ClinPharmR.pdf

80. Groenland SL, van Nuland M, Verheijen RB, et al. Therapeutic Drug Monitoring of Oral Anti-Hormonal Drugs in Oncology. *Clin Pharmacokinet*. 2019;58(3):299-308. doi:10.1007/s40262-018-0683-0
81. Xtandi, INN-enzalutamide. Accessed August 6, 2025. https://ec.europa.eu/health/documents/community-register/2016/20161212136636/anx_136636_it.pdf
82. “Enzalutamide”-FDA. Xtandi- CLINICAL PHARMACOLOGY AND BIOPHARMACEUTICS REVIEW(S). Published online 2022. https://www.accessdata.fda.gov/drugsatfda_docs/nda/2012/203415Orig1s000ClinPharmR.pdf
83. Benoist GE, van Oort IM, Burger DM, Mehra N, van Erp NP. The impact of patient characteristics on enzalutamide pharmacokinetics and how this relates to treatment toxicity and efficacy in metastatic prostate cancer patients. *Cancer Chemother Pharmacol*. 2020;85(4):753-760. doi:10.1007/s00280-020-04039-7
84. Gasperoni L, Giunta EF, Montanari D, Masini C, De Giorgi U. New-generation androgen receptor signaling inhibitors (ARSIs) in metastatic hormone-sensitive prostate cancer (mHSPC): pharmacokinetics, drug-drug interactions (DDIs), and clinical impact. *Expert Opin Drug Metab Toxicol*. 2024;20(6):491-502. doi:10.1080/17425255.2024.2353749
85. Otsuka Y, Poondru S, Bonate PL, et al. Physiologically-based pharmacokinetic modeling to predict drug-drug interaction of enzalutamide with combined P-gp and CYP3A substrates. *J Pharmacokinet Pharmacodyn*. 2023;50(5):365-376. doi:10.1007/s10928-023-09867-7
86. Lyon AR, López-Fernández T, Couch LS, et al. 2022 ESC Guidelines on cardio-oncology developed in collaboration with the European Hematology Association (EHA), the European Society for Therapeutic Radiology and Oncology (ESTRO) and the International Cardio-Oncology Society (IC-OS). *Eur Heart J*. 2022;43(41):4229-4361. doi:10.1093/eurheartj/ehac244
87. Pharmacokinetic Interactions Between Abiraterone, Apalutamide, Darolutamide or Enzalutamide and Antithrombotic Drugs: Prediction of Clinical Events and Review of Pharmacological Information - PubMed. Accessed October 28, 2025. <https://pubmed.ncbi.nlm.nih.gov/37126188/>
88. Groenland SL, van Eerden R a. G, Westerdijk K, et al. Therapeutic drug monitoring-based precision dosing of oral targeted therapies in oncology: a prospective multicenter study. *Ann Oncol Off J Eur Soc Med Oncol*. 2022;33(10):1071-1082. doi:10.1016/j.annonc.2022.06.010
89. Beumer JH. Without Therapeutic Drug Monitoring, There Is No Personalized Cancer Care. *Clin Pharmacol Ther*. 2013;93(3):228-230. doi:10.1038/clpt.2012.243
90. van der Kleij MBA, Guchelaar NAD, Mathijssen RHJ, et al. Therapeutic Drug Monitoring of Kinase Inhibitors in Oncology. *Clin Pharmacokinet*. 2023;62(10):1333-1364. doi:10.1007/s40262-023-01293-9

91. Spector R, Park GD, Johnson GF, Vesell ES. Therapeutic drug monitoring. *Clin Pharmacol Ther.* 1988;43(4):345-353. doi:10.1038/clpt.1988.42
92. Abdul-Aziz MH, Brady K, Cotta MO, Roberts JA. Therapeutic Drug Monitoring of Antibiotics: Defining the Therapeutic Range. *Ther Drug Monit.* 2022;44(1):19-31. doi:10.1097/FTD.0000000000000940
93. Brunet M, van Gelder T, Åsberg A, et al. Therapeutic Drug Monitoring of Tacrolimus-Personalized Therapy: Second Consensus Report. *Ther Drug Monit.* 2019;41(3):261-307. doi:10.1097/FTD.0000000000000640
94. Johannessen Landmark C, Johannessen SI, Patsalos PN. Therapeutic drug monitoring of antiepileptic drugs: current status and future prospects. *Expert Opin Drug Metab Toxicol.* 2020;16(3):227-238. doi:10.1080/17425255.2020.1724956
95. Couderc S, Mory C, Darnaud L, Saint-Marcoux F. [Therapeutic drug monitoring of antidepressants: Why venlafaxine is the most monitored drug? A review of literature]. *Therapie.* 2021;76(6):725-733. doi:10.1016/j.therap.2021.01.052
96. Kahan BD, Keown P, Levy GA, Johnston A. Therapeutic drug monitoring of immunosuppressant drugs in clinical practice. *Clin Ther.* 2002;24(3):330-350; discussion 329. doi:10.1016/s0149-2918(02)85038-x
97. Alnaim L. Therapeutic drug monitoring of cancer chemotherapy. *J Oncol Pharm Pract Off Publ Int Soc Oncol Pharm Pract.* 2007;13(4):207-221. doi:10.1177/1078155207081133
98. Reynolds DJ, Aronson JK. ABC of monitoring drug therapy. Making the most of plasma drug concentration measurements. *BMJ.* 1993;306(6869):48-51. doi:10.1136/bmj.306.6869.48
99. Hon YY, Evans WE. Making TDM work to optimize cancer chemotherapy: a multidisciplinary team approach. *Clin Chem.* 1998;44(2):388-400.
100. Galpin AJ, Evans WE. Therapeutic drug monitoring in cancer management. *Clin Chem.* 1993;39(11 Pt 2):2419-2430.
101. Teng JFT, Mabasa VH, Ensom MHH. The role of therapeutic drug monitoring of imatinib in patients with chronic myeloid leukemia and metastatic or unresectable gastrointestinal stromal tumors. *Ther Drug Monit.* 2012;34(1):85-97. doi:10.1097/FTD.0b013e31823cdec9
102. Yu H, Steeghs N, Nijenhuis CM, Schellens JHM, Beijnen JH, Huitema ADR. Practical guidelines for therapeutic drug monitoring of anticancer tyrosine kinase inhibitors: focus on the pharmacokinetic targets. *Clin Pharmacokinet.* 2014;53(4):305-325. doi:10.1007/s40262-014-0137-2
103. Giamas G, Man YL, Hirner H, et al. Kinases as targets in the treatment of solid tumors. *Cell Signal.* 2010;22(7):984-1002. doi:10.1016/j.cellsig.2010.01.011
104. Widmer N, Bardin C, Chatelut E, et al. Review of therapeutic drug monitoring of anticancer drugs part two--targeted therapies. *Eur J Cancer Oxf Engl 1990.* 2014;50(12):2020-2036. doi:10.1016/j.ejca.2014.04.015

105. Simsek C, Esin E, Yalcin S. Metronomic Chemotherapy: A Systematic Review of the Literature and Clinical Experience. *J Oncol*. 2019;2019:5483791. doi:10.1155/2019/5483791
106. Klümpen HJ, Samer CF, Mathijssen RHJ, Schellens JHM, Gurney H. Moving towards dose individualization of tyrosine kinase inhibitors. *Cancer Treat Rev*. 2011;37(4):251-260. doi:10.1016/j.ctrv.2010.08.006
107. Partridge AH, Avorn J, Wang PS, Winer EP. Adherence to therapy with oral antineoplastic agents. *J Natl Cancer Inst*. 2002;94(9):652-661. doi:10.1093/jnci/94.9.652
108. Wilkinson GR. Drug metabolism and variability among patients in drug response. *N Engl J Med*. 2005;352(21):2211-2221. doi:10.1056/NEJMra032424
109. Gross AS. Best practice in therapeutic drug monitoring. *Br J Clin Pharmacol*. 1998;46(2):95-99. doi:10.1046/j.1365-2125.1998.00770.x
110. Relling MV, Fairclough D, Ayers D, et al. Patient characteristics associated with high-risk methotrexate concentrations and toxicity. *J Clin Oncol Off J Am Soc Clin Oncol*. 1994;12(8):1667-1672. doi:10.1200/JCO.1994.12.8.1667
111. Evans WE, Relling MV. Clinical pharmacokinetics-pharmacodynamics of anticancer drugs. *Clin Pharmacokinet*. 1989;16(6):327-336. doi:10.2165/00003088-198916060-00001
112. DeVita VT, Lawrence TS, Rosenberg SA. DeVita, Hellman, and Rosenberg's cancer: Principles & practice of oncology: Tenth edition. In: *DeVita, Hellman, and Rosenberg's Cancer: Principles & Practice of Oncology: Tenth Edition*. Wolters Kluwer Health Adis (ESP); 2015:1-2280. Accessed October 28, 2025. <https://pure.johnshopkins.edu/en/publications/devita-hellman-and-rosenbergs-cancer-principles-amp-practice-of-o/>
113. Thomas-Schoemann A, Blanchet B, Bardin C, et al. Drug interactions with solid tumour-targeted therapies. *Crit Rev Oncol Hematol*. 2014;89(1):179-196. doi:10.1016/j.critrevonc.2013.08.007
114. Gao B, Yeap S, Clements A, Balakrishnar B, Wong M, Gurney H. Evidence for therapeutic drug monitoring of targeted anticancer therapies. *J Clin Oncol Off J Am Soc Clin Oncol*. 2012;30(32):4017-4025. doi:10.1200/JCO.2012.43.5362
115. Moore MJ, Erlichman C. Therapeutic drug monitoring in oncology. Problems and potential in antineoplastic therapy. *Clin Pharmacokinet*. 1987;13(4):205-227. doi:10.2165/00003088-198713040-00001
116. Bardin C, Veal G, Paci A, et al. Therapeutic drug monitoring in cancer--are we missing a trick? *Eur J Cancer Oxf Engl 1990*. 2014;50(12):2005-2009. doi:10.1016/j.ejca.2014.04.013
117. Crotti S, Posocco B, Marangon E, Nitti D, Toffoli G, Agostini M. Mass spectrometry in the pharmacokinetic studies of anticancer natural products. *Mass Spectrom Rev*. 2017;36(2):213-251. doi:10.1002/mas.21478

118. Chace DH, Kalas TA, Naylor EW. Use of tandem mass spectrometry for multianalyte screening of dried blood specimens from newborns. *Clin Chem.* 2003;49(11):1797-1817. doi:10.1373/clinchem.2003.022178
119. Hopfgartner G, Bourgoigne E. Quantitative high-throughput analysis of drugs in biological matrices by mass spectrometry. *Mass Spectrom Rev.* 2003;22(3):195-214. doi:10.1002/mas.10050
120. Understanding the ion source parameters in Analyst® and SCIEX OS software: GS1, GS2, TEM and CUR. Accessed October 29, 2025. https://sciex.com/support/knowledge-base/articles/ion-source-parameters-gs1-gs2-cur-temperature_en_us
121. Taylor G. Disintegration of Water Drops in an Electric Field. *Proc R Soc Lond Ser A.* 1964;280:383-397. doi:10.1098/rspa.1964.0151
122. Dülcks Th, Juraschek R. ELECTROSPRAY AS AN IONISATION METHOD FOR MASS SPECTROMETRY. *J Aerosol Sci.* 1999;30(7):927-943. doi:10.1016/S0021-8502(98)00781-2
123. XX. On the equilibrium of liquid conducting masses charged with electricity : The London, Edinburgh, and Dublin Philosophical Magazine and Journal of Science: Vol 14, No 87. Accessed October 22, 2025. <https://www.tandfonline.com/doi/abs/10.1080/14786448208628425>
124. M10 Bioanalytical Method Validation and Study Sample Analysis | FDA. Accessed October 23, 2025. <https://www.fda.gov/regulatory-information/search-fda-guidance-documents/m10-bioanalytical-method-validation-and-study-sample-analysis>
125. ICH M10 on bioanalytical method validation - Scientific guideline | European Medicines Agency (EMA). March 14, 2019. Accessed September 24, 2025. <https://www.ema.europa.eu/en/ich-m10-bioanalytical-method-validation-scientific-guideline>
126. Shah VP, Midha KK, Dighe S, et al. Analytical methods validation: bioavailability, bioequivalence and pharmacokinetic studies. Conference report. *Eur J Drug Metab Pharmacokinet.* 1991;16(4):249-255. doi:10.1007/BF03189968
127. Booth B, Arnold ME, DeSilva B, et al. Workshop report: Crystal City V--quantitative bioanalytical method validation and implementation: the 2013 revised FDA guidance. *AAPS J.* 2015;17(2):277-288. doi:10.1208/s12248-014-9696-2
128. Selecting the correct weighting factors for linear and quadratic calibration curves with least-squares regression algorithm in bioanalytical LC-MS/MS assays and impacts of using incorrect weighting factors on curve stability, data quality, and assay performance - PubMed. Accessed October 16, 2025. <https://pubmed.ncbi.nlm.nih.gov/25157966/>
129. Polson C, Sarkar P, Incledon B, Raguvaran V, Grant R. Optimization of protein precipitation based upon effectiveness of protein removal and ionization effect in liquid chromatography–tandem mass spectrometry. *J Chromatogr B.* 2003;785(2):263-275. doi:10.1016/S1570-0232(02)00914-5

130. “Abiraterone”-FDA. Zytiga- CLINICAL PHARMACOLOGY AND BIOPHARMACEUTICS REVIEW. Published online 2010. https://www.accessdata.fda.gov/drugsatfda_docs/nda/2011/202379orig1s000clinpharmr.pdf
131. “Enzalutamide”-EMA. Xtandi- summary of product characteristics. Published online 2024. https://www.ema.europa.eu/en/documents/product-information/xtandi-epar-product-information_en.pdf
132. “Darolutamide”- FDA. Nubeqa- MULTI-DISCIPLINE REVIEW. Published online 2018. https://www.accessdata.fda.gov/drugsatfda_docs/nda/2019/212099Orig1s000MultidisciplineR.pdf
133. “Apalutamide”- FDA. Apalutamide-MULTI-DISCIPLINE REVIEW. Published online 2018. https://www.accessdata.fda.gov/drugsatfda_docs/nda/2018/210951orig1s000multidiscipliner.pdf
134. Benoist GE, van der Meulen E, Lubberman FJE, et al. Analytical challenges in quantifying abiraterone with LC-MS/MS in human plasma. *Biomed Chromatogr BMC*. 2017;31(11). doi:10.1002/bmc.3986
135. van Nuland M, Venekamp N, de Vries N, de Jong K a. M, Rosing H, Beijnen JH. Development and validation of an UPLC-MS/MS method for the therapeutic drug monitoring of oral anti-hormonal drugs in oncology. *J Chromatogr B Analyt Technol Biomed Life Sci*. 2019;1106-1107:26-34. doi:10.1016/j.jchromb.2019.01.001
136. Buck SAJ, de Bruijn P, Ghobadi-Moghaddam-Helmantel IM, et al. Validation of an LC-MS/MS method for simultaneous quantification of abiraterone, enzalutamide and darolutamide in human plasma. *J Chromatogr B Analyt Technol Biomed Life Sci*. 2023;1225:123752. doi:10.1016/j.jchromb.2023.123752
137. Research C for DE and. Bioanalytical Method Validation Guidance for Industry. April 29, 2020. Accessed September 24, 2025. <https://www.fda.gov/regulatory-information/search-fda-guidance-documents/bioanalytical-method-validation-guidance-industry>
138. Nykänen P, Korjamo T, Gieschen H, Zurth C, Koskinen M. Pharmacokinetics of Darolutamide, its Diastereomers and Active Metabolite in the Mouse: Response to Saini NK et al. (2020). *Drug Metab Lett*. 2021;14(1):9-16. doi:10.2174/1872312814666201112121129
139. Mueller-Schoell A, Groenland SL, Scherf-Clavel O, et al. Therapeutic drug monitoring of oral targeted antineoplastic drugs. *Eur J Clin Pharmacol*. 2021;77(4):441-464. doi:10.1007/s00228-020-03014-8
140. Janssen JM, Dorlo TPC, Beijnen JH, Huitema ADR. Evaluation of Extrapolation Methods to Predict Trough Concentrations to Guide Therapeutic Drug Monitoring of Oral Anticancer Drugs. *Ther Drug Monit*. 2020;42(4):532. doi:10.1097/FTD.0000000000000767